THE EFFECT OF SI AND MO ON THE ISOTHERMAL TRANSFORMATION
TREATMENT AND TEMPERING OF A BAINITIC MEDIUM C STEEL

A THESIS SUBMITTED TO
THE GRADUATE SCHOOL OF NATURAL AND APPLIED SCIENCES
OF
MIDDLE EAST TECHNICAL UNIVERSITY

BY

GÜLTEN KAFADAR

IN PARTIAL FULFILLMENT OF THE REQUIREMENTS
FOR
THE DEGREE OF DOCTOR OF PHILOSOPHY
IN
METALLURGICAL AND MATERIALS ENGINEERING

DECEMBER 2021

Approval of the thesis:

THE EFFECT OF SI AND MO ON THE ISOTHERMAL TRANSFORMATION TREATMENT AND TEMPERING OF A BAINITIC MEDIUM C STEEL

submitted by **GÜLTEN KAFADAR** in partial fulfillment of the requirements for the degree of **Doctor of Philosophy** in **Metallurgical and Materials Engineering, Middle East Technical University** by,

Prof. Dr. Halil Kalıpçılar
Dean, Graduate School of **Natural and Applied Sciences** _____

Prof. Dr. Cemil Hakan Gür
Head of the Department, **Metallurgical and Materials Eng** _____

Prof. Dr. Bilgehan Ögel
Supervisor, **Metallurgical and Materials Eng, METU** _____

Examining Committee Members:

Prof. Dr. Rıza Gürbüz
Metallurgical and Materials Eng, METU _____

Prof. Dr. Bilgehan Ögel
Metallurgical and Materials Eng, METU _____

Prof. Dr. Abbas Tamer Özdemir
Metallurgical and Materials Eng, Gazi University _____

Prof. Dr. Ziya Esen
Inter-Curricular Courses Dept, Çankaya University _____

Assoc. Prof. Dr. Caner Şimşir
Metallurgical and Materials Eng, METU _____

Date: 02.12.2021

I hereby declare that all information in this document has been obtained and presented in accordance with academic rules and ethical conduct. I also declare that, as required by these rules and conduct, I have fully cited and referenced all material and results that are not original to this work.

Name, Last name: Gülten Kafadar

Signature:

ABSTRACT

**THE EFFECT OF SI AND MO ON THE ISOTHERMAL
TRANSFORMATION TREATMENT AND TEMPERING OF A BAINITIC
MEDIUM C STEEL**

Kafadar, Gülten
Doctor of Philosophy, Metallurgical and Materials Engineering
Supervisor: Prof. Dr. Bilgehan Ögel

December 2021, 101 pages

Bainitic steels have become popular in recent years that generally include medium-high C(~0.5-1%), high Mn(~1-2%) and high Si (~1-2%) because of their high mechanical properties. However, their transformation time is very long (7-14 days). In this study, one of the main goal is to obtain bainitic steels which have shorter bainitic transformation times. This may be achieved by changing Mo and Si ratios in the alloys.

In this thesis study, isothermal transformation treatment and tempering of a bainitic medium C steel are investigated. This research work aims to study the effect of 2wt%Mo on bainitic transformation kinetics and bainite morphology in 0.6wt%C-1.2wt%Si-1.0wt%Mn (60SiMn5) steel. Different heat treatments were applied for bainitic transformation. In the first set of specimens, austenitization was done at 950°C. It is followed by an isothermal holding at just above M_S and higher temperatures. Second set of specimens were austenitized at 950°C, rapidly cooled in salt bath and isothermally treated between 200°C–300°C for different time intervals. Another set of specimens were rapidly cooled in oil after an austenitization treatment and then tempered in the temperature range of 200°C–550°C. Hardness testing and

tensile testing were applied to investigate the mechanical properties. In 60SiMn5 specimens, the amount of retained austenite increases with increasing the amount of bainite but no retained austenite is observed in bainitic 2wt% Mo addition of 60SiMn5 specimens. 2wt% Mo addition of 60SiMn5 specimens shows the secondary hardening effect peak upon tempering at 500°C. The examination of the secondary hardening would also contribute to the behavior of Mo in tempered bainitic steels.

Keywords: Bainite Transformation; Microstructure; Secondary Hardening; Bainite; Tempering

ÖZ

BEYNİTİK ORTA KARBONLU ÇELİĞİN İZOTERMAL DÖNÜŞÜM İŞLEMİ VE TEMPERLENMESİ ÜZERİNE Sİ VE MONUN ETKİSİ

Kafadar, Gülten
Doktora, Metalurji ve Malzeme Mühendisliği
Tez Yöneticisi: Prof. Dr. Bilgehan Ögel

Aralık 2021, 101 sayfa

Genellikle orta-yüksek C (~0.5-1%), yüksek Mn (~1-2%) ve yüksek miktarda Si (~1-2%) içeren beynitik çelikler yüksek mekanik özellikleri nedeniyle son yıllarda oldukça popüler bir hale gelmiştir. Ama dönüşüm süreleri çok uzun sürmektedir (7-14 gün). Bu çalışmada, beynitik dönüşüm süreleri daha kısa olan beynitik çeliklerin elde edilmesi ana hedeflerden biridir. Bu, alaşımlardaki Mo ve Si oranları değiştirilerek sağlanabilir.

Bu tez çalışmasında, orta karbonlu beynitik çeliğin izotermal dönüşüm işlemi incelenmiştir. Bu araştırma, ağırlıkça %2 Mo'nun beynitik dönüşüm kinetiği ve beynit morfolojisi üzerindeki etkisini ağırlıkça %0.6C-1.2%Si-1.0%Mn (60SiMn5) çelikte incelemeyi amaçlamaktadır. Beynitik dönüşüm için farklı ısıl işlemler uygulanmıştır. İlk set numunelerde 950°C'de östenitleme yapılmıştır. Bunu, M_S'nin hemen üzerinde ve daha yüksek sıcaklıklarda bir izotermal işlem izler. İkinci set numuneler 950°C'de östenitlenmiş, tuz banyosunda hızla soğutulmuş ve farklı zaman aralıklarında 200°C-300°C arasında izotermal işlem uygulanmıştır. Başka bir numune seti, östenitleme işleminden sonra hızla yağda soğutulmuş ve ardından 200°C-550°C sıcaklık aralığında temperlenmiştir. Mekanik özellikleri araştırmak için sertlik testi ve çekme testi uygulanmıştır. 60SiMn5 numunelerinde beynit miktarının artmasıyla kalıntı östenit miktarı artar, ancak ağırlıkça %2'si Mo

ilavesinde 60SiMn5 beynitik numunelerinde kalıntı östenit görülmez. %2 Mo ilavesi olan 60SiMn5 numunelerinde, 500°C'de temperleme neticesinde ikincil sertleşme tepe noktası oluşur. İkincil sertleşmenin incelenmesi, Mo'nun temperlenmiş beynitik çeliklerdeki davranışına da katkıda bulunacaktır.

Anahtar Kelimeler: Beynit Dönüşümü; Mikroyapı; İkincil Sertleşme; Beynit; Temperleme

To my special mom, super dad, best sister ever, only love and also my little

princess *İpek* to be born

ACKNOWLEDGMENTS

TABLE OF CONTENTS

xii

LIST OF TABLES

LIST OF FIGURES

FIGURES

xv

LIST OF ABBREVIATIONS

B_F	Bainite Transformation Final Temperature
B_S	Bainite Transformation Start Temperature
CCT	Continuous-Cooling-Transformation
CP	Complex Phase
FC	Furnace Cooling
HV	Vickers Hardness
HV30	Vickers Hardness under 30 kg load
LTB	Low Temperature Bainite
M_F	Martensite Final Temperature
M_S	Martensite Start Temperature
PSE	Product of Strength and Elongation
RA	Retained Austenite
RT	Room Temperature
SEM	Scanning Electron Microscopy
TRIP	Transformation-Induced Plasticity
TTT	Time-Temperature-Transformation
XRD	X-Ray Diffraction

CHAPTER 1

INTRODUCTION

In recent years, the pressure on automotive industry for safer, more energy efficient and environmentally friendly cars lead to the replacement of mild steels with high-strength steels at an increasing trend [1]. Despite the competition from aluminum alloys and magnesium alloys, steel is still a leading material that offers automakers a robust and economical material for body structure.

Since, the discovery of bainitic microstructure and named in honor of E. Bain, many commercial low carbon bainitic steels become available in the market. These include creep resistant steels [2, 3], bainitic forging steels [4, 5] and complex phase (CP) steels with bainitic constituents [6, 7]. However, especially at high %C and %Mn contents, the bainitic transformation limit may be reached, beyond which austenite will no longer transform to bainite leaving blocky austenite regions in the microstructure. These blocky austenite regions together with the carbides precipitated within and between the bainite sheaves degrade the toughness of bainitic steels.

In recent years, Bhadeshia and Caballero has developed a series of high carbon high silicon carbide free bainitic steels with an ultimate tensile strength of 2.0 GPa and a toughness as high as $30MPa.m^{1/2}$ [8-10]. The presence of high %Si suppresses the carbide precipitation within bainite sheaves (bainitic ferrite). The transformation carried out at lower temperatures (very close to Martensite Start (M_S)) also prevents the blocky austenite formation and helps the retention of retained austenite between the bainite sheaves and improves the toughness by resistance to crack propagation.

However, at low temperatures, the bainitic transformation can be very sluggish and may extend to 2 days-9 days [11-14]. It is found that the growth of bainite cannot be sustained once the carbon concentration of the austenite reaches the T_0 curve of the

1

phase diagram [15-17]. The points where the free energies of austenite and ferrite are exactly the same, which have the same chemical composition, is called the T_0 curve. Bhadeshia and Caballero has shown that several alloying elements like Al and Co can shift the T_0 to higher carbon concentrations and increase the rate of reaction [13,14,18]. On the other hand, Mn has an opposite effect. Although it decreases the M_S temperature and enhances strength of bainite due to transformation at low temperatures, Mn also decreases the rate of the reaction. In a study, however, using a lower content of Mn shifted the T_0 curve to higher carbon concentrations and permitted a higher degree of transformation to bainitic ferrite without too much loss in strength [19].

In studies of high strength bainitic steels, the Mo content is kept low, i.e., in the range 0.2%-0.4% to avoid temper embrittlement. However, Mo as an alloying element have several important effects on steel. It suppresses primary ferrite and pearlite and hence enhances bainite formation [20-23]. Depending on the heat treatment procedure Mo may cause secondary hardening in steels, by replacing coarse cementite precipitation with a much finer alloy carbide dispersion [20]. Mo is also used as solid-solution strengthening element.

The aim of this study is to produce the finest possible bainitic microstructure by transformation at the lowest possible temperature by decreasing bainite transformation temperatures, and increasing the maximum volume fraction of bainite in the final microstructure.

This study is focused on isothermal transformation treatment of a bainitic medium C steel. In this experiment, two main parameters are investigated: transformation temperature and Mo, Si content. The effect of these parameters on bainite morphology, retained austenite content, carbide precipitation and mechanical properties are investigated.

The following chapters include literature review, experimental, results and discussion, and conclusions, respectively. In the second chapter, important points about bainitic formation, carbide-free bainitic steels, and low temperature bainitic

steels will be mentioned. In the third chapter, the experimental methods of nano bainitic transformation on low alloyed steels will be explained. In the fourth chapter, microstructural and mechanical results will be investigated, discussed and compared with the literature together. In the final part, the results obtained from the study and its contributions to the literature will be indicated.

CHAPTER 2

LITERATURE REVIEW

Different microstructures may be required place of use of the steels. For example, hot rolled, or cold rolled, or heat-treated steels have different performances and so different microstructures may be achieved. Some traditional techniques during heat treatment may provide good mechanical properties. Especially, quenching causes to big increases in the strength values. Therefore, this method is preferred to increase the strength of the material. However, the cost of the quenching process is so high. The steel needs to be heated to the 800ºC-900ºC range and then quenched to achieve a martensitic microstructure. In addition, after the quenching process, the quenched steel needs to temper for two hours. This tempering process also increases the cost [24].

The use of bainitic steels is preferred in various mobile vehicles [25]. The reason is that there is a decrease in the total weight of the vehicle. Advanced bainitic steels have a good elongation. This means that they have good ductility. The reason of this ductility is their microstructure in which bainitic ferrite provides ductility. Bainite phase is a hard phase. The combination of these phases may create good stretch flangeability and bendability. A uniform fine lath microstructure is obtained in advanced bainitic steels with bainitic ferrite matrix and bainite phases. Also, martensite phase may cause differences in hardness. These heterogeneities provide good deep drawability.

When we considered all these effects, bainite phase has an importance especially for mechanical properties of the material. The strength values of the bainite phases are so close to the strength values of the martensite. In addition to these, this phase has a tough microstructure and tempering is not needed. It is very attractive that both the

toughness and strength values expected to be obtained in maraging steels can be achieved and it is 9 times cheaper [26].

2.1   BAINITE FORMATION

Looking at the TTT diagram of a eutectoid carbon steel (Figure 2.1) as an example, the martensitic structure can only be observed at low temperatures around 250°C-550°C, while the pearlitic structure is observed in the range of 550°C-720°C. In this temperature range, a new structure was found. This structure is slower than fine pearlite and faster than martensite [20,27]. Edgar Bain and Davenport (1930) first found these structures which are their generic terms are bainite and observed in the optical microscopy (Figure 2.2). This microstructure was expressed as acicular, dark etching aggregate [15].
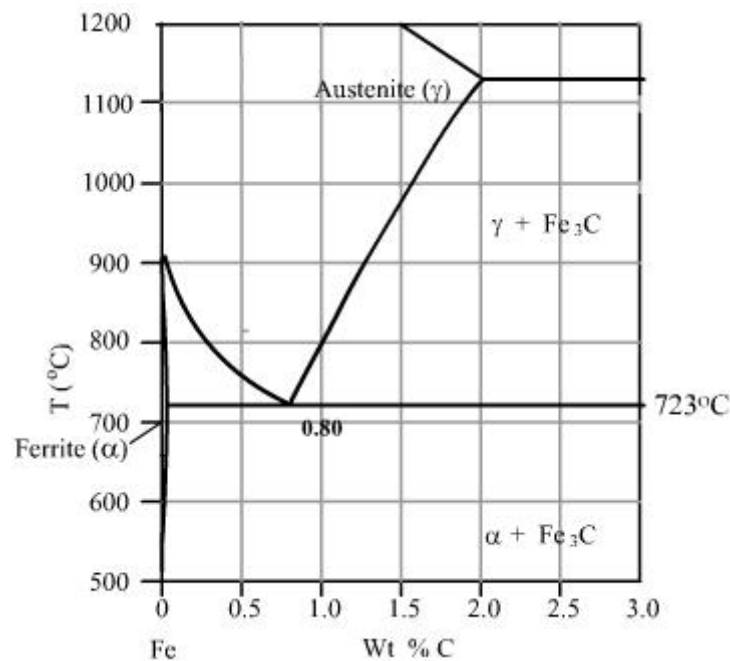
Figure 2.1. Fe-C phase diagram of a eutectoid steel.
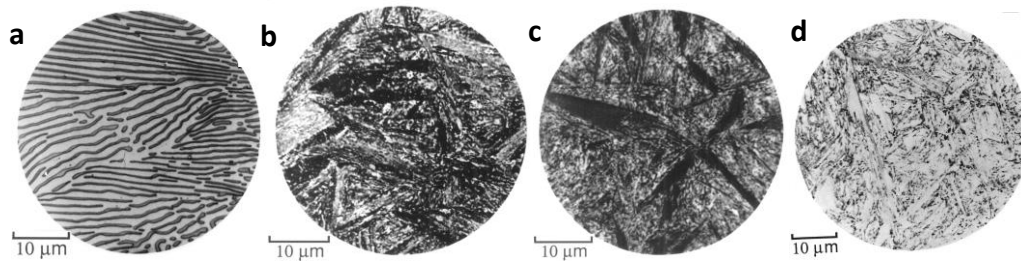
Figure 2.2. Optical micrographs of a eutectoid steel (a) pearlitic structure, (b:c) bainitic structure, (d) martensitic structure [27].

The change in transformation temperature reveals two different bainitic structures, upper bainite and lower bainite.

2.1.1 Upper Bainite

Upper bainite has a bulk structure that fills austenite grains whereas lower bainite has an acicular structure that separates austenite grains. It is obtained as a result of isothermal heat treatment between upper bainite (350°C-550°C) in eutectoid steels. Upper bainite consists of thin ferrite plates 0.2 μm thick and about 10 μm long. The plates are formed in clusters and this structure is known as bundle. In each bundle, the plates are parallel to each other, and each plate has its own crystal arrangement. The individual plates within the bundle are called the sub-units. The sub-units are usually separated by cementite particles or low irregular boundaries. Upper bainite occurs in two distinct stages. In the first step, bainitic ferrite is formed with very low carbon solubility (0.02wt%). After the ferrite is formed, the remaining austenite becomes enriched with carbon and eventually the cementite particles precipitate into ferrite subunits in the remaining austenite layers. [15,20].

2.1.2   Lower Bainite

The lower bainite is very similar to the upper bainite in terms of microstructure and crystallographic features. If the transformation temperature is quite low and close to the M_S temperature of the steel, all the carbon supersaturated in the bainitic ferrite plates will not be able to escape to the austenite and carbides will precipitate inside bainitic ferrite and in the carbon enriched austenite [28,29]. This microstructure is known as lower bainite. This bainite transformation may be seen clearly in Figure 2.3 [15]. In the lower bainite, carbide particles are precipitated in ferrite plates.
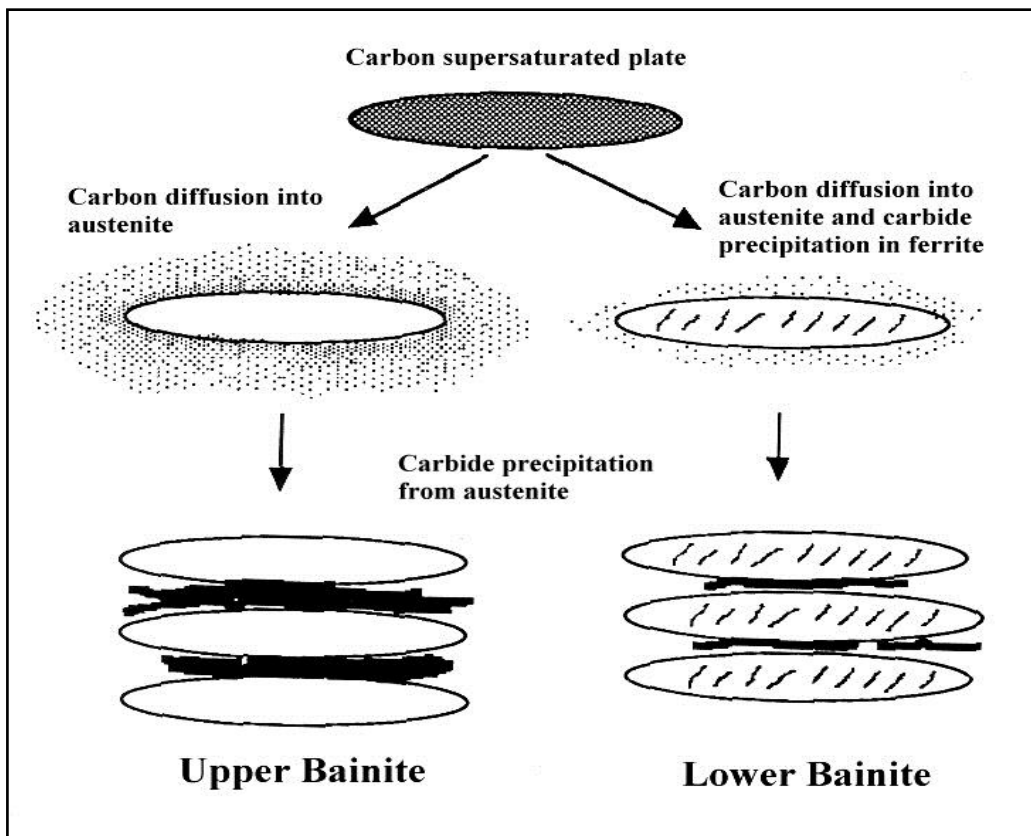
Figure 2.3. A schematic view of carbon diffusion during the bainite transformation [15].

Bhadeshia explained that only lower bainite is expected in steels with carbon concentrations exceeding 0.4 %. Figure 2.4 shows the calculated lower bainite

transformation start temperatures for plain carbon steels as a function of transformation temperature.
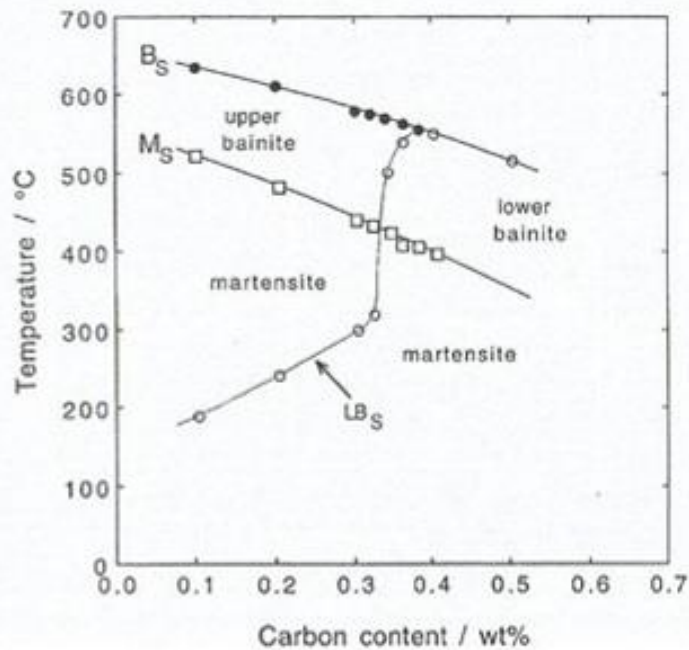
Figure 2.4. Calculated lower bainite transformation start temperatures for plain carbon steels as a function of transformation temperature [15].

In order to produce bainitic steel, it becomes critical that the pearlite and ferrite region on the CCT diagram should be pushed as far to the right as possible to allow for the bainitic formation (Figure 2.5). At this stage, the role of alloying elements is quite large.
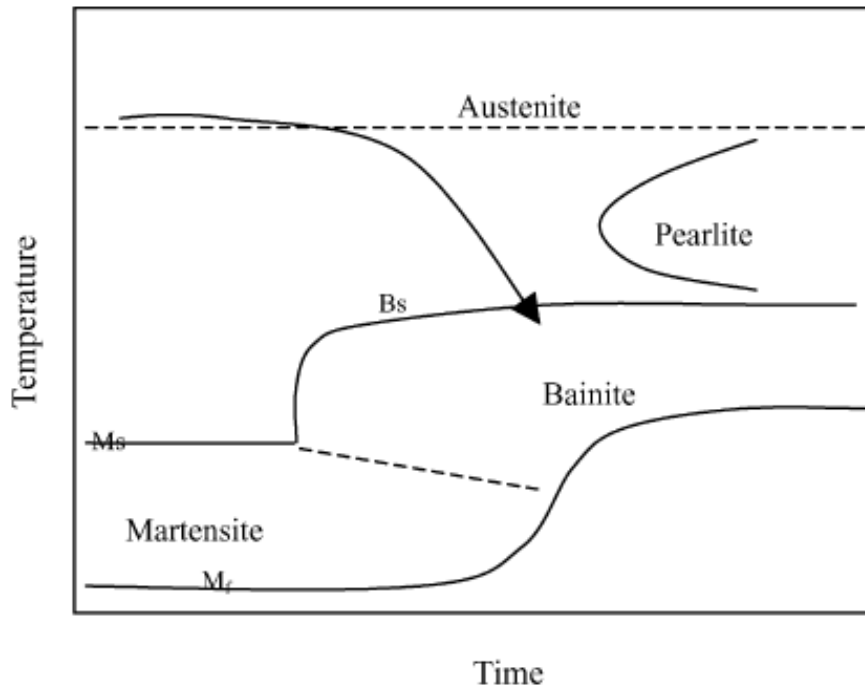
Figure 2.5. A schematic view of CCT diagram.

2.1.3   The Behavior of Alloying Elements

Bainitic transformation is of great importance in the heat treatment of steels. In alloy steels, pearlite and bainitic transformations are distinguished from each other. Alloying elements accelerate the formation of bainitic ferrite by separating the ferrite or ferrite-austenite interfaces.

It may be valuable here to mention about the growth mechanism of bainitic ferrite in lower bainitic transformation. Upon an isothermal transformation at low temperatures, the bainitic ferrite grows into austenite. After the growth, the supersaturated carbon in ferrite is partitioned with austenite due to a displacive mechanism [28,29]. At this stage carbide precipitation takes place both in ferrite and between austenite/ferrite boundaries. However, it has been shown that in steels containing high Si, the carbide precipitation in bainitic ferrite is retarded [30]. Silicon is very important alloying element in the alloy design. As a result, more carbon is

partitioned between ferrite and austenite causing super saturation of austenite. The austenite with excess carbon cannot transform to martensite upon cooling and retain as thin austenite films between ferrite layers. A certain amount of austenite may remain in the microstructure at room temperature (RT) when the bainite transformation is completed. This austenite is called retained austenite (RA) [31].

Carbon is highly soluble in austenite and is a strong austenite stabilizer, which slows down the reaction kinetics. High amount of Si and C, bainite plate thickness and amount of residual austenite are among the factors affecting the yield strength. When the amount of high carbon residual austenite increases, the ductility also increases. [32]. Silicon is very important alloying element in the carbide-free bainitic steels. It dissolves very slightly in cementite. It especially prevents the carbide precipitation, improves mechanical properties of the alloy. Some Cr and Mn addition in the alloy increases the hardness. [11-14,33]. High amount of Si (>1.5wt%) delays the cementite precipitation at high temperatures like 500°C and therefore, it stabilizes austenite.

Alloys designed by Yoozbashi et. al. are given in Table 2.1. They developed the new alloy by revising the Steel A and Steel B obtained in their previous research. The main purpose here is to reduce the amount of C (from 1 to 0.69 wt%) and Co (from 1.5 to 0.14 wt%) [19]. By reducing the amount of Co, both a cost-effective solution is created and good mechanical properties are obtained. When considering other studies, it was seen that Co and Al were added to give the ductility and strength and to accelerate bainitic transformation. [14,34]. This effect can also be achieved by reducing the austenite grain size. The resulting microstructure has finer grains, higher bainitic ferrite amount and higher hardness [14].

Table 2.1 The chemical compositions of the new nanostructured bainitic steel [19].

	C wt%	Si wt%	Mn wt%	Al wt%	Cr wt%	Co wt%
Steel A	1	1.5	1.9	-	1.25	-
Steel B	0.8	1.5	2	1	1	1.5
New Alloy	0.69	1.92	1.38	0.75	1.39	0.14

Molybdenum as an alloying element is so important in the alloy design. It delays the formation of ferrite and pearlite by splitting the bainite and pearlite noses in the C curve of the continuous cooling transformation diagram, (providing the bainite phase in wider cooling rate during continuous cooling) and so increases the formation of bainite (depressing the bainite transformation start temperature to lower level above the martensite transformation start temperature) [35].

Manganese is a preferred alloying element due to some properties in the bainitic steels. These are to decrease the bainite transformation temperature and improve mechanical properties. Huang et al. [36] investigated the effect of alloying elements for same carbon amount (Table 2.2). They use time–temperature–transformation (TTT) diagrams to analyze this effect. Calculations showed that it is still possible to accelerate the transformation kinetics. According to this research, reducing Mn has a much greater effect than increasing Co in terms of accelerating the bainite reaction which can bring significant cost reductions. They revealed that Mn reduction has an important effect on accelerating bainite formation at low temperatures [36].

Table 2.2 The chemical composition of the bainitic steel [36].

C wt%	Si wt%	Mn wt%	Al wt%	Cr wt%	Mo wt%	Balance
0.8	1.9	0.1	0.7	1.9	0.25	Fe

Soliman et.al. designed alloys including different amount of alloying elements (Table 2.3). In alloys X, Y and Z, Al and Co are added to accelerate the bainite

transformation and Mn is set to 0.9 wt%, 0.3 wt%, respectively [37,38]. Amel-Farzad H. et. al. designed an alloy not including Mn element [39]. Decreasing or removal of Mn has a twofold effect:

- The degree of bainitic transformation increases because the T_0 curve shifts to the right.

- The transformation rate increases because the thermal stability of the retained austenite lowers.

Table 2.3 The chemical compositions of bainitic steel [40].

Alloy	C wt%	Si wt%	Mn wt%	Al wt%	Cr wt%	Mo wt%	Co wt%	Balance
X	0.67	2.10	0.92	0.90	1.30	0.24	1.73	Fe
Y	0.55	2.10	0.37	0.90	1.47	0.46	1.8	Fe
Z	1.15	2.15	-	0.89	0.58	0.25	1.58	Fe

Alloy Z achieved a hardness value of 694 HV after treatment at 200ºC for about 10 days. In alloy X, acceleration of bainite formation was obtained by decreasing the carbon content. Bainite formation rate and its total amount increase by decreasing the carbon content.

Table 2.4 The chemical composition of bainitic steel [37-39].

C (%)	Si (%)	Mn (%)	Cr(%)	Mo (%)	V (%)	Fe (%)
0.98	1.46	1.89	1.26	0.26	0.09	Bal.

Caballero et. al designed a low temperature bainitic steel. Its chemical composition is in Table 2.4. They concluded that a significant amount of bainite can be obtained if the transformation temperature is kept low, i.e. 200 ºC and the transformation time kept at around two days. The transformation time required to obtain a completely

bainitic microstructure is approximately 6 days (Figure 2.6). Refining prior austenite grain size and alloying with Al and Co could reduce the transformation time from a week to a day. The idea is to increase nucleation sites and reduce the driving force for bainite transformation. Precipitation of cementite in the bainitic ferrite was observed after a transformation time of ten days at 200 ºC. This cementite phase was found to be extremely fine, approximately 20 nm wide and 175 nm long [40].
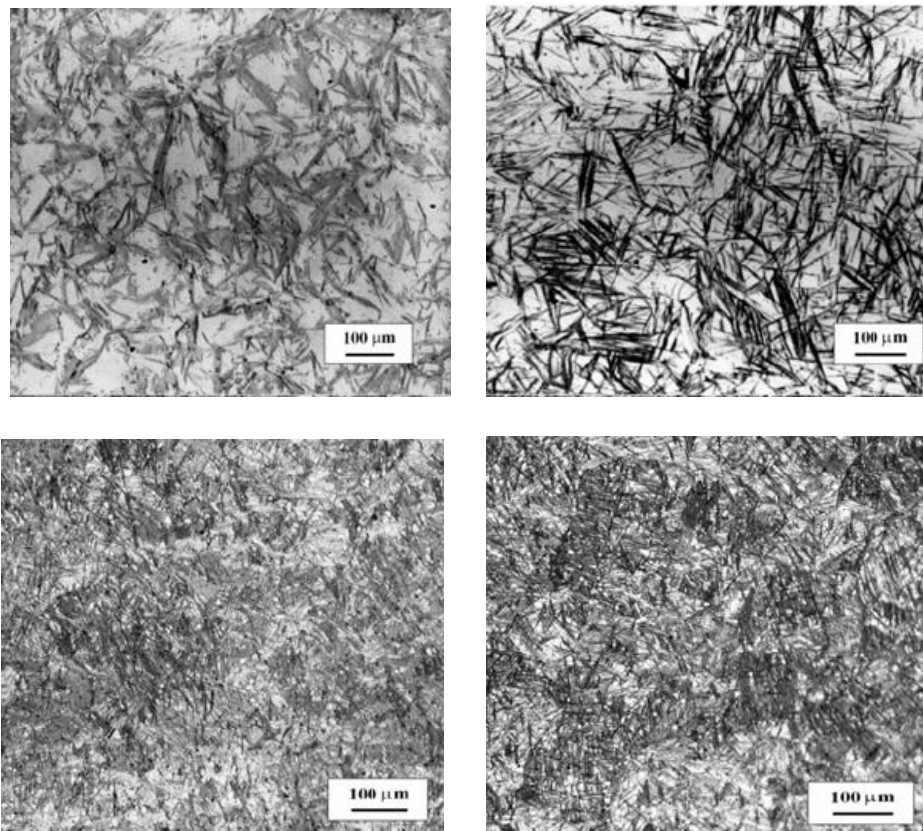
Figure 2.6. Optic micrographs of the bainitic steel at 200°C (a) for 1 day, (b) for 2 days, (a) for 4 days and (d) for 6 days [40].

The phases formed with the change in the transformation time and their hardness change (Figure 2.7). During the transformation at 200ºC, a significant decrease in hardness occurred because the bainite replaces some of the martensite, then the hardness increases with an increase in the fraction of fine-bainite which has a

14

hardness comparable to that of the mixture of martensite and austenite at zero transformation time.
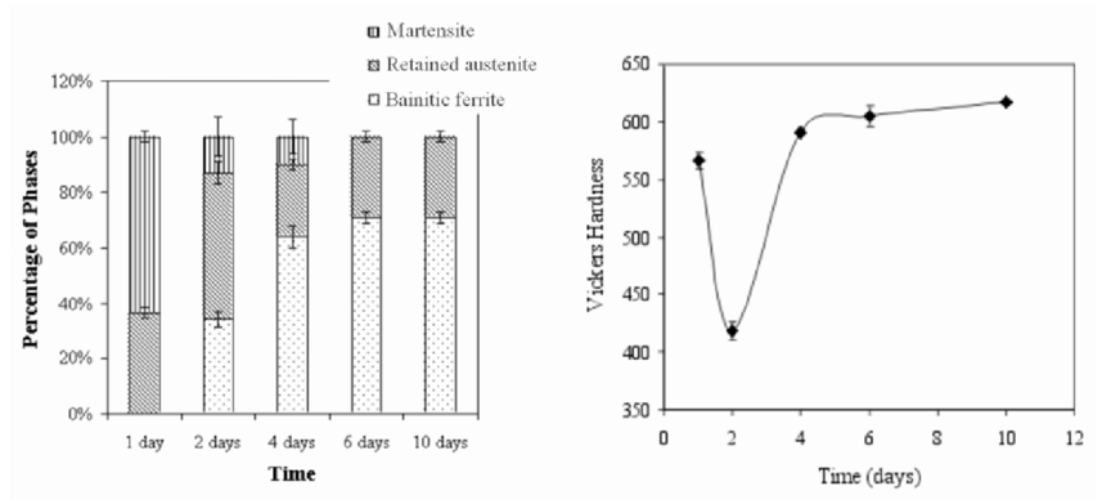
Figure 2.7. The changes of phases and hardness values in bainitic steel isothermal treated 200 ℃ for 1 to 10 days.

2.1.4 Carbide Precipitation

There are two types of precipitated carbide particles: those growing from carbon-rich austenite, which separates the bainitic ferrite layers, and precipitates from super saturated ferrite. Depending on the chemical composition and temperature, the carbides in ferrite sometimes form as cementite and sometimes as other transitional carbides. It is important which carbide precipitates first. Cementite particles are undesirable due to the damage initiation effect on the microstructure. One of the most effective ways to prevent the presence of cementite particles is to add silicon to the steel. Silicon retards cementite formation and carbides usually precipitate as epsilon carbide inside the bainitic ferrite [15, 20].

Normally tempering is not applied to the bainitic steels. However, it is known that Mo has several beneficial effects on alloy steels. It yields a secondary hardening peak at around 550℃ when sufficient amount is added as an alloying element. Even when

the amount of %Mo is low, the softening of martensite delays during tempering [20]. This effect is attributed to the fact that the relatively coarse cementite dispersion is replaced by a new and much finer alloy carbide precipitation. There are several studies on tempering behavior of bainite. However, as far as gathered from the literature, the effect of Mo on tempering of bainite is very limited [41,42].

In steels where there is high concentration of silicon, cementite is usually seen as carbide. But orthorhombic carbides, c-carbides and transient carbides are also carbides that can be seen in bainite and tempered bainite [15, 20].

2.2 TRIP STEELS

TRIP steels actually fall into the advanced high strength steel class. They are especially preferred in the automotive sector because they meet the two most important demands of weight reduction and safety [43]. In transformation- induced plasticity (TRIP) steels; the microstructure contains enough residual austenite to stress induced the phase (martensite or bainite) [44]. This causes an increase in strength and ductility. The effect of retained austenite is so important in TRIP steels. The mechanical properties of TRIP steels are controlled by the residual austenite in the microstructure [45]. TRIP steels are preferred in the automotive industry as they provide good mechanical properties [46].

In a mixed microstructure consisting of bainitic ferrite and austenite, the ductile films of austenite were deeply dispersed between the ferrite plates and they have a crack blunting effect. They cause the transformation of austenite to martensite under the influence of the tension field of a growing crack. Therefore, they further contribute to toughness. This effect is named as TRIP effect [20].

Nowadays, TRIP-aided bainitic steels with high silicon content consisting of carbide-free bainite matrix and retained austenite films have been studied. During the bainitic transformation, the presence of high %Si suppresses the carbide

16

precipitation within bainite sheaves and the surrounding austenite is stabilized due to the rejection of carbon from ferrite to austenite.

Depending on the carbon content, the TRIP steels can exhibit a wide range of properties. Bhadeshia and Caballero has developed a series of high carbon carbide free bainitic steels containing high C and high Si with an ultimate tensile strength in the range 2.0 GPa and a toughness of as high as 30MPa.m$^{1/2}$ [8-10].

2.3   T$_0$ CONCEPT

T$_0$ is a critical temperature to obtain the incomplete reaction of bainite during the bainite formation. The bainite formation has a subunit growth. In this growth, excess of carbon transforms to austenite and forms residual austenite. Cementite formation is observed between the ferrite plates. This process occurs until the value of carbon concentration of the residual austenite is equal to the carbon concentration of the free energy of bainite.

The variation of carbon concept of austenite (x$_y$) can be calculated with this equation (Eq.1.) [47].

$$x_y = \bar{x} + v_b \frac{(x-s)}{(1-v_b)}$$..Eq.1

where $\bar{x}$ is the average carbon content of the alloy.
     v_b is the volume fraction of bainitic ferrite.
     s is the amount of carbon in solid solution in the bainitic ferrite.

The points where the free energies of austenite and ferrite are exactly the same, which have the same chemical composition, is called the T$_0$ point. The curve formed by the changing temperature according to the changing amount of carbon describes the T$_0$ curve. If the amount of carbon is on the lower side of the curve, bainitic transformation does not occur. If the amount of carbon is on the upper side of the curve, bainitic transformation is possible [18].
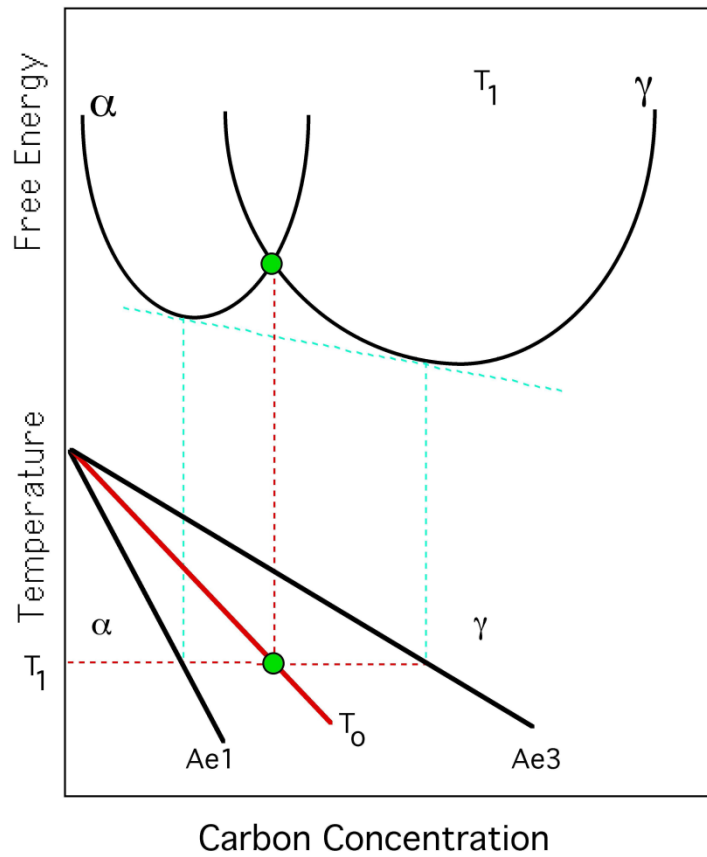
Figure 2.8. Definition of the T_0 curve [18].

The main aim of the T_0 concept is to increase the maximum amount of bainite that can be formed (Figure 2.8 and 2.9). The permitted fraction of bainite is determined by

i) lowering the carbon amount of the alloy,

ii) changing the amount of the substitutional alloying elements,

iii) decreasing transformation temperature.

$$V_{\alpha_b} = \frac{x_{T_0} - \overline{x}}{x_{T_0} - x_\alpha}$$
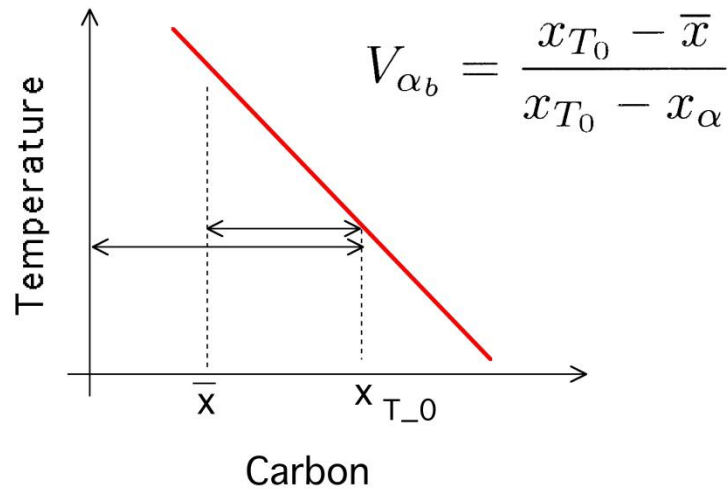
Figure 2.9. Lever rule applied to the T_0 curve to determine the allowable fraction of bainite.

The point where the free energies of austenite and ferrite are exactly the same, which have the same chemical composition, is called the T_0 point (Figure 2.10). However, if the stored energy of ferrite is also taken into account, then T_0 replaces with T_0' (400 J mol^{-1}). However, the stored energy term does not change the overall result, because the T_0 curve just shifts slightly and the relative positions are not affected [48].

If the carbon content of the residual austenite exceeds the T_0 curve on the phase diagram, the maximum amount of bainite that can be obtained at any temperature is limited [18].
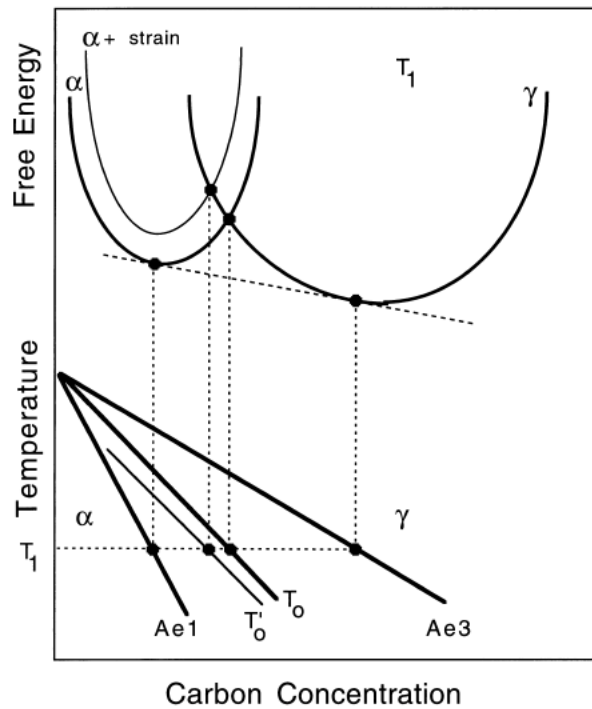
Figure 2.10. Definition of the T_0 and T_0' curve [18].

2.4 ALLOY DESIGN

The main purpose of alloy design is to provide the maximum amount of bainitic ferrite formation. Some limitations may be encountered in this process, such as the hardness of the steel preventing the formation of proeutectoid ferrite during cooling.

The desired microstructure consists of bainitic ferrite and austenite. In the alloy design, some points need attention. In high strength steels, cementite initiates the fracture. Bainitic ferrite contains almost no carbon. Since carbon shows a brittle effect on ferritic microstructures, bainitic ferritic microstructures provide an advantage in terms of strength. Fine grain size of ferrite plates is less than $1\mu m$ thick. Grain refinement is used to increase the hardness and toughness of the properties [20].

For a steel with a certain composition, the highest temperature at which bainite can be obtained is the bainite start temperature (B_S), and the highest temperature at which martensite can be obtained is the martensite start temperature (M_S).

Alloying elements play an important role in determining the martensite and bainite formation temperatures. The extent of this effect is explained by empirical formulas.

$B_S(°C) = 830 - 270(wt\%C) - 90(wt\%Mn) - 37(wt\%Ni) - 70(wt\%Cr) - 83(wt\%Mo)$ by Steven & Haynes [49].

$M_S(°C) = 539 - 423(wt\%C) - 30.4(wt\%Mn) - 17.7(wt\%Ni) - 12.1(wt\%Cr) - 7.5(wt\%Mo) + 10(wt\%Co) - 7.5(wt\%Si)$ by Andrews [50].

2.5   LOW TEMPERATURE BAINITE

Nano bainitic steels can have strength, ductility and even acceptable toughness values [51].

It is expected that the fine bainitic microstructure consists of nanoscale bainitic ferrite layers and thin retained austenite films. It may be obtained by transforming the bainite at low temperatures and to add an alloying element that would retard precipitation of carbide.

This fine bainitic microstructure was obtained in a high carbon high silicon steel by isothermal heat treatment at a low temperature of 200 ºC (Figure 2.11). Microstructure is formed by 20-40 nm thick plates of ferrite and films of carbon enriched austenite.
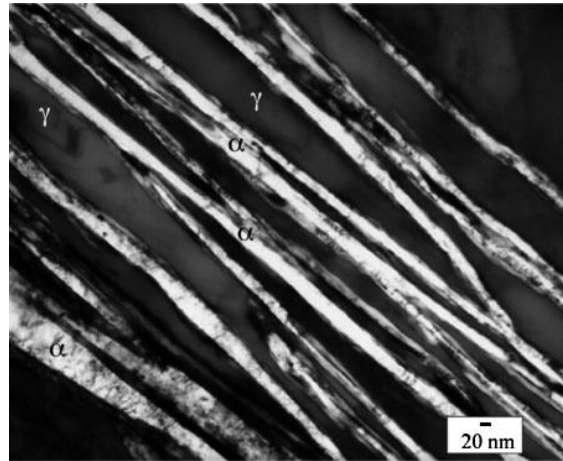
Figure 2.11. TEM micrograph of bainitic microstructure at 200 ºC [51].

Bhadeshia and his team worked on two silicon containing steels, Fe-0.2C-2Si-3Mn and Fe-0.4C-2Si-3Mn. The aim was to obtain the optimum alloy having carbidefree bainitic steels microstructure.

For this purpose, Caballero and his team designed different sets of alloys. In the first set designed bainitic steels, they used the steels as the reference on the above research of Bhadeshia.

In this set of designed bainitic steels, the amount of carbon is selected as 0.3 wt % [8]. The amount of carbon is important to obtain high strength (minimum 1100 MPa). 130MPa.m^{½} toughness and 1600-1700 MPa strength values are obtained with these two steels (Ni1 & Ni2) for bainitic microstructures [8]. The chemical compositions of these steels may be seen in Table 2.5.

Table 2.5 The chemical compositions of the first set of designed bainitic alloys [8].

Alloy	C (%)	Si (%)	Mn (%)	Ni (%)	Cr(%)	Mo (%)	V (%)
Mn	0.32	1.45	1.97	<0.02	1.26	0.26	0.10
Ni1	0.31	1.51	<0.01	3.52	1.44	0.25	0.1
Ni2	0.30	1.51	<0.01	3.53	1.42	0.25	<0.005

For the first set of designed bainitic alloys, as seen in Figure 2.12, Ni1 and Ni2 alloys have mainly bainitic ferrite and retained austenite. These alloys contain high amount of carbon. This carbon content cause to the formation of residual austenite after bainite transformation. Quantitative datas for Mn, Ni1, and Ni2 is shown in Table 2.6. Bainitic ferrite in Ni1 and Ni2 alloys has high volume fraction. This may cause that retained austenite forms as films between the subunits and bainitic ferrite.
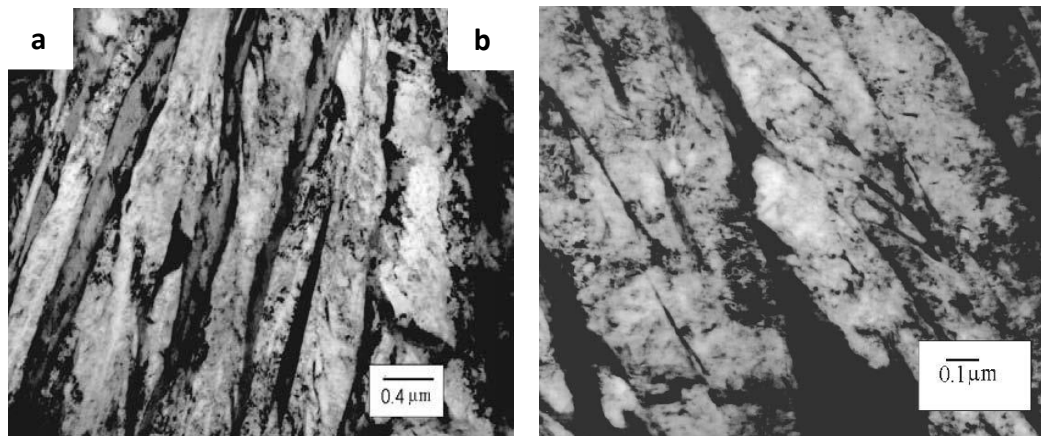
Figure 2.12. Transmission electron micrographs of bainitic ferrite and retained austenite films (a) Ni1 alloy; (b) Ni2 alloy [8].

Table 2.6 Quantitative data of Mn, Ni1, and Ni2 alloys.

Alloy	Bainitic Ferrite (vf)	Martensite (vf)	RetainedAustenite (vf)
Mn	0.26	0.67	0.7
Ni1	0.62	0.26	0.12
Ni2	0.81	0.11	0.08

Caballero et. al. designed new set of designed bainitic steels. In these steels, alloys are rearranged because nickel addition is not so feasible due to economic reasons. Instead, alloys with manganese addition are designed. The similar chemical composition of Ni2 steel is used to obtain the bainitic microstructure because Ni2 steel has the best results in the first set of designed bainitic steels. Two step cooling is preferred to obtain the fully bainitic microstructure by considering the kinetic model. The chemical compositions of these steels may be seen in Table 2.7.

Table 2.7 The chemical compositions of the new set of designed bainitic alloys (wt%) [14].

Alloy	C	Si	Mn	Ni	Cr	Mo	V
0.3BAIN 1	0.29	1.50	2.25	--	--	0.26	--
0.3BAIN 2	0.29	1.46	1.97	--	0.46	0.25	--
0.3BAIN 3	0.29	1.49	1.56	--	1.47	0.25	--
0.3BAIN 4	0.27	1.71	1.53	1.47	0.17	0.24	--

The combination of the cooling process and low carbon content increases the amount of bainitic ferrite and decreases the amount of retained austenite and martensite (Table 2.8). These microstructures may be seen clearly in Figure 2.13.

Table 2.8 Quantitative data of new designed alloys.

Alloy	Bainitic Ferrite (vf)	Martensite (vf)	Retained Austenite (vf)
0.3BAIN 1	0.76	0.21	0.03
0.3BAIN 2	0.77	0.13	0.10
0.3BAIN 3	0.88	0.2	0.10
0.3BAIN 4	0.88	0.09	0.03
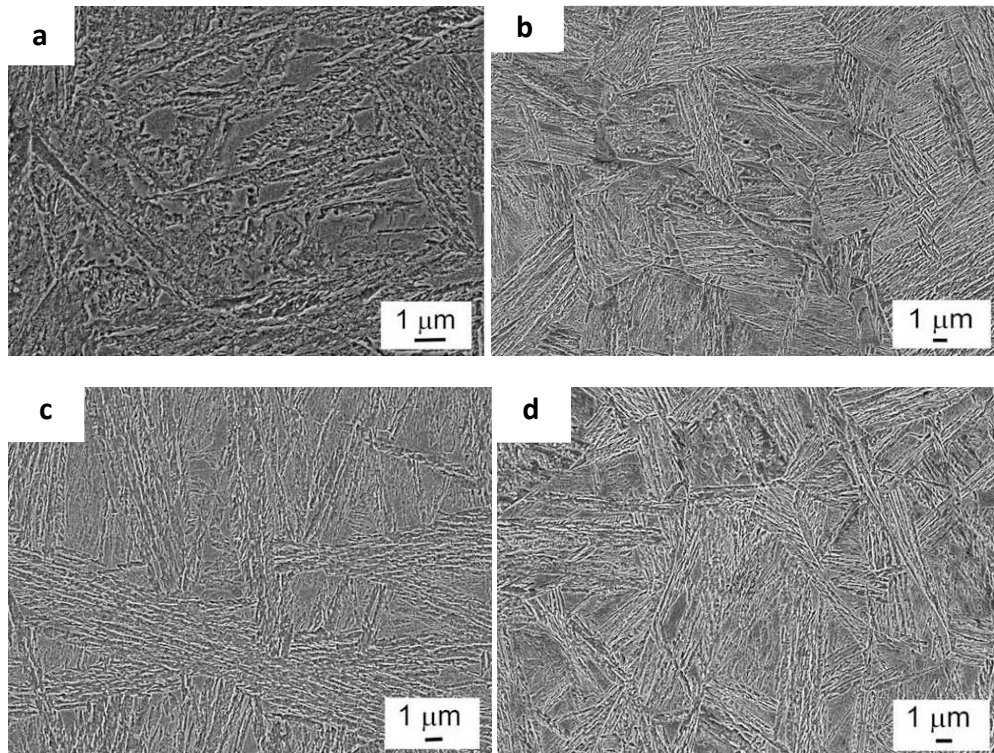
Figure 2.13. SEM micrographs from 0.3BAIN1 to 0.3BAIN4 air cooled (a) 600°C, (b:d) 500°C, respectively.

These new alloys have similar curves and B_S and M_S temperatures, but different diffusional noses. The calculated TTT diagrams (Figure 2.14) determined to obtain the desired fully bainitic microstructure with two-step cooling.
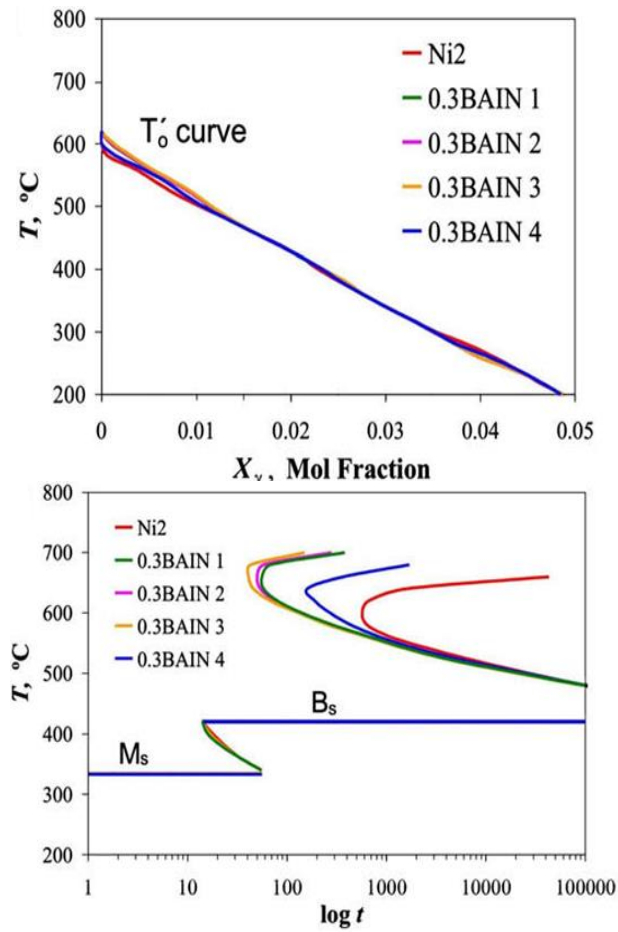
Figure 2.14. a) T_0' curve and b) TTT diagram of the designed steels [52].

Microstructural characterization revealed that from the 0.3BAIN1 to 0.3BAIN4 alloys have the desired microstructure consisting of carbide-free upper bainite. The best results were obtained after air cooling from every temperature tested for 0.3 BAIN 4. High volume fraction bainitic ferrite and fine grained microstructures were obtained. These properties increased the mechanical performance of these materials.

2.6   MOTIVATION OF THE THESIS STUDY

As mentioned in Tenaglia's study [53], rolled/forged homogenized steels are used in most studies. However, this thesis study focus on cast and homogenized steels while

observing the effect of alloying elements. In this study, the effect of isothermal treatment temperature and time on the microstructure and mechanical properties is observed. The stability of the microstructures and mechanical response of the alloys as a result of long-term heat treatments applied to a particular alloy (0.6%C-1.0%Mn-1.2%Si and 0.6%C-1.0%Mn-1.2%Si-2%Mo) was discussed.

In the literature, the effect of Mo on tempering behavior of bainitic steels are not studied extensively. In this context, this thesis study will be interest to the effect of Mo on tempering behavior of a carbide free bainitic steel which contains 1.2%Si. It would be interesting to study the effect of 2%Mo on bainitic transformation kinetics and bainite morphology in a high Si and medium carbon (0.6%C) steel. To examine the secondary hardening effect of Mo in a bainitic microstructure would also contribute to the behavior of Mo in tempered bainitic steels. The bainitic transformation behavior and resulting microstructures are compared in a 0.6%C-1.2%Si-1.0%Mn steel with and without 2%Mo addition.

CHAPTER 3

EXPERIMENTAL

3.1 Alloys

The first steel is commercial 60SiMn5. This alloy has been supplied by Asil Çelik A.Ş. This alloy will be referred as C-Mn-Si alloy during this thesis study. The second steel is laboratory-cast 60SiMn5 steel with 2wt%Mo addition. This steel is prepared as follows. The melt is prepared using an induction furnace under an air atmosphere. After the steel containing 0.6% C is completely melted, Si is added to increase silicon level and to decrease oxygen in solution. When the steel is deoxidized sufficiently the other alloying elements Mn and Mo are added to complete the alloying stage before melt delivery. After alloying, the mold is preheated to fill the mold cavity completely and to prevent premature freezing during casting. Finally, the steel alloy is poured into permanent molds preheated to 180°C -200°C and cast as a plate with dimensions 220x215x17 mm^3. Homogenization is done at 1150°C for 24 hours. This alloy will be referred as C-Mn-Si-Mo alloy during this thesis study. The chemical compositions of the alloys used in this study is given in Table 3.1.

Table 3.1 Chemical compositions of the C-Mn-Si and C-Mn-Si-Mo alloys (wt. %).

Alloy	C	Si	Mn	Mo	Cr	Ni	Al
C-Mn-Si	0.6	1.2	1.0	0.03	0.19	0.07	0.02
C-Mn-Si-Mo	0.59	1.17	0.89	2.02	0.20	0.08	0.02

3.2 Experimental Method

The M_S temperatures and isothermal bainite transformation kinetics curve (TTT) was calculated using the JMat Pro. The calculated M_S temperatures are checked using the Andrew's equation [50] for M_S:

$M_S(°C) = 539-423(wt\%C)-30.4(wt\%Mn)-17.7(wt\%Ni)-12.1(wt\%Cr)-7.5(wt\%Mo) +10(wt\%Co)-7.5(wt\%Si)$

The calculated value of 242.03°C for C-Mn-Si alloy and 231.55°C for C-Mn-Si-Mo alloy according to Andrew's diagram. The calculated Ms temperatures for C-Mn-Si and for C-Mn-Si-Mo alloys using JMat Pro are presented as 254°C and 233°C, respectively. Considering the Andrew's equation and TTT diagram results, the isothermal transformation temperatures are selected as 250°C and 300°C for C-Mn-Si alloy, whereas they are 230°C and 280°C for C-Mn-Si-Mo alloy.

3.2.1 Heat Treatment Studies

Before the isothermal treatment studies, homogenization was applied to the C-Mn-Si-Mo steel at 1150ºC. For both steel grades, the first set of specimens were austenitized at 950ºC for 45 min and quenched into salt bath for isothermal treatment between 200ºC-300ºC for different time intervals. The second set of specimens were quenched in oil from 950ºC and then tempered in the temperature range of 200ºC-550ºC for 90 min. As the third set of specimens, several bainitic specimens are also tempered in the temperature range of 200ºC-550ºC for 90 min for comparison purposes. Heat treatment sets are summarized and given a label for simplicity. For example, for the specimens labelled as IT-200-1 and Mo-Q-T-500:

IT-200-1

Transformation time (h, min)

Treatment temperature (°C)

Isothermal treatment

Mo-Q-T-500

Tempering temperature (°C)

Tempering

Quenching

C-Mn-Si-Mo alloy
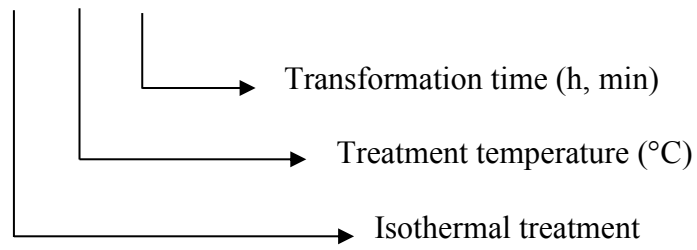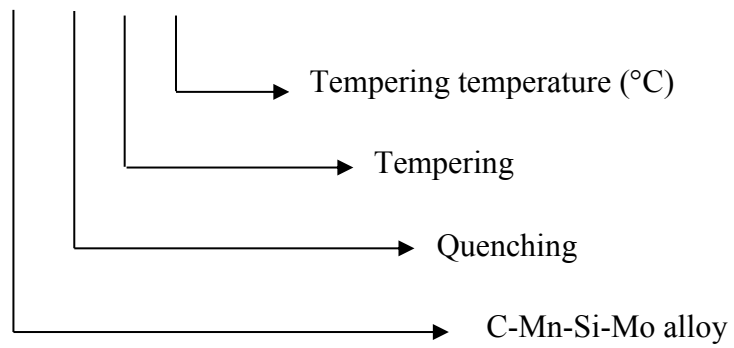
The detailed information obtained in Table 3.2, Table 3.3 and Table 3.4.

Table 3.2 First Set of Specimens.

Steel Type	Isothermal Treatment Temperature (ºC)					Transformation Time (h)							Label ID
C-Mn-Si C-Mn-Si-Mo	**200**	230	250	280	300	1/4	**1**	3	6	12	24	48	IT-200-1
C-Mn-Si C-Mn-Si-Mo	**200**	230	250	280	300	1/4	1	3	**6**	12	24	48	IT-200-6
C-Mn-Si C-Mn-Si-Mo	**200**	230	250	280	300	1/4	1	3	6	**12**	24	48	IT-200-12
C-Mn-Si C-Mn-Si-Mo	**200**	230	250	280	300	1/4	1	3	6	12	**24**	48	IT-200-24
C-Mn-Si C-Mn-Si-Mo	200	**230**	**250**	280	300	1/4	**1**	3	6	12	24	48	IT-250-1
C-Mn-Si C-Mn-Si-Mo	200	**230**	**250**	280	300	1/4	1	3	6	**12**	24	48	IT-250-12
C-Mn-Si C-Mn-Si-Mo	200	**230**	**250**	280	**300**	**1/4**	1	3	6	**12**	24	48	IT-300-1/4
C-Mn-Si C-Mn-Si-Mo	200	**230**	**250**	280	**300**	1/4	**1**	3	6	**12**	24	48	IT-300-1
C-Mn-Si C-Mn-Si-Mo	200	**230**	**250**	280	**300**	1/4	1	**3**	6	**12**	24	48	IT-300-3
C-Mn-Si **C-Mn-Si-Mo**	200	**230**	250	280	300	1/4	**1**	3	6	12	24	48	Mo-IT-230-1
C-Mn-Si **C-Mn-Si-Mo**	200	**230**	250	280	300	1/4	1	3	6	**12**	24	48	Mo-IT-230-12
C-Mn-Si **C-Mn-Si-Mo**	200	**230**	250	280	300	1/4	1	3	6	12	**24**	48	Mo-IT-230-24
C-Mn-Si **C-Mn-Si-Mo**	200	**230**	250	280	300	1/4	1	3	6	12	24	**48**	Mo-IT-230-48
C-Mn-Si **C-Mn-Si-Mo**	200	230	250	**280**	300	1/4	**1**	3	6	12	24	48	Mo-IT-230-1
C-Mn-Si **C-Mn-Si-Mo**	200	**230**	250	280	300	1/4	1	3	6	**12**	24	48	Mo-IT-230-12

Table 3.3 Second Set of Specimens.

Steel Type	Quenching	Tempering Temperature (ºC)				Label ID
C-Mn-Si C-Mn-Si-Mo	**yes**	**200**	400	500	550	Q-T-200
C-Mn-Si C-Mn-Si-Mo	**yes**	200	**400**	500	550	Q-T-400
C-Mn-Si C-Mn-Si-Mo	**yes**	200	400	**500**	550	Q-T-500
C-Mn-Si C-Mn-Si-Mo	**yes**	200	400	500	**550**	Q-T-550
C-Mn-Si **C-Mn-Si-Mo**	**yes**	**200**	400	500	550	Mo-Q-T-200
C-Mn-Si **C-Mn-Si-Mo**	**yes**	200	**400**	500	550	Mo-Q-T-400
C-Mn-Si **C-Mn-Si-Mo**	**yes**	200	400	**500**	550	Mo-Q-T-500
C-Mn-Si **C-Mn-Si-Mo**	**yes**	200	400	500	**550**	Mo-Q-T-550

Table 3.4 Third Set of Specimens.

Steel Type	Isothermal treatment temperature (°C)		Tempering temperature (°C)				Label ID
C-Mn-Si C-Mn-Si-Mo	230	**250**	**200**	400	500	550	IT-250-12-FC-T-200
C-Mn-Si C-Mn-Si-Mo	230	**250**	200	**400**	500	550	IT-250-12-FC-T-400
C-Mn-Si C-Mn-Si-Mo	230	**250**	200	400	**500**	550	IT-250-12-FC-T-500
C-Mn-Si C-Mn-Si-Mo	230	**250**	200	400	500	**550**	IT-250-12-FC-T-550
C-Mn-Si **C-Mn-Si-Mo**	**230**	250	**200**	400	500	550	Mo-IT-230-48-FC-T-200
C-Mn-Si **C-Mn-Si-Mo**	**230**	250	200	**400**	500	550	Mo-IT-230-48-FC-T-400
C-Mn-Si **C-Mn-Si-Mo**	**230**	250	200	400	**500**	550	Mo-IT-230-48-FC-T-500
C-Mn-Si **C-Mn-Si-Mo**	**230**	250	200	400	500	**550**	Mo-IT-230-48-FC-T-550

Isothermal transformation was conducted in a salt bath with a sufficient thermal capacity to avoid appreciable temperature fluctuations during operation. Dry Heat Sterilizer/Oven is used for long isothermal heat treatments and tempering. Its maximum working temperature is 250 °C. The photographs of these furnaces can be seen in Figure 3.1.

(a)

(b)

(c)

Figure 3.1. The photographs of (a) Muffle furnace, (b) Salt bath, (c) Dry heat oven.

3.3 Characterization Methods

3.3.1 Optical Microscopy Studies

Optical microscopy studies are conducted to examine the microstructures, phases present and phase morphologies. Huvitz Digital Microscope HDS-5800, Korea is used as an optical microscope. Firstly, each sample is cut from the middle part into two equal parts along the horizontal direction with Buehler Isomet 5000 Linear Precision Saw, USA. These samples are mounted during the metallographic preparation. The metallographic preparation includes grinding (Metkon Gripo 2V Grinder, Turkey), polishing (Mecapol P230 Polisher, France for 6μm and 1μm), and etching (2% Nital).

3.3.2 Scanning Electron Microscopy Studies

SEM studies are conducted to investigate the phases present and phase morphologies. SEM (Nova Nano SEM 430, FEI LTD, Oregon, USA) equipped with an EDX analyzer system is used for examination. Firstly, each sample is cut from the middle part into two equal parts along the horizontal direction with Buehler Isomet 5000 Linear Precision Saw, USA. These samples are mounted during the metallographic preparation. The metallographic preparation includes grinding (Metkon Gripo 2V Grinder, Turkey), polishing (Mecapol P230 Polisher, France for 6μm and 1μm), and etching (2% Nital).

3.3.3 Carbide Extraction

Carbide extraction from the specimens is performed in an electrolytic cell which is connected to a direct current source and containing stainless steel sheets as the cathode. Extraction is carried out at a current density of $0.01A/cm^2$ in an electrolyte

of 10%HCl-Methanol. The weight percentages are determined by weighing the filter paper before and after the filtration. In the oven, the filter papers are dried for 2 h at 70ºC.

3.3.4 Mechanical Characterization

3.3.4.1 Tensile Tests

Tensile test specimens are prepared according to ASTM E8/E8M − 16a standard. INSTRON 5582 Universal Testing Machine is used for tension tests. For each heat treatment, 2 specimens are tested.

3.3.4.2 Macro Hardness Tests

Macro hardness measurements are conducted to determine the hardness of the specimens. These measurements are taken on the Vickers scale using the EMCO test machine (M4U-025) and under 30 kg load. The hardness values are taken as the average of 8 indentations for each specimen.

3.3.5 Retained Austenite Determination

Quantitative X-ray diffraction analysis is employed by comparing the integrated X-ray diffraction intensity of ferrite and austenite phases to determine the volume percent of retained austenite. X-ray diffraction (XRD) specimens are sectioned to ensure the removal of the decarburized layer. Then, after grinding and final polishing using 1μm diamond paste, the samples are simply etched and then repolished to minimize the effect of plastic deformation on the surface which may otherwise affect the amount of austenite. XRD analysis is carried out using a Bruker-D8 Advance diffractometer with monochromated Cu-Kα radiation (wavelength of 0.154183 nm) operating at 40 kV and 40 mA. Scanning is performed in the 2Ө range of 20–120∘ at

a scanning rate of $1^{\circ}\,\mathrm{min}^{-1}$. The volume fraction of the retained austenite is calculated from the integrated intensities of (111), (200), (220) austenite peaks, and the (110), (200), (211) ferrite peaks.

CHAPTER 4

RESULTS AND DISCUSSION

In this study, C-Mn-Si and C-Mn-Si-Mo alloys were used. Carbon amount is important in the alloy design. If the percentage of carbon is high, M_S temperature decreases, the transformation shifts to very long periods, the amount of retained austenite increases. If the percentage of carbon is low, M_S temperature will be too high. A high M_S temperature would yield thicker bainite sheaves which would lower the strength. The carbon content is kept at around 0.6%C to obtain a fine bainitic structure [9,54] and to suppresses the bainite start temperature. Si addition is an important parameter in these steels because increased amounts of Si prevent the cementite precipitation [18,36,55]. High Si retards the bainitic transformation rate. Mn content is limited to 1.0% for several purposes: Mn suppresses the M_S temperature which is necessary to obtain a fine structured strong bainite. On the other hand, above 1%Mn, the bainitic reactions become very sluggish [10-12,36]. Molybdenum could shift the pearlite transformation line of CCT to its right and restrain the formation of ferrite, but not retard bainite transformation. It also raises the temperature of the maximum rate of pearlite transformation, and reduces the temperature of the maximum rate of bainite. This would result in the separation of the pearlite line and the bainite transformation line, and consequently make the bainite transformation easier under the same cooling condition.
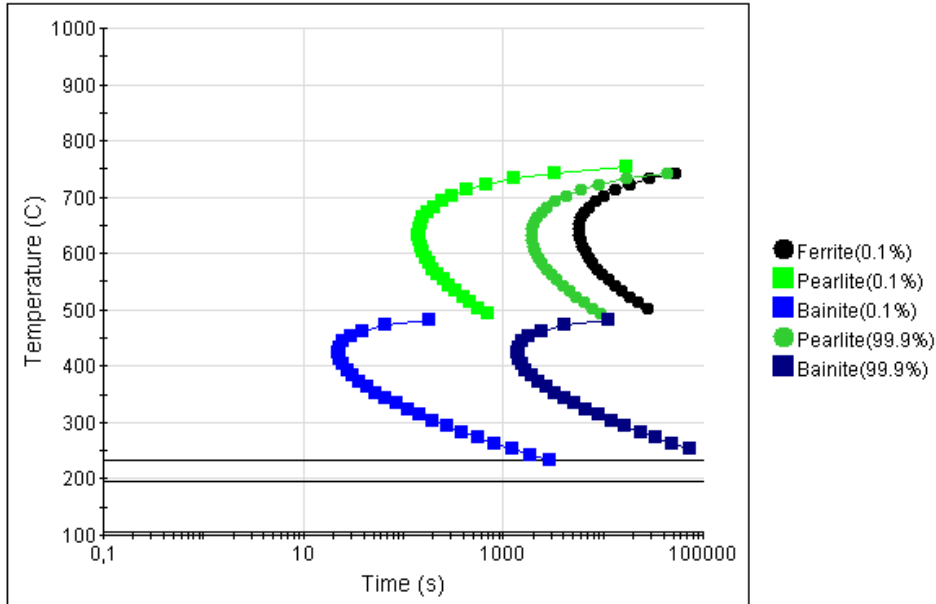
To analyze the C-Mn-Si and C-Mn-Si-Mo alloy composition before the experiment, TTT diagrams were calculated via JMat Pro. Figure 4.1 shows the TTT plots for the two alloys using JMat Pro software. The calculated time intervals for bainitic transformation at different temperatures are given in Table 4.1.
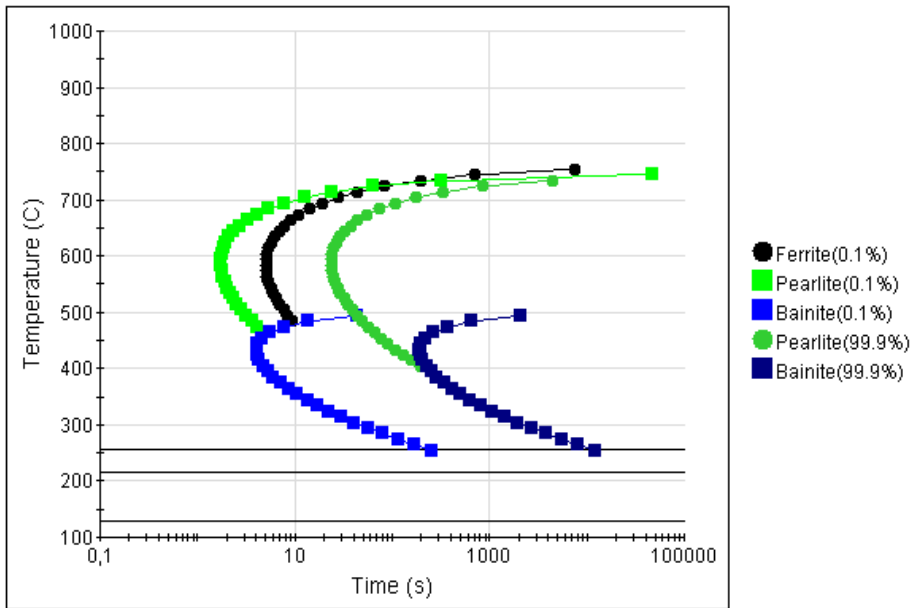
Figure 4.1. TTT diagrams of C-Mn-Si and C-Mn-Si-Mo alloys, respectively.

Table 4.1. The calculated bainite transformation times extrapolated from the calculated TTT diagram for C-Mn-Si and C-Mn-Si-Mo alloys.

C-Mn-Si	Bainite					
Ms=250°C	200°C		250°C		300°C	
	1%B	100%B	1%B	100%B		
	15 min	830 min (14 h)	5 min	215 min (4 h)	1 min	50 min
C-Mn-Si-Mo	Bainite					
Ms=230°C	230°C		280°C			
	1%B	100%B	1%B	100%B		
	50 min	2500 min (42 h)	6 min	400 min (7 h)		

4.1   Microstructural Examination

4.1.1   Isothermal Treatment Studies of C-Mn-Si alloy

Four set specimens were prepared for C-Mn-Si alloy (Table 4.1):
a) As-Quenched Specimens
b) Isothermally Treated Specimens at 200°C
c) Isothermally Treated Specimens at 250°C
d) Isothermally Treated Specimens at 300°C

Initially, the austenitization temperature was selected 900°C. In Figure 4.2, the scanning electron micrographs are given which belong to isothermal treated specimens at 250°C for 24 hours. The microstructure of 900-IT-250-24 consists of a mixture of bainite, some amount of martensite and widmanstatten ferrite regions.
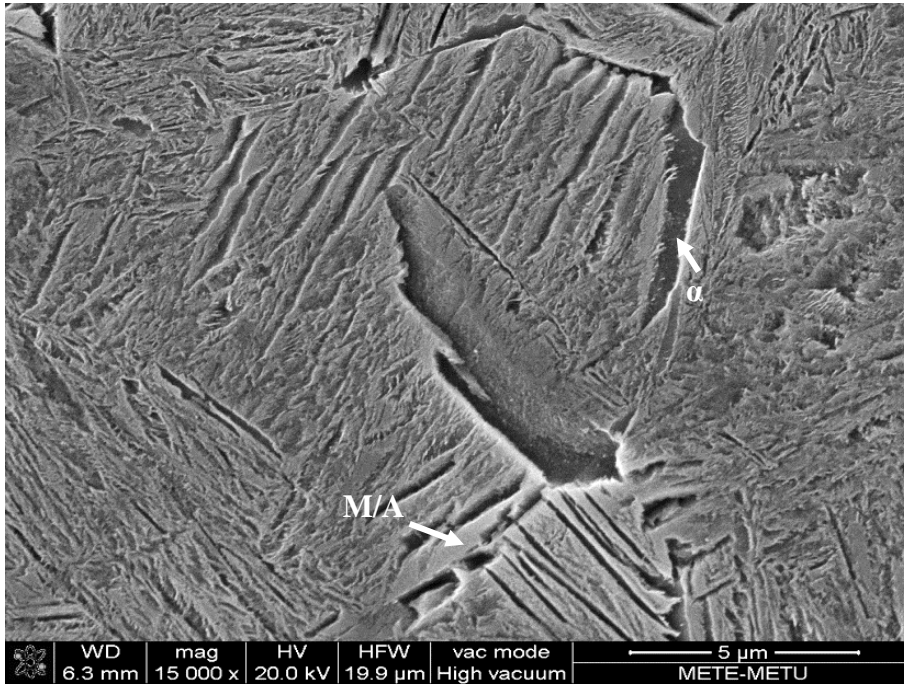
Figure 4.2. SEM micrograph of 900-IT-200-12.

Carbon must diffuse during the nucleation of both widmanstatten ferrite and bainite. Nucleation probably occurs by a process akin to the dissociation of arrays of dislocations. This follows from the observation that the activation energy for nucleation is directly proportional to the driving force, rather than the inverse square relationship implied by a heterophase fluctuation model of nucleation. Both Widmanstatten ferrite and bainite develop from the same nucleus; it develops into bainite if the growth is possible at the temperature where nucleation becomes possible. Otherwise it evolves into widmanstatten ferrite. It is seen from the TTT plots that ferrite shifts quite to the right. One of the most important reasons of this is the effect of Si.

Due to the presence of the widmanstatten ferrite, austenitization temperature was increased from 900°C to 950°C and four set specimens were prepared:

a) As-Quenched Specimens

b) Isothermally Treated Specimens at 200°C

c) Isothermally Treated Specimens at 250°C

d) Isothermally Treated Specimens at 300°C

Heat treatment flow of C-Mn-Si alloy can be seen in Figure 4.3.
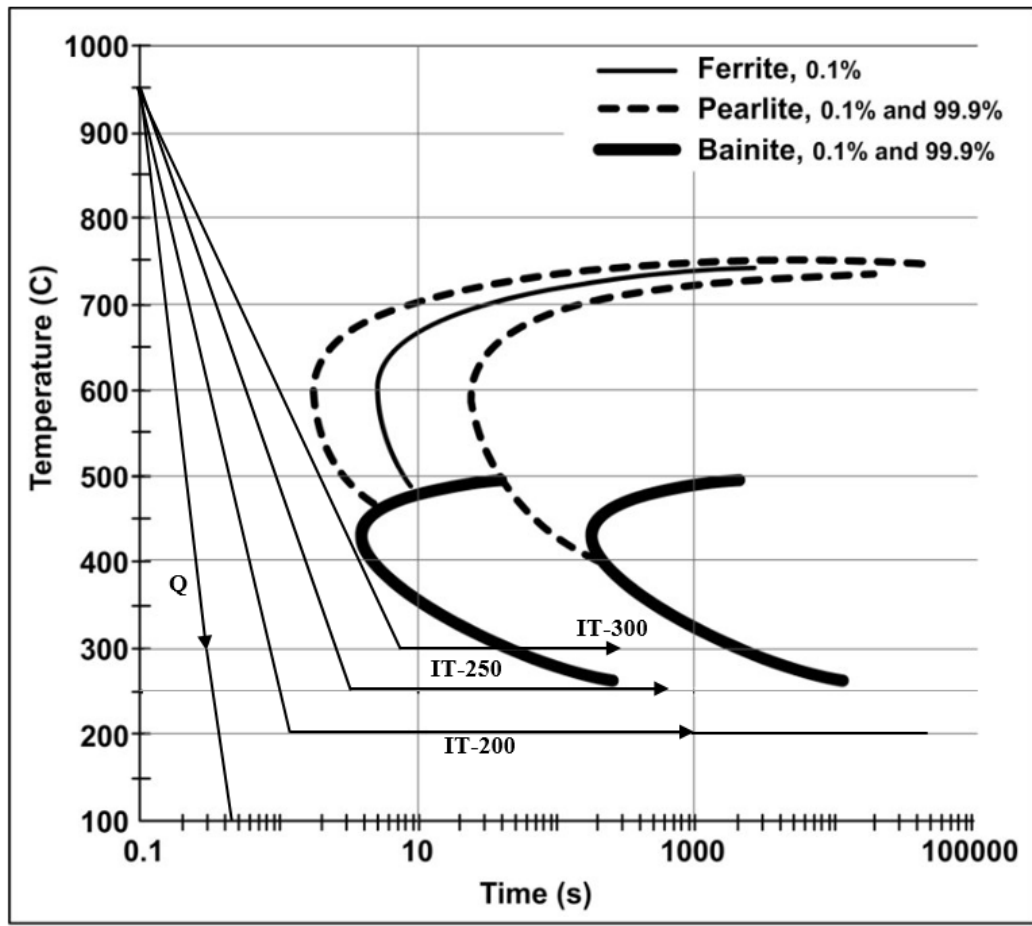
Figure 4.3. Heat treatment flow of C-Mn-Si alloy.

As-Quenched Specimens

Figure 4.4 shows the SEM micrograph of Q. The microstructure is fully martensitic.
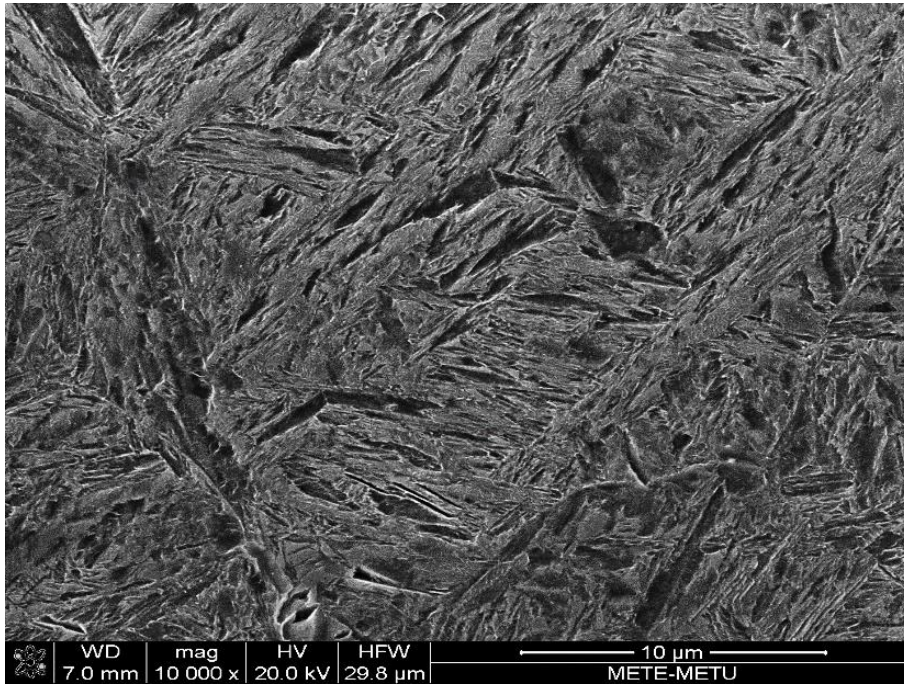
Figure 4.4. SEM micrograph of Q.

Isothermal treated specimens (200°C)

1hour isothermal treatment at 200°C (IT-200-1) produces little amount of bainite (Figure 4.5). As the time is extended, bainite begins to appear in the following samples (Figure 4.6). After 14 hours, the structure is completely bainitic (Figure 4.7).
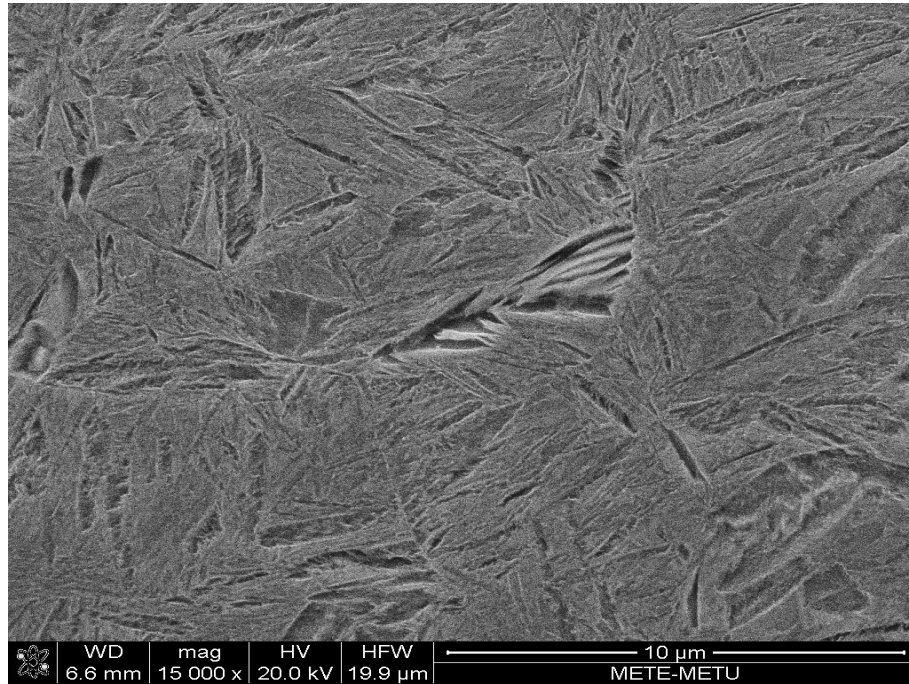
Figure 4.5. SEM micrograph of IT-200-1h.

Figure 4.6(b) shows that the microstructure is mostly bainitic tough some amout of martensite may be present. Calculated TTT diagram supports this phenomena.
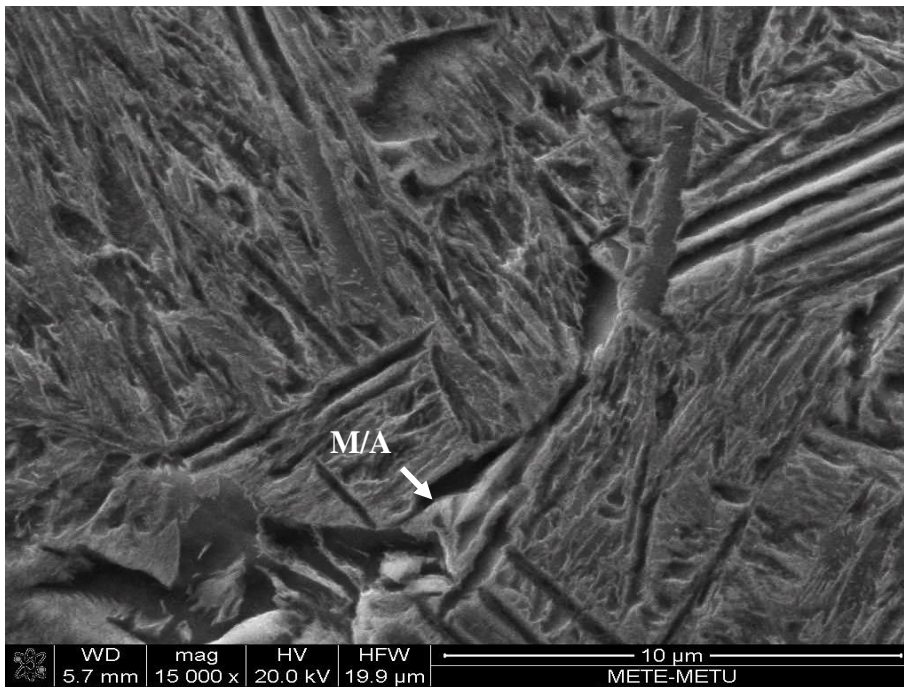
(a)
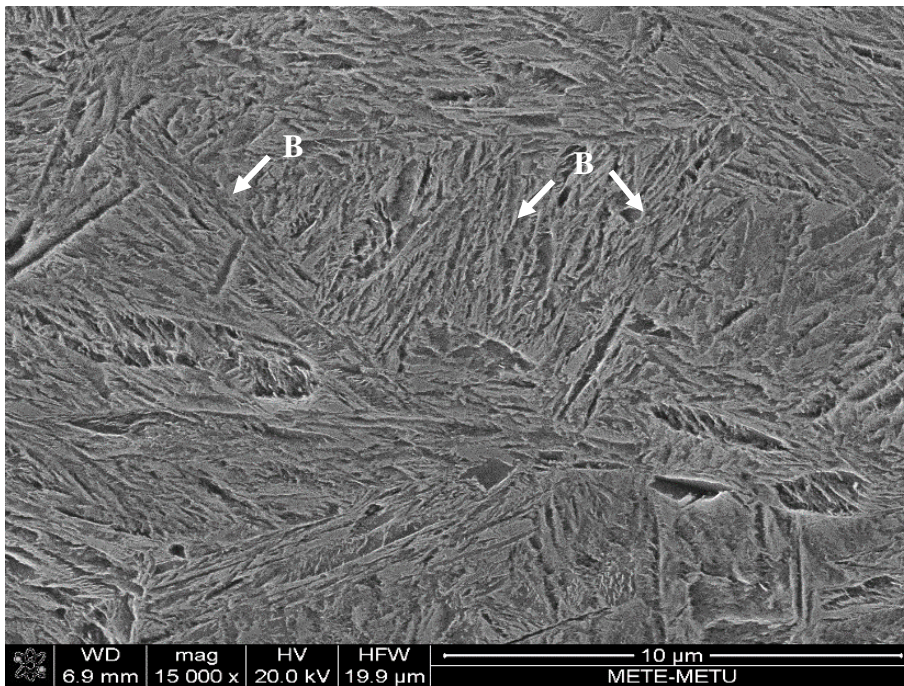
(b)

Figure 4.6. SEM micrographs of (a) IT200-6 and (b) IT200-12.
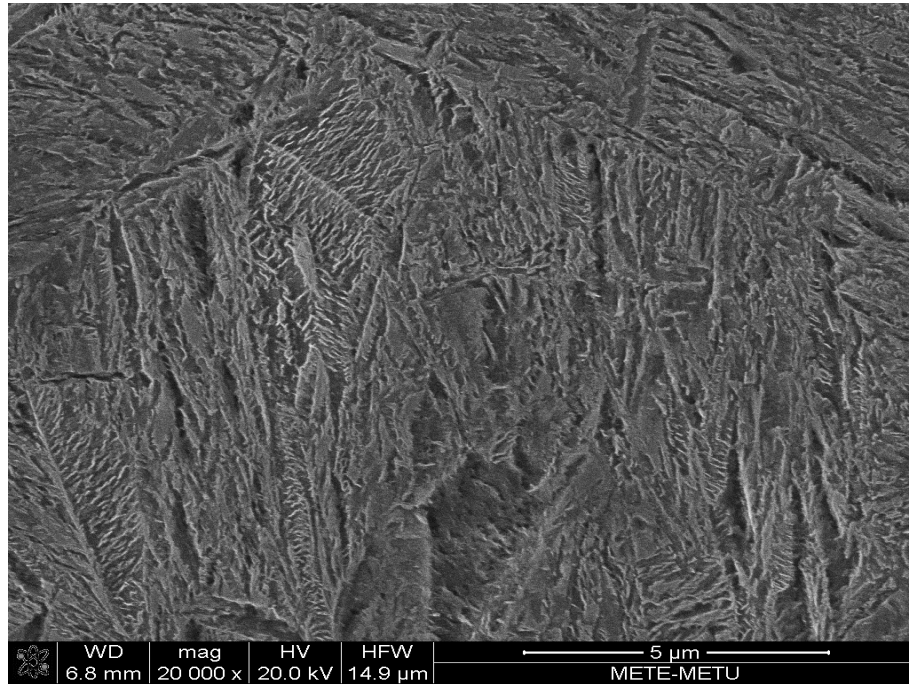
Figure 4.7. SEM micrograph of IT200-24.

Isothermal treated specimens (250°C)

The microstructure of IT250-1 consists of a mixture of bainite and M/A regions. (Figure 4.8). After 4 hours, the microstructure is completely bainitic (Figure 4.9).
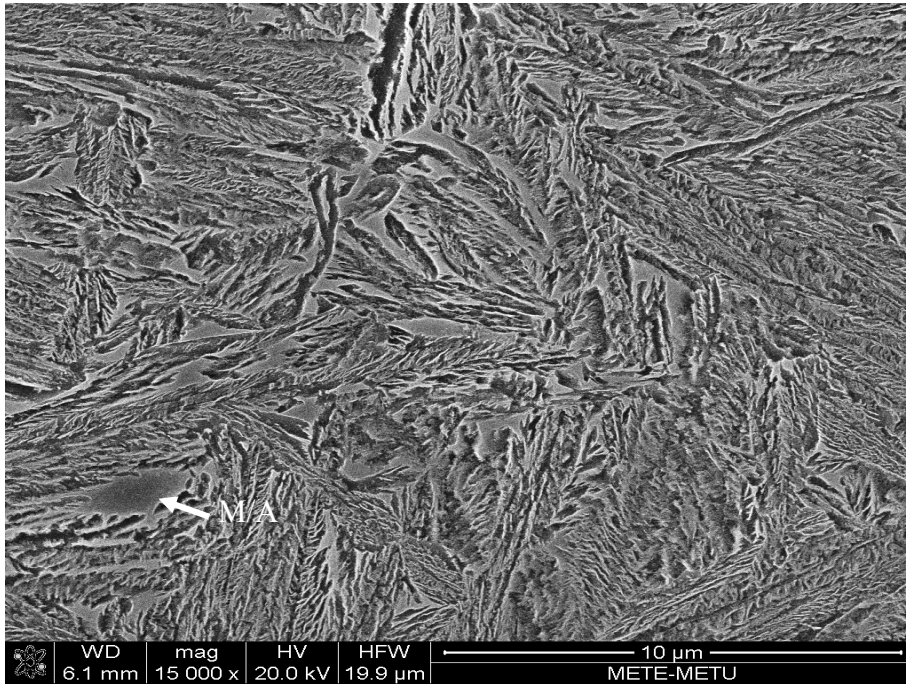
Figure 4.8. SEM micrograph of IT-250-1.
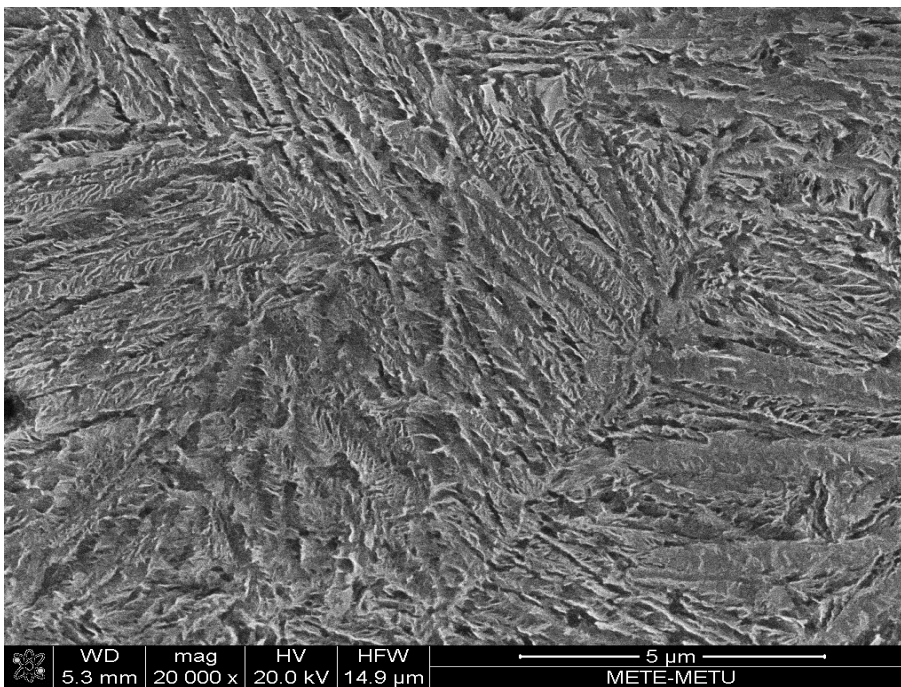
Figure 4.9. SEM micrograph of IT-250-12.

Isothermal treated specimens (300°C)

The microstructure of 60SiMn5 alloy isothermal treated at 300°C for 15min consists of a mixture of bainite and M/A regions (Figure 4.10). After 1 hour, according to the calculated TTT diagrams the microstructure should be completely bainitic (Figure 4.11). However, the M/A regions could be detected even after a treatment of 3h in the salt bath (Figure 4.12).

Figure 4.10. SEM micrograph of IT-300-1/4.

Figure 4.11. SEM micrograph of IT-300-1.
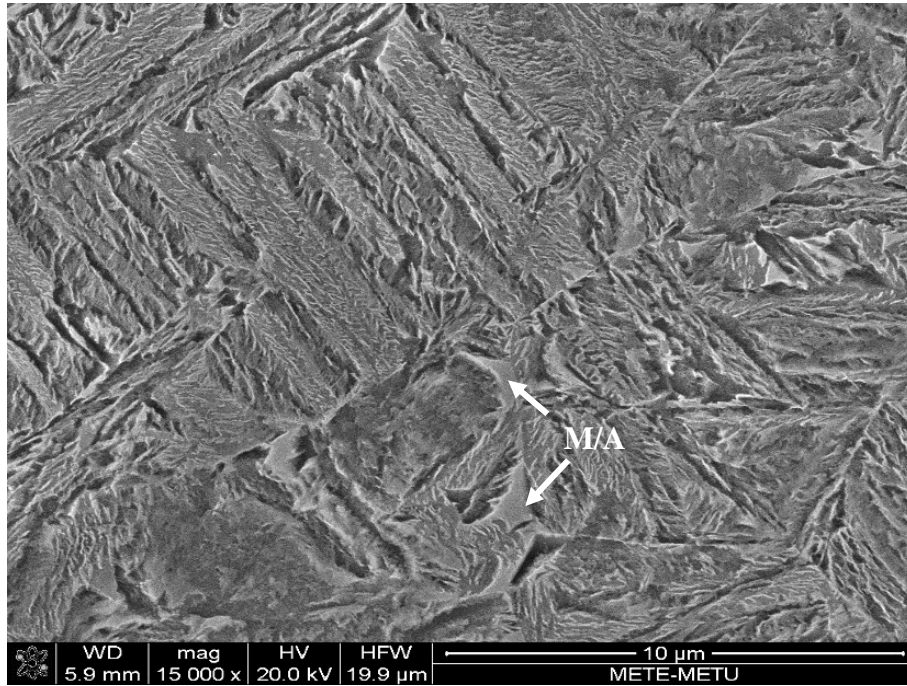
(a)

(b)

Figure 4.12. SEM micrographs of IT300-3.

The obtained phases in the microstructures according to the changing transformation temperature and time in C-Mn-Si steel can be summarized as follows (Table 4.2):

Table 4.2. The obtained phases as a result of heat treatments.

Specimen	Obtained Phases
Q	Martensite
IT-200-1	M/A+little bainite
IT-200-6	M/A+bainite
IT-200-12	M/A+bainite
IT-200-24	**100% bainite**
IT-250-1	M/A+bainite
IT-250-12	**100% bainite**
IT-300-1	M/A+bainite
IT-300-3	M/A+bainite

4.1.2   Isothermal Treatment Studies of C-Mn-Si-Mo Alloy

To prevent the local melting at the grain boundaries, the steel is heated to 1050°C. The samples were homogenized at 1100°C for 1 hour then the furnace. Then samples were cooled in the furnace. The obtained microstructure may be seen in Figure 4.13.
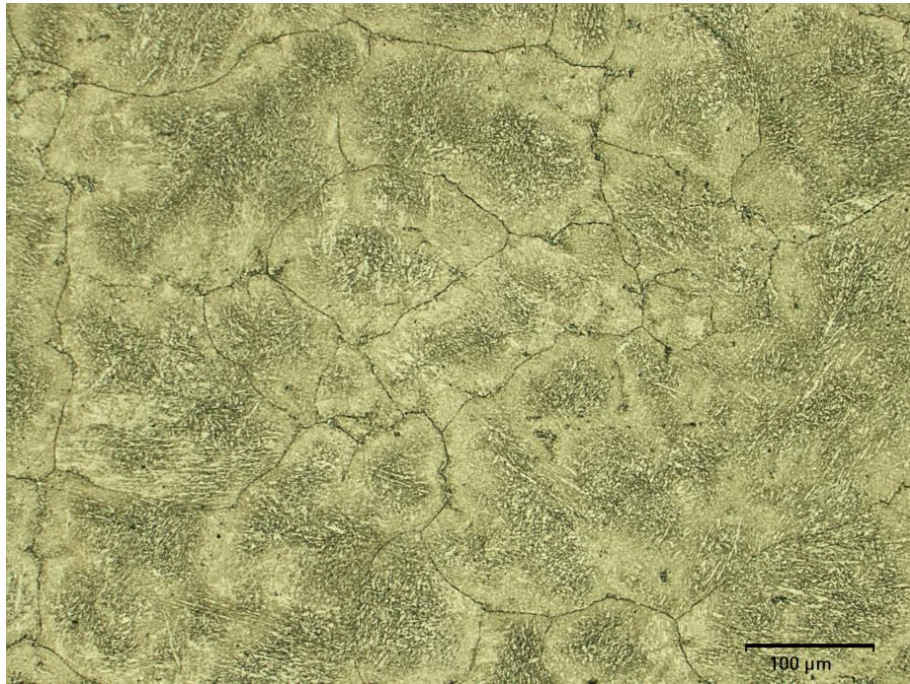
(a)
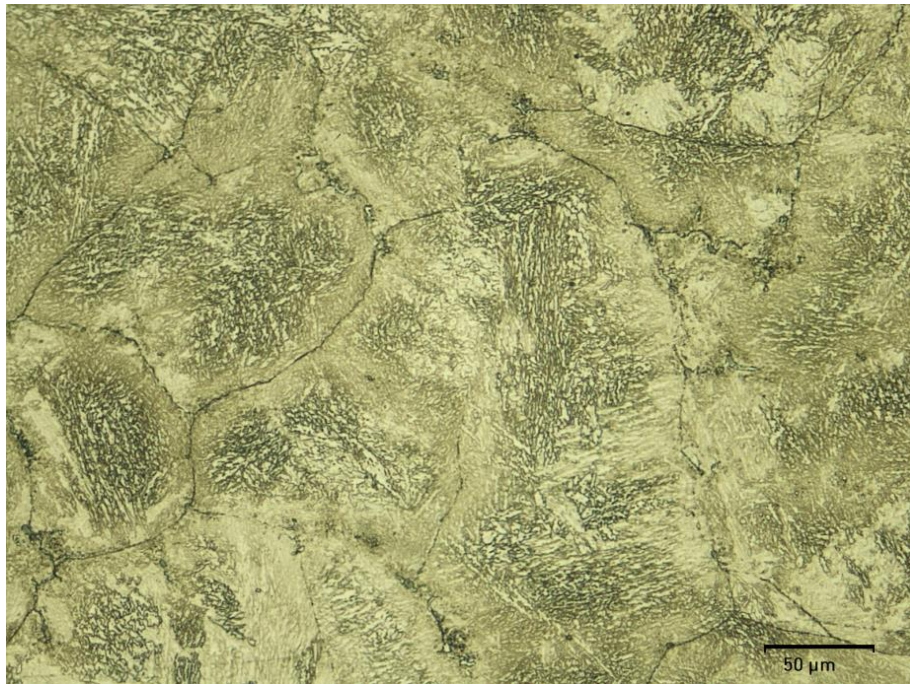
(b)
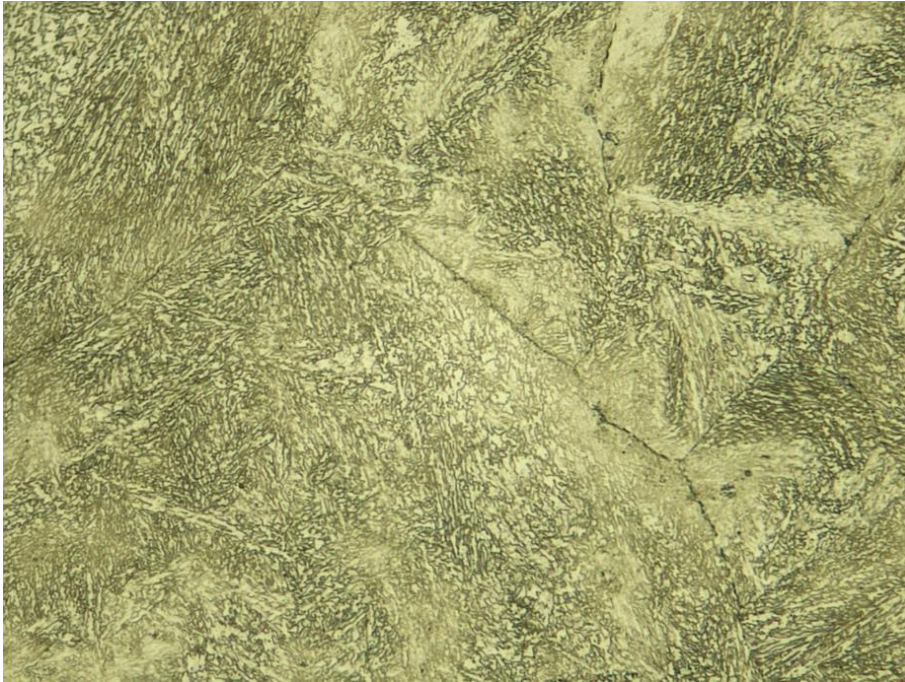
(c)

Figure 4.13. Optic micrographs of homogenized C-Mn-Si-Mo alloy.

The schematic representation of homogenization is given in the Figure 4.14.
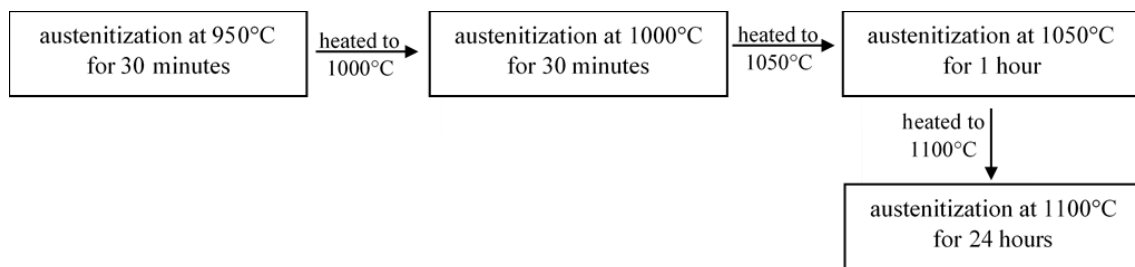
Figure 4.14. Schematic representation of the homogenization process.

Three set specimens were prepared:

a) As-Quenched Specimens

b) Isothermally Treated Specimens at 230°C

c) Isothermally Treated Specimens at 280°C

Heat treatment flow of C-Mn-Si-Mo alloy can be seen in Figure 4.15.
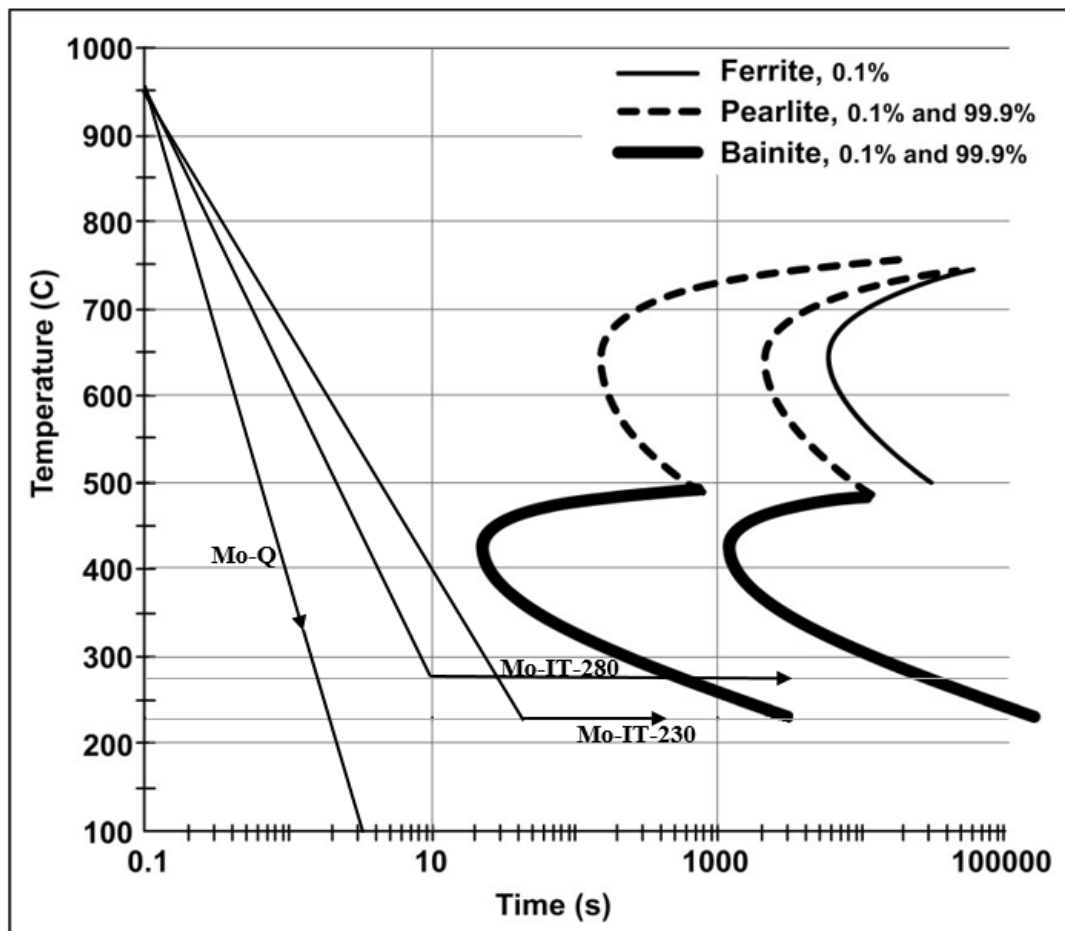
Figure 4.15. Heat treatment flow of C-Mn-Si-Mo alloy.

As-Quenched Specimens

Figure 4.16 shows the SEM micrograph of Mo-Q. The microstructure is fully martensitic.
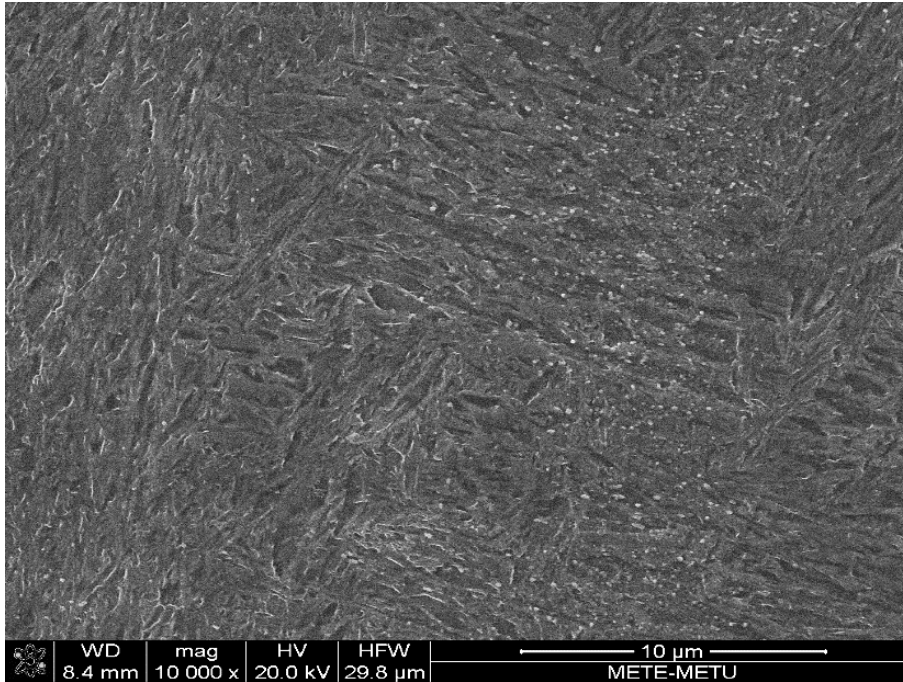
Figure 4.16. SEM micrograph of Mo-Q.

Isothermal treated specimens (230ºC)

The microstructures of C-Mn-Si-Mo alloy isothermal treated at 230°C for 1 hour and 12 hour consists of bainite and if there is martensite it cannot be resolved (Figure 4.17 and 4.18). As the time is extended, bainite begins to appear more in the following samples (Figure 4.19). After 42 hours, the structure is completely bainitic (Figure 4.20).
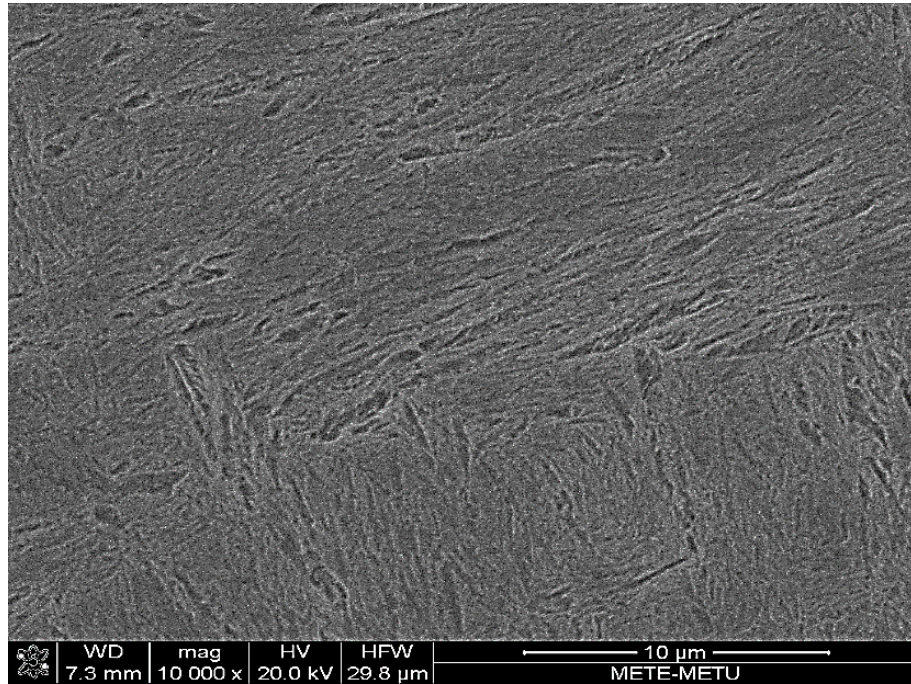
Figure 4.17. SEM micrograph of IT-230-1.
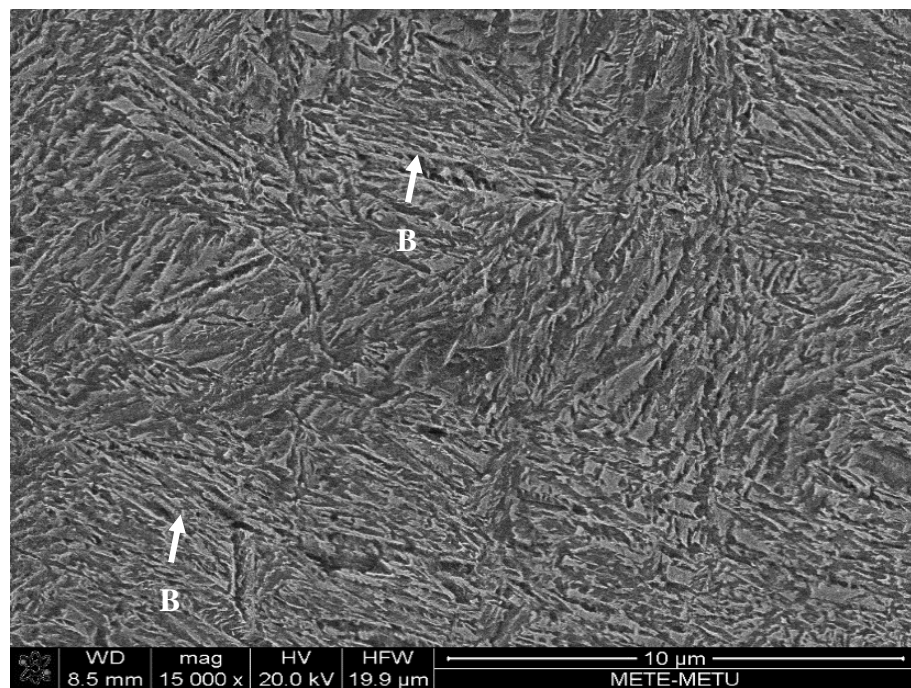
Figure 4.18. SEM micrograph of Mo-IT-230-12.
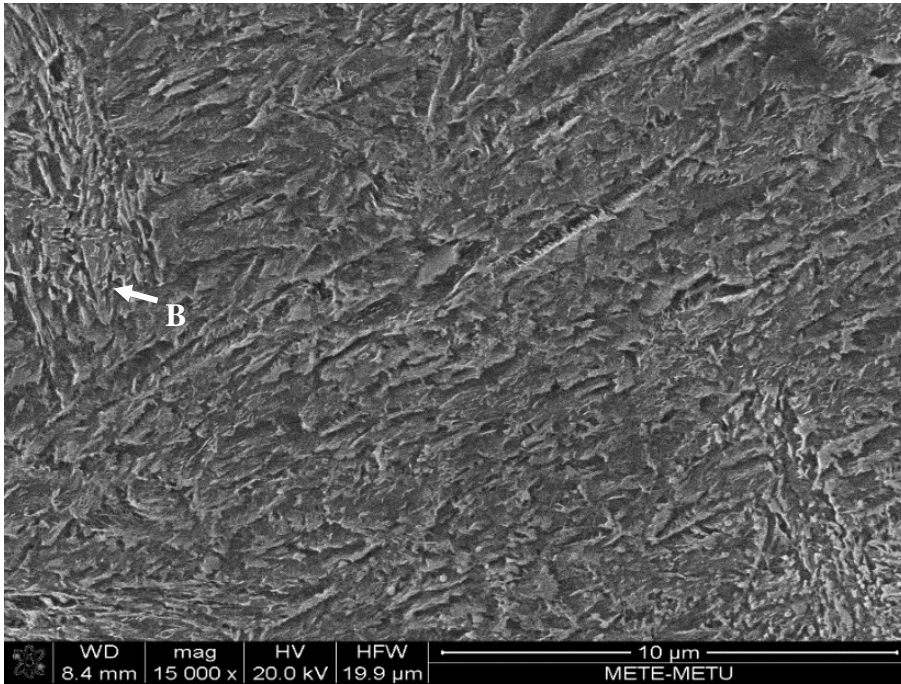
(a)
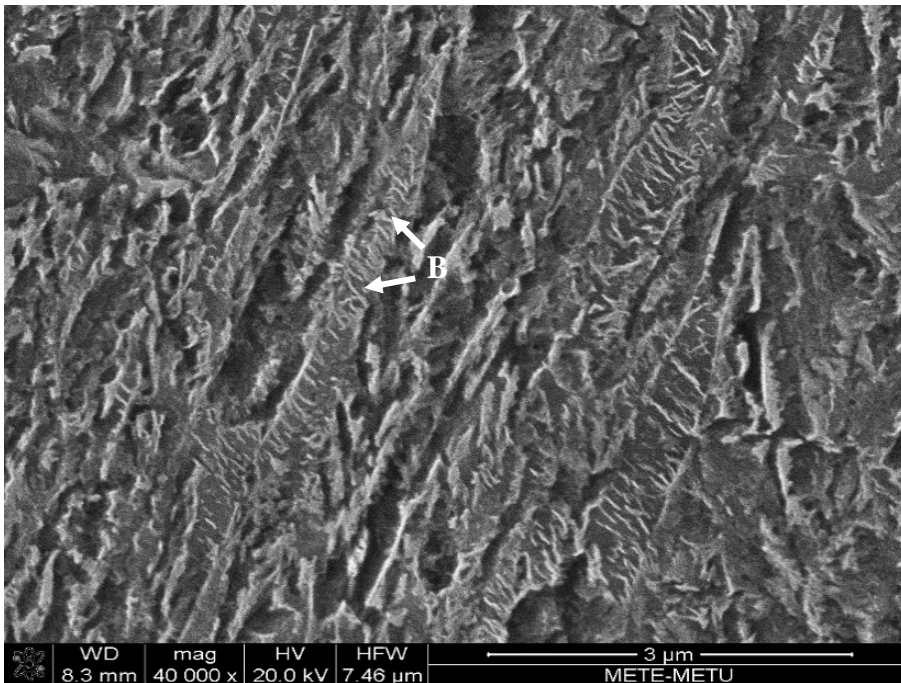
(b)

Figure 4.19. SEM micrographs of Mo-IT-230-24.
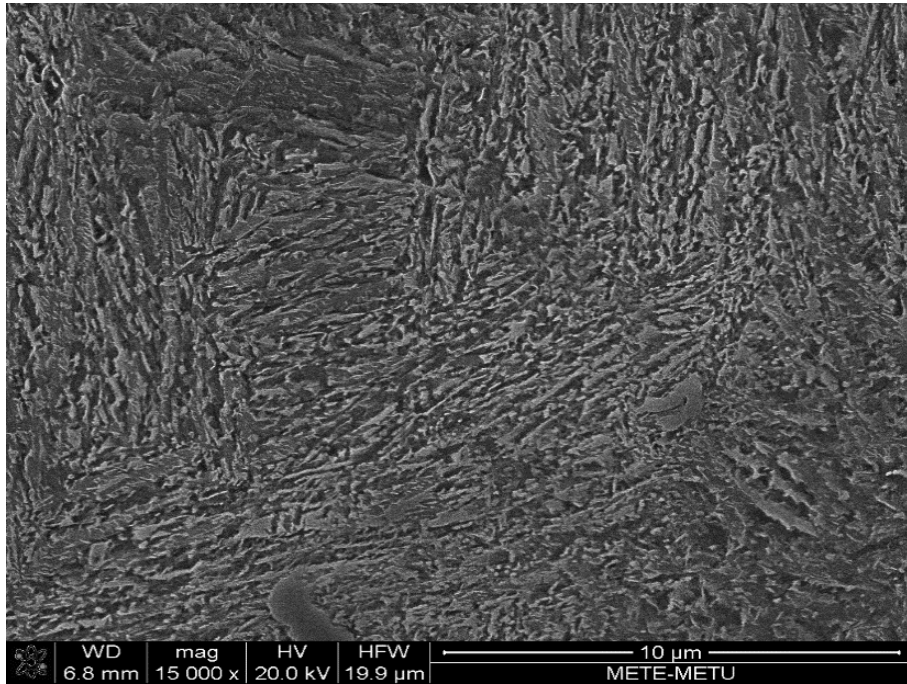
(a)
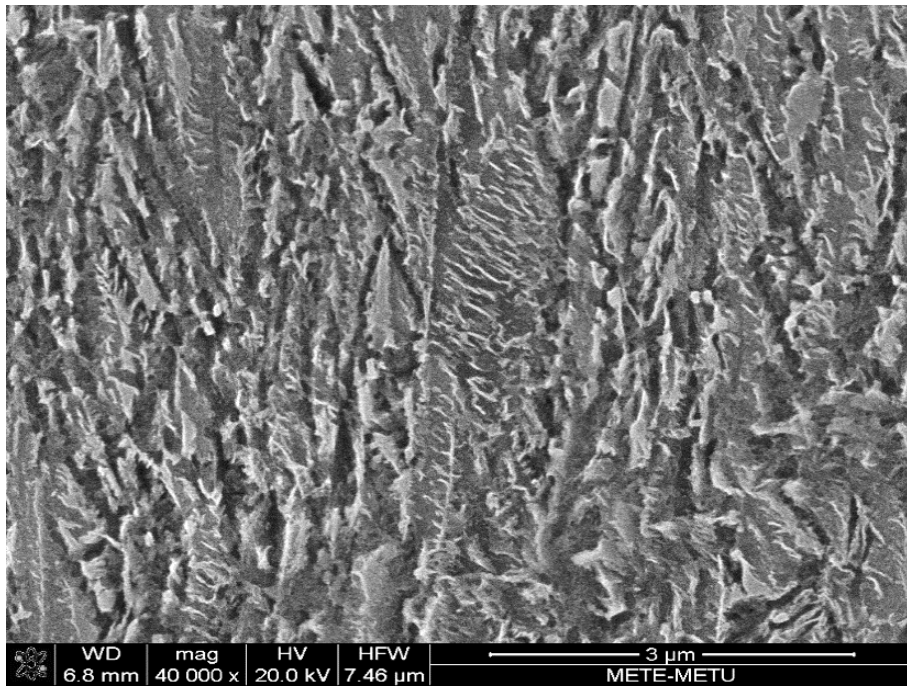
(b)

Figure 4.20. SEM micrographs of Mo-IT-230-48.

Isothermal treated specimens (280ºC)

The microstructures of C-Mn-Si-Mo alloy isothermal treated at 280°C for 1 hour consists of bainite and if there is martensite it cannot be resolved (Figure 4.21). After 7 hours, the structure is completely bainitic (Figure 4.22).
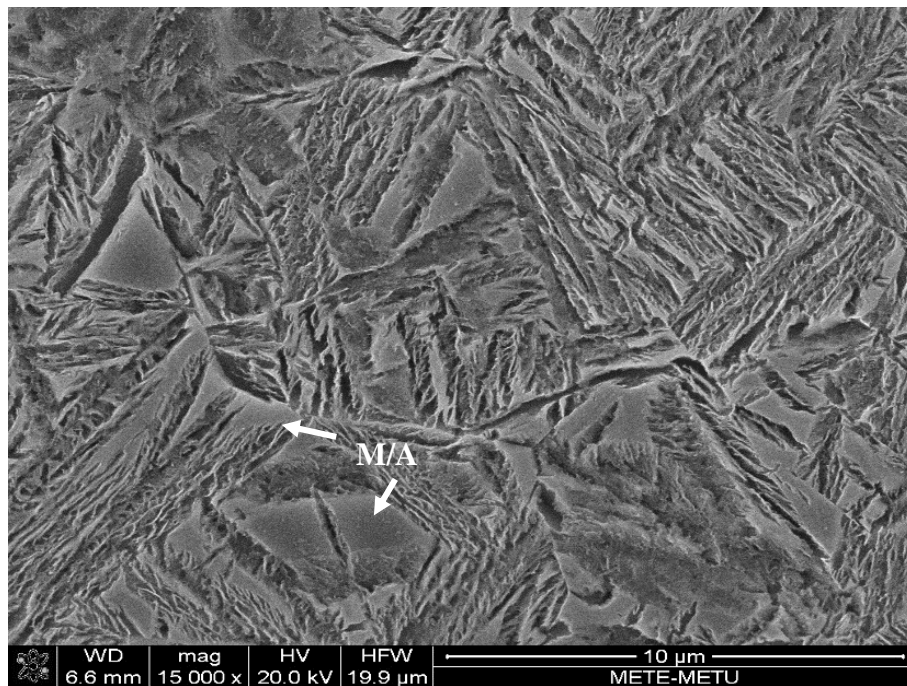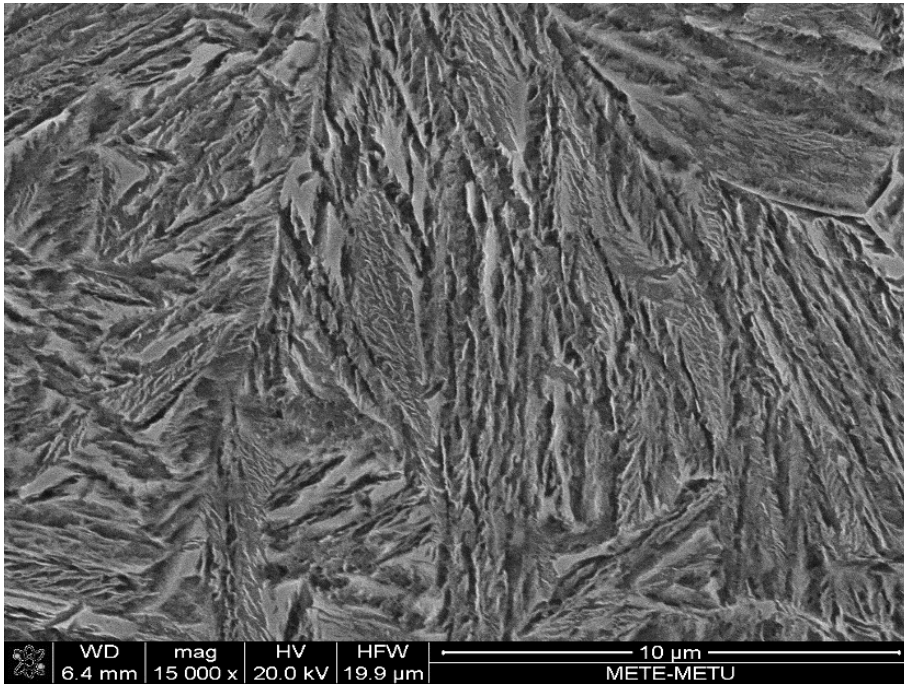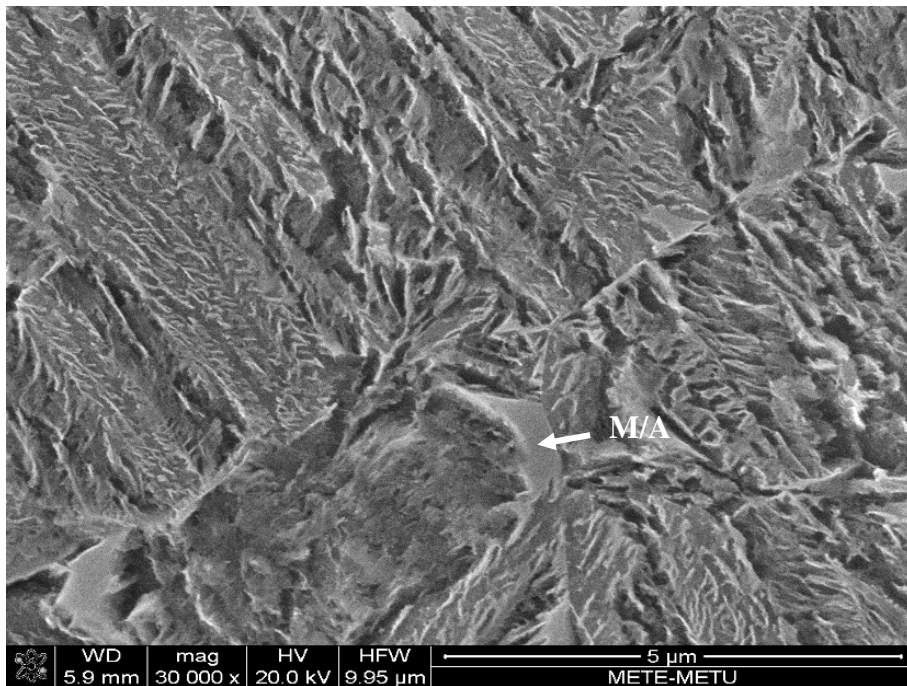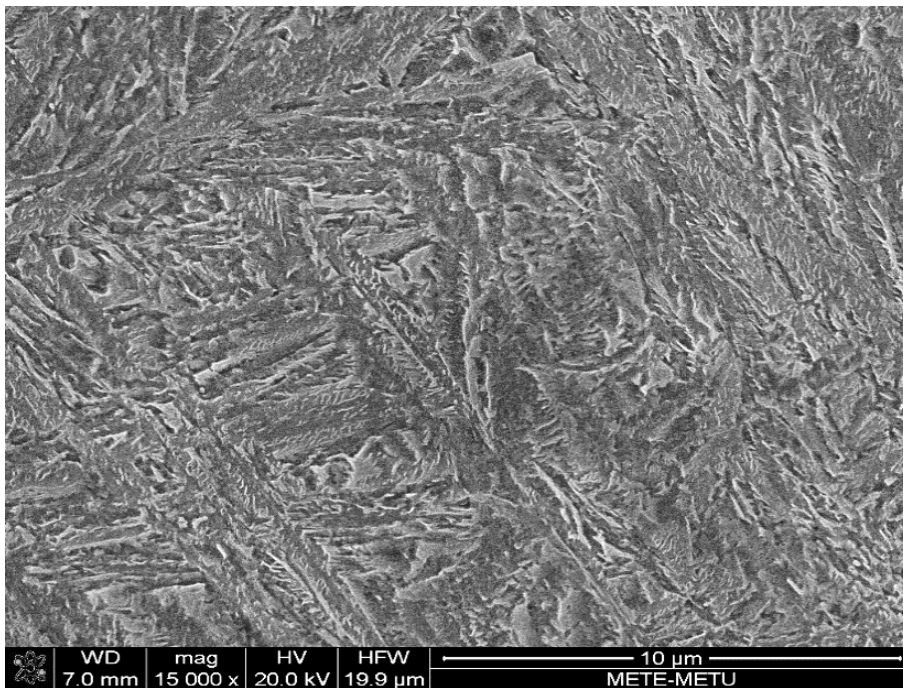

(a)
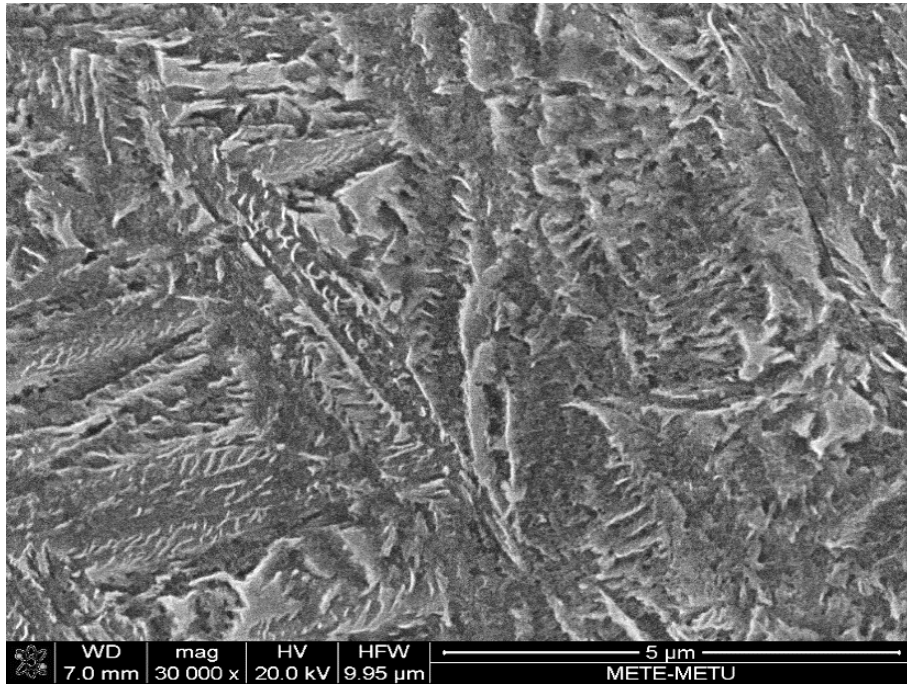
(b)

Figure 4.21. SEM micrograph of Mo-IT-280-1.
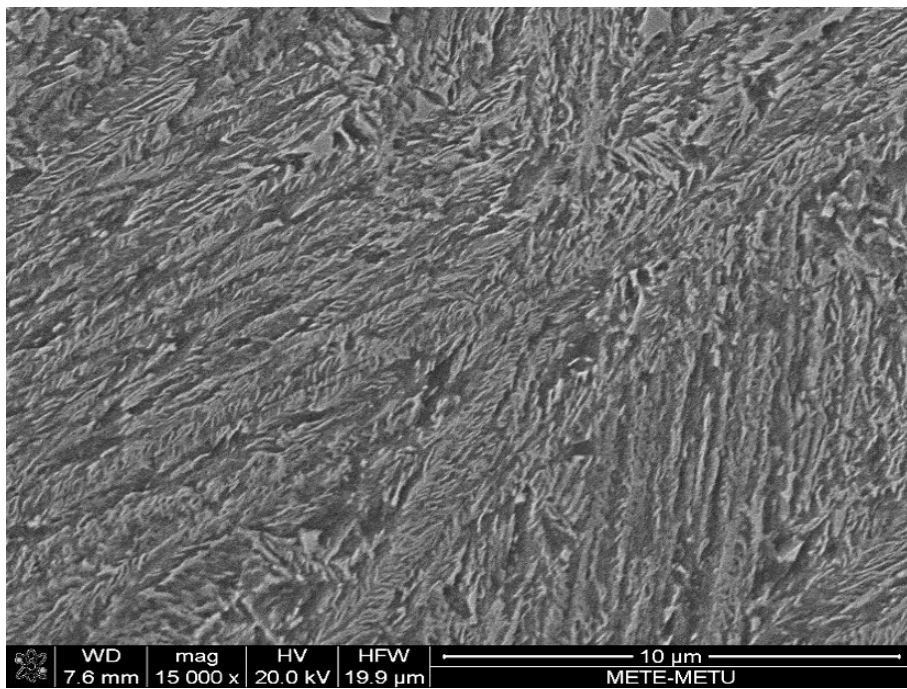
Figure 4.22. SEM micrograph of Mo-IT-280-12.

The obtained phases in the microstructures with respect to transformation temperature and time in C-Mn-Si-Mo steel is summarized in Table 4.3.

Table 4.3. The obtained phases as a result of heat treatments.

Specimen	Obtained Phases
Mo-Q	Martensite
Mo-IT-230-1	Bainite
Mo-IT-230-12	Bainite
Mo-IT-230-24	Bainite
Mo-IT-230-48	**100% bainite**
Mo-IT-280-1	Bainite
Mo-IT-280-12	**100% bainite**

4.2 Carbide Extraction Studies

For the C-Mn-Si and C-Mn-Si-Mo steels, the possible carbide types that can form in the microstructure were investigated from the literature. The possible carbide types, their approximate compositions, space groups and the carbides detected in the specimens are given in Table 4.4 [56-59]. The carbide extraction results of tempered specimens are also included to the analysis. It is known that addition of Si above a definite percentage retards the carbide precipitation in bainite. For this reason, IT-250-12 and FC were used for C-Mn-Si alloy; Mo-IT-230-48 and Mo-FC were used for C-Mn-Si-Mo alloy.

Table 4.4 The possible carbides, approximate composition, space groups and carbide consisting specimens.

Carbide	Approximate composition	Space group	Matching Specimen
Cementite (Θ)	Fe_3C	Orthorhombic Pnma	FC
Ɛ-carbide	$Fe_{2-3}C$	Hexagonal P63/mmc or P6322	Mo-IT-230-48
X-carbide	$Fe_{2.2}C$	Monoclinic C2/c	
ℷ-carbide	Fe_2C	Orthorhombic Pnnm	
Iron molybdenum carbide	Fe_3Mo_3C	Cubic Fd-3m	Mo-FC
Molybdenum carbide	Mo_2C	Hexagonal Pbcn	Mo-IT-230-48-FC-500

The carbide residues were analyzed using XRD. Furnace Cooling (FC) is the equilibrium state for the alloys. As the equilibrium carbide types in these specimens are known, FC specimens would be a good reference and starting point. The peaks taken from the carbide residue of FC specimens fit Fe_3C carbide as expected. It was observed that there is no any carbide peak in 100% bainitic specimens of C-Mn-Si alloy. Interestingly, the peaks obtained from the carbide residue of Mo-IT-230-48 specimens fit Ɛ-carbide. This finding indicates that Si cannot prevent carbide precipitation in bainite, if there is Mo as an alloying element. Ɛ-carbide is the first carbide formed at low temperatures during tempering of martensite under normal conditions [20]. In this study, it is observed that it also precipitates in bainite at low temperatures. M_2C is a carbide precipitated at secondary hardening temperatures in Mo-containing steels (500^oC) during tempering and in this study, similarly, it

precipitates at the same temperature. It is important to mention that M_2C precipitation in the bainite structure is an important observation. ϵ-carbides precipitate just as in tempered martensitic steels. It is observed that ϵ-carbide is replaced by M_6C in Mo-FC specimens. The peaks fit M_2C carbide in the bainitic specimens (Mo-IT-230-48-FC-500).

For C-Mn-Si-Mo specimens, M_6C is not stable at tempering temperature. The analysis conducted using Jmat Pro, at equilibrium conditions, around 2.3% Mo_2C formation is expected during tempering. The effect of secondary hardening differs for bainitic and martensitic specimens. In secondary hardening; the carbon is in solid solution in martensite and M_2C would precipitate in martensite. M_6C should not be seen. In Jmat Pro analysis; around 1% M_2C is observed at the austenitization temperature. When it comes to room temperature; it is considered that some of the precipitated carbide may come from the austenitization temperature, and although there is no carbon precipitation in ferrite, it is not thought to have a significant effect on the bainitic transformation. The difference in secondary hardening behaviour between tempered martensitic and tempered bainitic specimens that in bainitic transformation, there is no carbon precipitation in carbide free bainite.

4.3   Tempering Studies

Two different sets of samples were used for C-Mn-Si steel:

1)Martensitic specimens (Q-T-200, Q-T-400, Q-T-500, Q-T-550)

2)Bainitic   specimens   (IT-250-12-FC-T-200,   IT-250-12-FC-T-400, IT-250-12-FC-T-500, IT-250-12-FC-T-550)

Two different sets of samples were used for C-Mn-Si-Mo steel:

1)Martensitic specimens (Mo-Q-T-200, Mo-Q-T-400, Mo-Q-T-500, Mo-Q-T-550)

2)Bainitic specimens (Mo-IT-230-48-FC-T-200, Mo-IT-230-48-FC-T-400, Mo-IT-230-48-FC-T-500, Mo-IT-230-48-FC-T-550)

The martensitic and bainitic samples were achieved by tempering the heat treated steels at 200°C, 400°C, 500°C, 550°C for 1,5 hours. The hardness values of the martensitic and bainitic specimens can be seen at Section 4.4.1 in Table 4.5.

The comparison of the hardness of martensitic and bainitic C-Mn-Si alloy can be seen in Figure 4.23. The martensitic samples exhibit the expected behavior: An increase in tempering temperature from 200ºC to 550ºC causes a decrease in hardness values from approximately 700 HV to 400 HV. A drop in hardness for bainitic samples was also observed though the rate of decrease was lower: The hardness decreases from 600 HV to approximately 360 HV upon tempering in the range 200ºC-550ºC. Both bainitic and martensitic steels yielded nearly same hardness values after tempering at 550ºC. In C-Mn-Si steel, a secondary hardening peak is not observed both in martensitic and bainitic specimens.
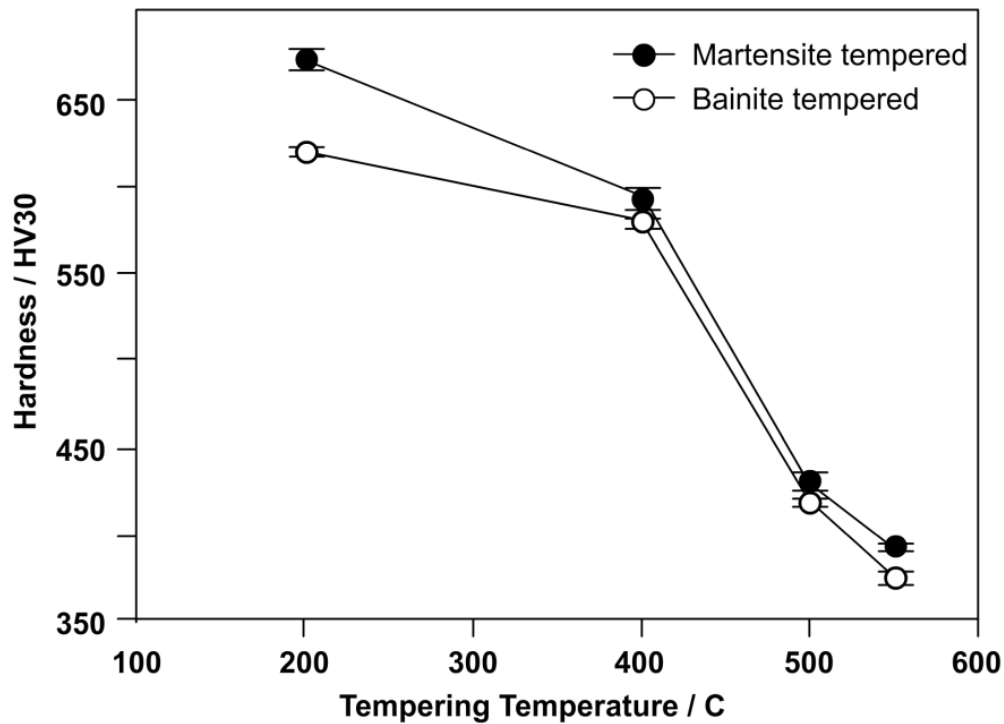
Figure 4.23. The hardness of martensitic and bainitic C-Mn-Si alloy.

The comparison of the hardness of martensitic and bainitic 'C-Mn-Si-Mo alloy' is seen in Figure 4.24. The carbon solubility in bainitic ferrite is low. As secondary hardening in Mo-containing steels results from alloy carbide precipitation, the potential of secondary hardening would be low due to low carbon content of bainitic ferrite. At 500°C, in martensitic specimen a slight increase in hardness from 628HV to 637HV is observed when compared to that of tempered at 400°C. This increase is most probably due to the secondary hardening effect. The presence of M_2C carbides in tempered specimen also gives an evidence that there is a secondary hardening effect.
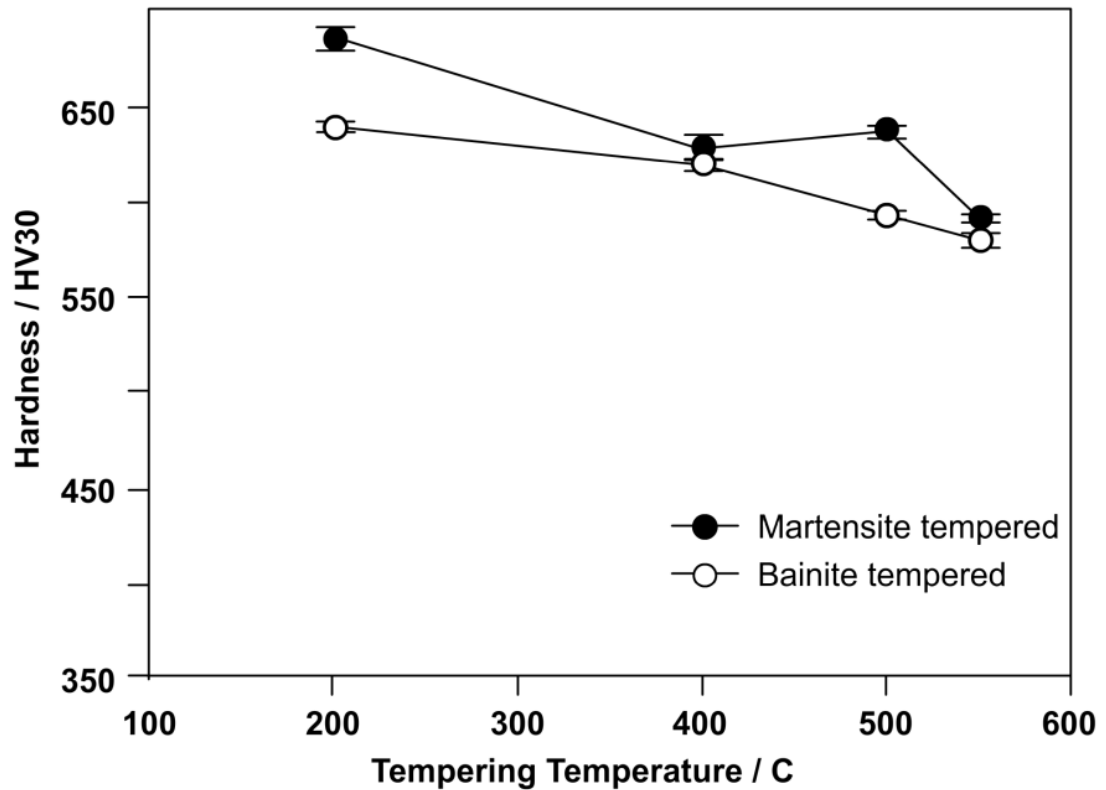
Figure 4.24. The hardness results of martensitic and bainitic C-Mn-Si-Mo specimens.

The bainitic IT-250-12 and Mo-IT-230-48 specimens are tempered at 200°C, 400°C, 500°C, and 550°C for 1,5 hours. The comparison of the hardness of bainitic C-Mn-Si alloy and bainitic C-Mn-Si-Mo alloy can be seen in Figure 4.25. It is a well-known fact that the response of bainite to tempering is slow because the long transformation stages of bainite also act as auto tempering [15,21,60-62]. Similar behavior is observed in this study as well. In C-Mn-Si steel, a secondary hardening peak is not observed in bainitic specimens.

At 500°C, tough not much, there is an increase in hardness due to the secondary hardening effect of molybdenum in C-Mn-Si-Mo alloy. Garcia-Mateo et.al [61] have shown that in a 1.0wt%C steel, the softening of bainite is not seen if tempering is carried out below 550°C. This effect is related to the carbides precipitated in bainite

which leads to some precipitation strengthening during the early stages of tempering. The hardness results obtained in this study for tempered C-Mn-Si alloys are closer to the results of Kang et. al [21], probably due to the similarity in the carbon content of the steels studied. In this study carried out by Kang et.al. [21], it has been found out that the microstructural coarsening becomes detectable together with precipitation of carbides upon tempering above 360°C which results in a sudden decrease in the hardness values. There are a few studies on the effect of Mo on the tempering of bainite. The retardation to softening in Mo-containing steels first shown by Baker and Nutting [42] and Irvine and Pickering [41] in a study based on low carbon steels. However, in this study, the carbon content of C-Mn-Si-Mo steel is high i.e., 0.6wt%. The bainite looses carbon by precipitation of epsilon carbide. It is possible that the amount of Mo (2wt%) is not enough to obtain a well-defined peak. In studies of high strength bainitic steels, the Mo content is kept low, i.e., in the range 0.2%-0.4% to avoid temper embrittlement. However, Mo as an alloying element has several important effects on steels. Mo exhibits a secondary hardening peak at around 500°C when a sufficient amount is added as an alloying element. The formation of secondary hardening peak in Mo-containing steels is related to the replacement of coarse cementite particles with much finer alloy carbides (M_2C and MC type) [20,63].
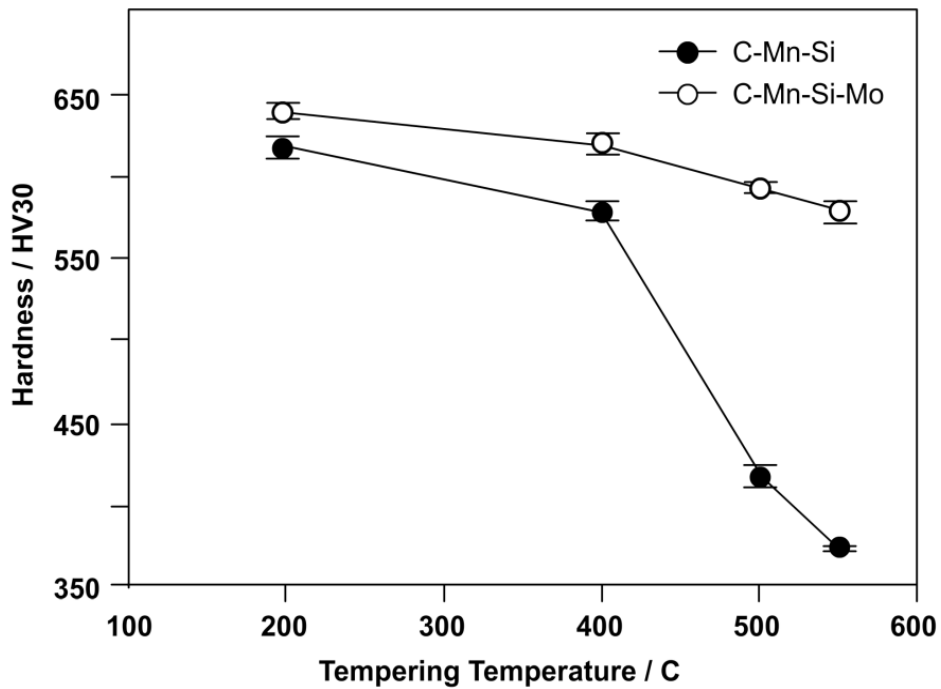
Figure 4.25. Hardness values of bainitic C-Mn-Si and bainitic C-Mn-Si-Mo alloy.

In this study, the secondary hardening potential of bainitic steel is lower than its martensitic counterpart most probably due to the early carbide precipitation during the bainitic transformation (which is named as auto tempering) and loss of some carbon for secondary hardening peak. On the other hand, upon tempering at 500°C and 550°C, bainite and martensite exhibit very similar hardness values in C-Si-Mn steel.

4.4 Mechanical Properties

4.4.1 Hardness Measurements

The hardnesses of C-Mn-Si and C-Mn-Si-Mo alloy can be seen at Table 4.5.

Table 4.5. Hardness measurements.

Specimen	Hardness (HV30)
Q	750±4.4
IT-200-1	685±4.5
IT-200-6	663±3.0
IT-200-12	652±3.4
IT-200-24	646±4.4
IT-250-1	655±4.6
IT-250-12	640±3.6
IT-300-1	581±4.6
IT-300-3	532±2.0
IT-300-3	522±4.6
Q-T-200	673±6.2
Q-T-400	592±5.7
Q-T-500	429±5.9
Q-T-550	391±1.4
IT-250-12-FC-T-200	619±2.6
IT-250-12-FC-T-400	579±4.0
IT-250-12-FC-T-500	417±2,9
IT-250-12-FC-T-550	373±2.9
Mo-Q	769±6.0
Mo-IT-230-1	691±6.6
Mo-IT-230-12	676±7.2
Mo-IT-230-24	665±5.3
Mo-IT-230-48	658±3.5
Mo-IT-280-1	630±5.3
Mo-IT-280-12	616±6.0
Mo-Q-T-200	686±4.7
Mo-Q-T-400	628±5.5

Table 4.5 (Cont'd)

Mo-Q-T-500	637±3.2
Mo-Q-T-550	590±5.2
Mo-IT-230-48-FC-T-200	639±4.6
Mo-IT-230-48-FC-T-400	620±4.2
Mo-IT-230-48-FC-T-500	593±1.8
Mo-IT-230-48-FC-T-550	579±3.1
Mo-Q-T-550	590±5.2

The hardness values of C-Mn-Si alloy and C-Mn-Si-Mo alloy at different tempering temperatures can be seen in Figure 4.26 and Figure 4.27, respectively. For C-Mn-Si alloy, in bainitic C-Mn-Si specimens (i.e. IT-200-1, IT-200-6, IT-200-12, and IT-200-24), as the transformation time increases, the hardness decreases. Similarly, in bainitic C-Mn-Si-Mo specimens (Mo-IT-230-1, Mo-IT-230-12, Mo-IT-230-24, and Mo-IT-230-48), as the transformation time increases, the hardness decreases. In both C-Mn-Si alloy and C-Mn-Si-Mo alloy, a decrease in hardness values with respect to time can be explained with an increase in percentage of bainite. Also, self tempering during transformation can also lower the hardness values.
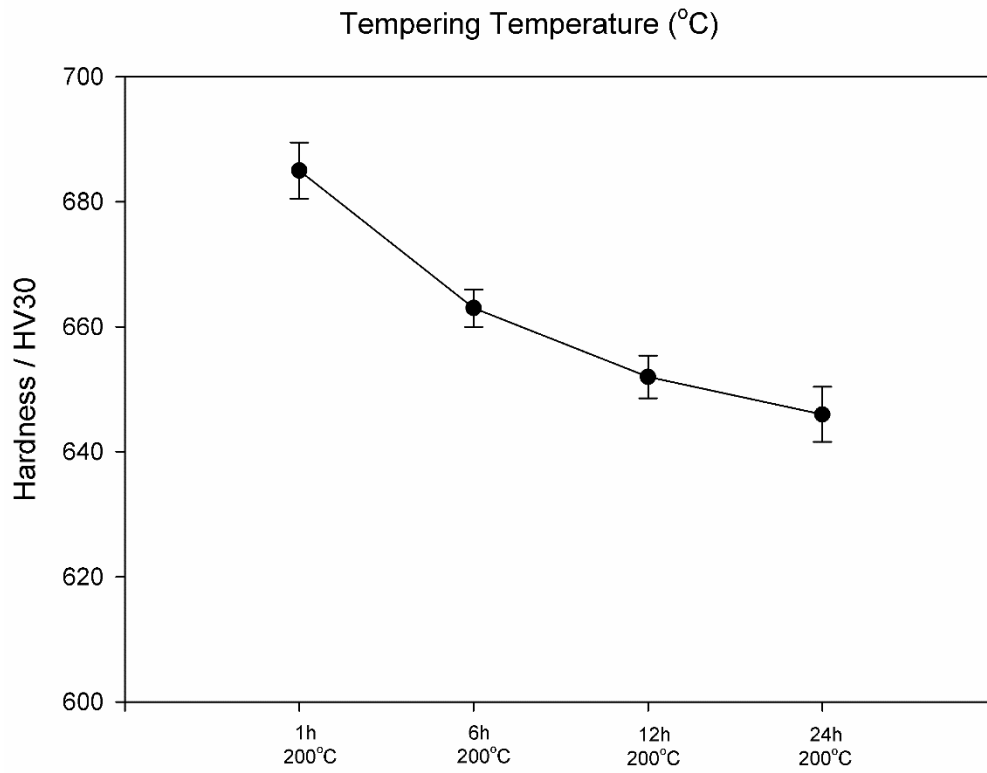
Figure 4.26. Hardness vs. tempering temperature of C-Mn-Si alloy.
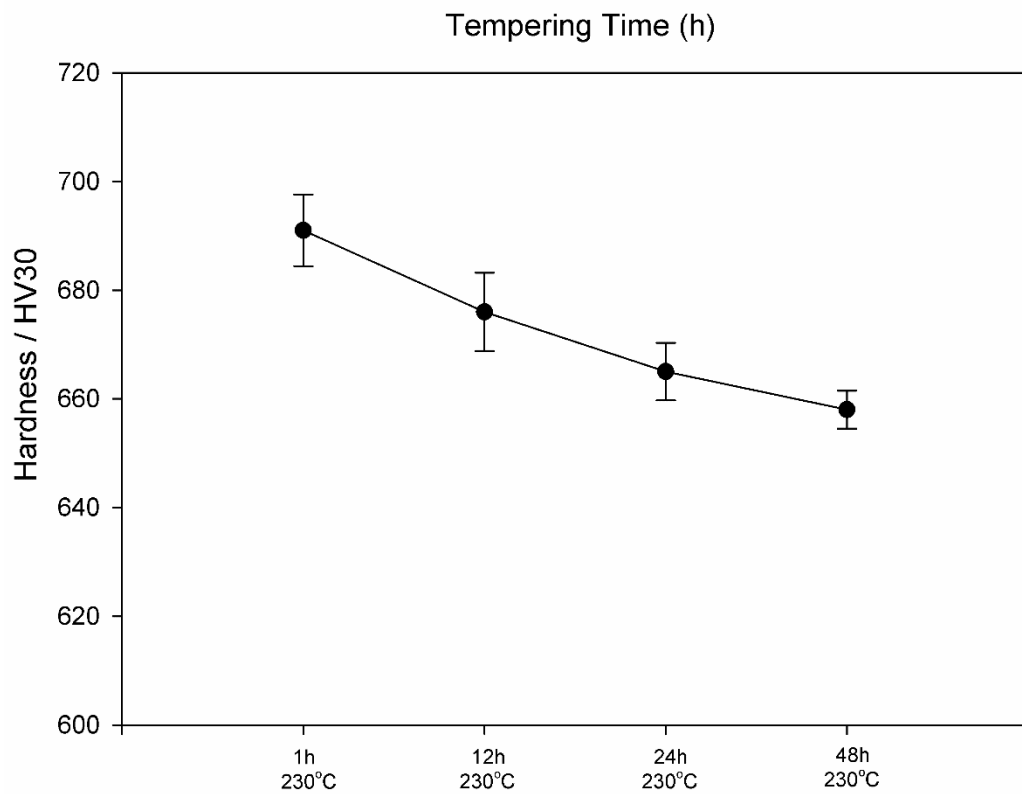
Figure 4.27. Hardness vs. tempering time of C-Mn-Si-Mo alloy.

4.4.2   Tensile Test Studies

Tensile testing is applied to nearly 100% bainitic specimens, IT-200-24, IT-250-12, and Q-T-400 for C-Mn-Si steel; Mo-IT-230-48, Mo-IT-280-12 and Mo-Q-T-400 (Table 4.4). The stress-strain curves given in Figure 4.28 are shown as examples for both alloys.

Table 4.6 Tensile testing of specimens.

Specimen	Ultimate Tensile Strength (MPa)	Yield Strength (MPa)	Elogation (%)	Hardness (HV30)	$\dfrac{\sigma_y}{\sigma_{UTS}}$	UTSx%elongation (MPa%)
IT-200-24	2211±0.7	1695±3.2	6.7±1.4	646±4.4	0.76	14813
IT-250-12	2053±4.9	1745±5.5	8.0±0.2	640±3.6	0.85	16424
IT-300-3	1730±2.2	1462±4.8	6.2±0.4	522±4.6	0.85	10726
Q-T-400	1916±4.9	1763±5.7	7.5±0.1	592±5.7	0.92	14370
Mo-IT-230-48	1356±4.7	1058±3.6	1.2±0.1	658±3.5	0.78	1627
Mo-IT-280-12	1175±4.9	870±4.3	1.4±0.1	616±6.0	0.74	1645
Mo-Q-T-400	1182±4.9	852±4.5	1.1±0.2	628±5.6	0.72	1300

Q-T-400 specimen was selected to compare the tensile strength of nearly 100% bainitic specimens because the hardness values of the specimens tempered at 400°C for 1.5 hours are close to that of bainitic specimens.

Tensile test measurements for C-Mn-Si steel show that specimens that have nearly fully bainitic microstructure have equal or higher tensile strength values than that of the tempered martensitic specimen. The fully bainitic C-Mn-Si alloy (IT-250-12) exhibited a UTS of 2050 MPa and 8% elongation. On the other hand, the martensitic specimen exhibited a UTS of 1900 MPa and 7.5% elongation. Moreover, the hardness of the IT-250-12 is much higher than that of martensitic specimen (640HV vs 590HV respectively).

As far as the bainitic specimens are concerned (Table 4.4), the strength of the IT-300-3 specimen is lower than that of IT-250-12 specimen (1730 MPa vs 2050 MPa) which can be explained by the differences in their sheave thicknesses (Figure

4.36). On the other hand, the higher UTS value of IT-200-24 specimen (2200 MPa) can be either due to thickness of bainite sheaves or the presence of some amount of martensite besides bainite, because the M_S temperature of C-Mn-Si alloy is 250°C.

In recent years, "Product of Strength and Elongation" (PSE) is emerged as an important parameter [64-66]. When the PSE values of all the specimens are compared, the IT-250-12 specimen has a considerable advantage with respect to other bainitic and martensitic specimens.

Stress strain curves of IT-250-12 and Mo-IT-230-48 specimens can be seen as an example in Figure 4.28. Tensile strength and yield strength values of bainitic and tempered martensitic C-Mn-Si-Mo specimens can be seen in Figure 4.29. Tensile strength values of C-Mn-Si-Mo steel are lower than expected. The inhomogeneties in the specimens have caused a brittle fracture by preventing the elongation.
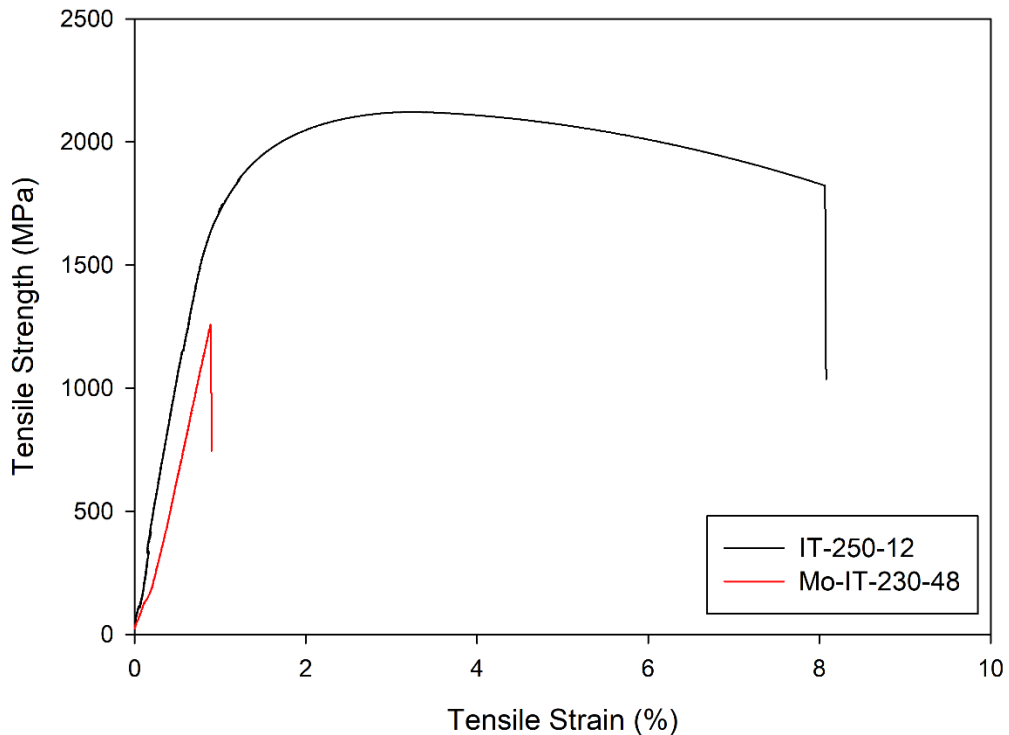
Figure 4.28. Stress strain curves of IT-250-12 and Mo-IT-230-48 specimens.
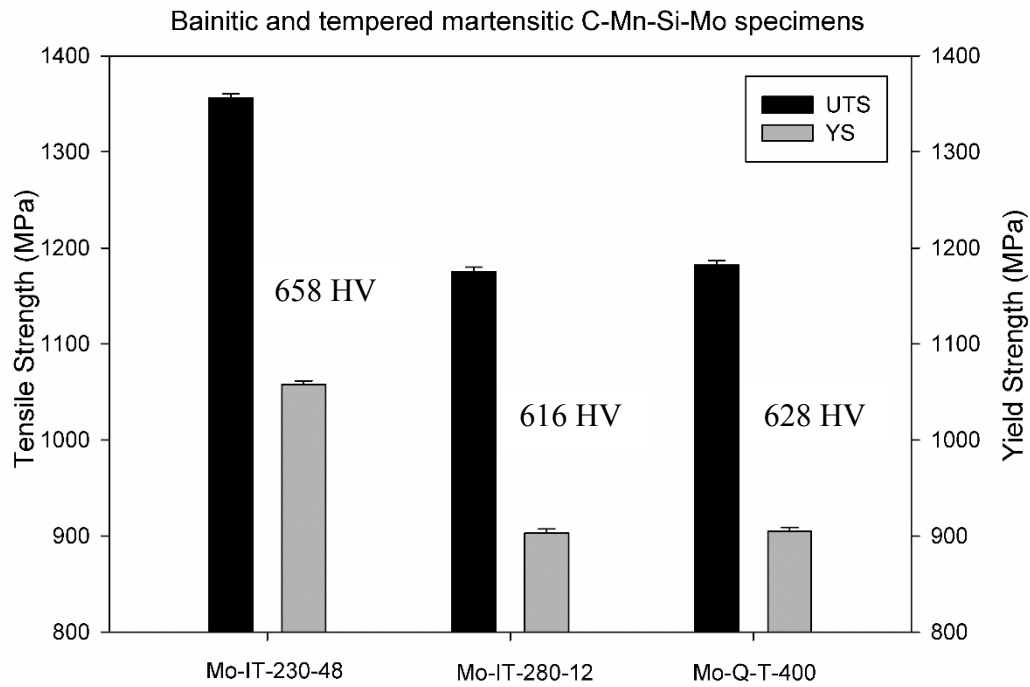
Figure 4.29. Comparison of tensile strength and yield strength values of bainitic and tempered martensitic C-Mn-Si-Mo specimens.

The hardnesses of all the samples are given in Figure 4.30. For comparison purposes, the hardnesses of quenched specimens which have fully martensitic structure are also given. As expected the hardnesses of isothermally treated samples with bainite phase are always lower than their martensitic counterparts. As far as the bainitic samples are concerned, an increase in transformation time causes a decrease in hardness values. This decrease in hardness can be explained by an increase in the bainite volume percentage and also due to recovery of bainitic structure.
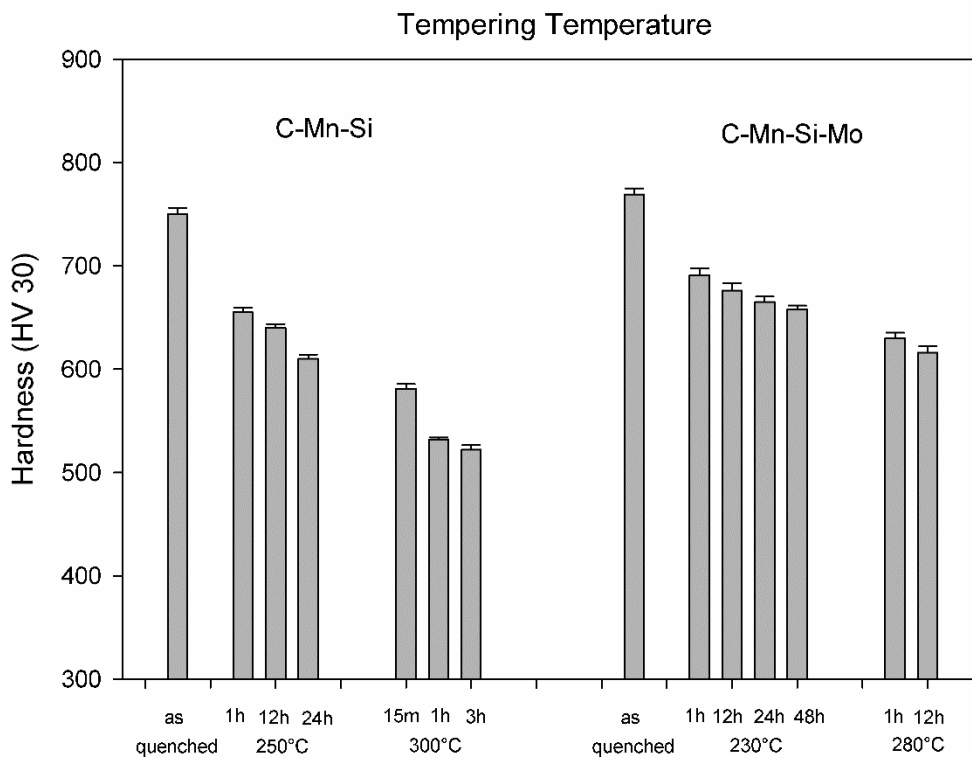
Figure 4.30. Hardness values of the isothermal treated C-Mn-Si and C-Mn-Si-Mo alloys.

The tensile strength values of 100% bainitic samples are given in Figure 4.31. C-Mn-Si-Mo steel was cast in the laboratory and forging was not performed. This steel has inhomogeneities. This causes that C-Mn-Si-Mo steel shows brittle behavior.

C-Mn-Si is a commercial and homogenized steel. This steel shows ductile behavior in tensile tests. The amount of residual austenite plays an important role in the tensile test results. The increase in the amount of retained austenite (especially the retained austenite films between the bainite sheaves) activates the strain-hardening mechanism and increases the tensile strength of the material [67,68].
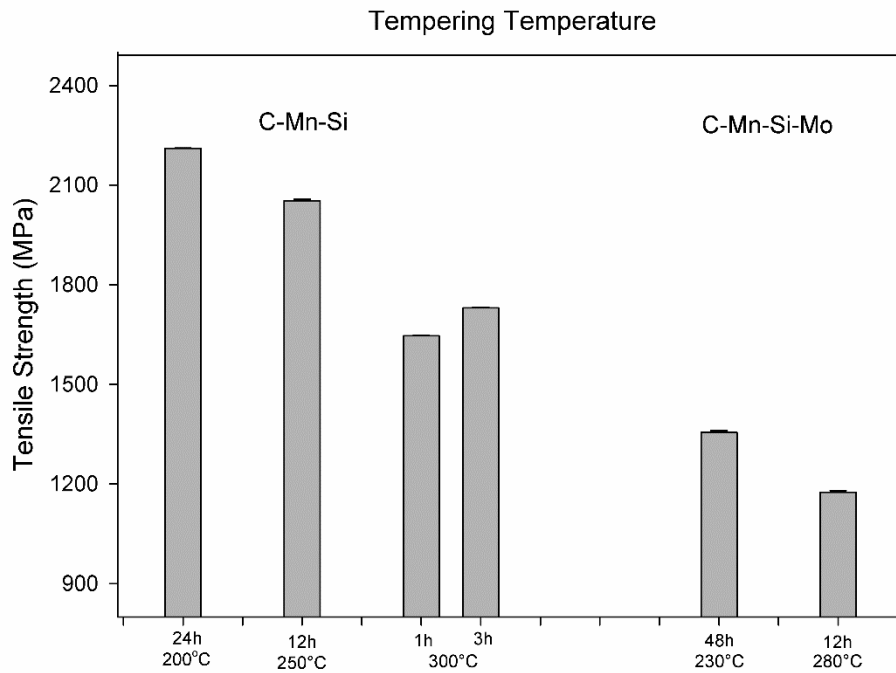
Figure 4.31. Tensile strength values of the isothermal treated C-Mn-Si and C-Mn-Si-Mo alloys.

4.5   Bainitic Transformation and Retained Austenite Determination

Quantitative X-ray diffraction analysis was done to to determine the volume percentage of retained austenite (Table 4.7). In contrast to C-Mn-Si steels, the bainitic C-Mn-Si-Mo steels do not exhibit any retained austenite or the amount is beyond the limits of detection for XRD.

Table 4.7 Retained austenite measurements.

Specimen	Amount of Retained Austenite (%)	Hardness (HV30)
Q	-	750±6
IT-200-1	<5	685
IT-200-6	<5	663
IT-200-12	8,30	652
IT-200-24	10,98	646
IT-250-1	6,7	655±4.6
IT-250-12	10,3	640±3.6
IT-300-1/4	11.3	581±4.6
IT-300-1	14.8	532±2
IT-300-3	14.8	522±4.6
Mo-Q	-	769±6
Mo-IT-230-1	-	691±6.6
Mo-IT-230-12	-	676±7.2
Mo-IT-230-24	-	665±5.3
Mo-IT-230-48	-	658±3.5
Mo-IT-280-1	<5	630±5.3
Mo-IT-280-12	<5	616±6

In C-Mn-Si steels, as the duration of isothermal treatment increases, the amount of retained austenite increases. As transformation continues, an increase in bainite content will result in more carbon rejection to austenite phase and enriching the austenite regions with respect to carbon and hence resulting in higher percentage of retained austenite.

In contrast to C-Mn-Si steels, in the bainitic C-Mn-Si-Mo steels, retained austenite phase cannot be detected. The retained austenite contents of all samples found by

XRD are shown in Figure 4.32. As shown in this figure, the bainitic specimens of C-Mn-Si alloy contain different amounts of retained austenite due to the isothermal transformation treatment but it could not be detected in C-Mn-Si-Mo alloy. When the RA contents of the bainitic specimens of C-Mn-Si alloy is concerned, an increase in the amount of bainitic ferrite in the structure causes an increase in the amount of RA as well (e.g. an increase in transformation time from 1 h to 12 h at 250°C causes an increase in the amount of RA from 6% to 10%, respectively). Another finding is that the amount of retained austenite is higher in the specimen transformed at 300°C (14%) with respect to the specimen transformed at 250°C (10%).
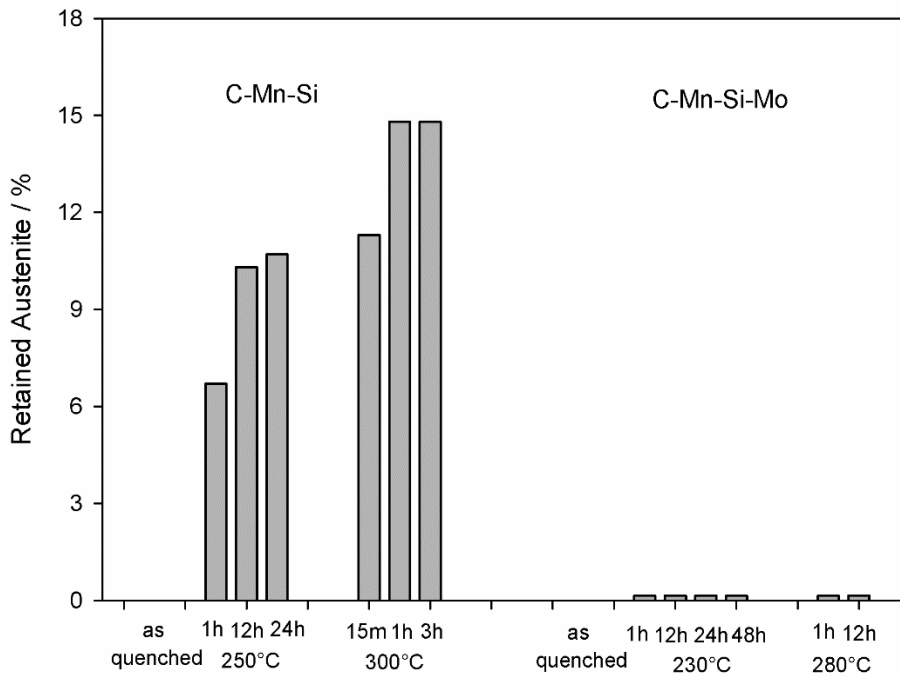
Figure 4.32. The retained austenite contents of all the specimens.

XRD patterns of Q, Mo-IT-230-48, and IT-250-12 specimens are shown in Figure 4.33. Oil-quenched specimens do not contain any RA. On the other hand, the bainitic structures of C-Mn-Si steel give rise to RA peaks.

80
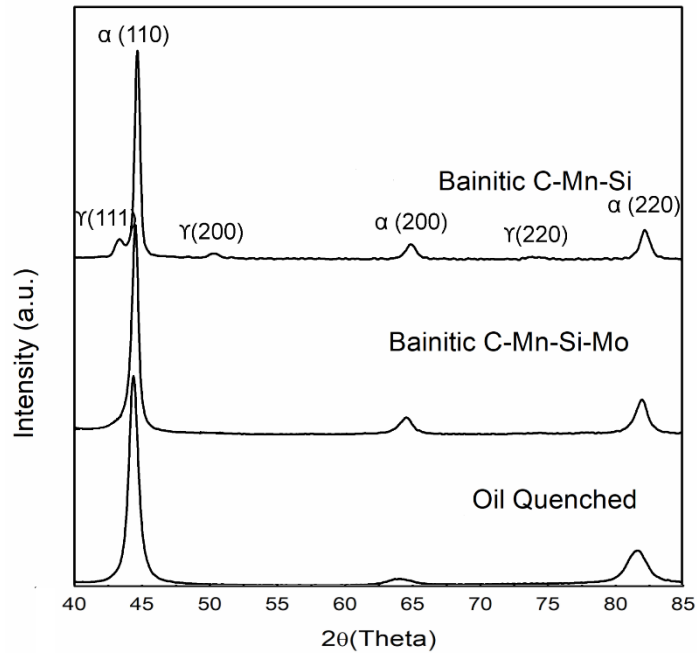
Figure 4.33. Comparison of XRD patterns of Q, Mo-IT-230-48, and IT-250-12 specimens. In IT-250-12 specimens, austenite peaks ɣ (111), ɣ (200), ɣ (220) are observed.

The change in retained austenite contents of C-Mn-Si specimens can be explained with the bainite growth mechanism in Si-containing steels and T_0' phenomena. In the isothermal transformation, the bainitic ferrite grows into austenite and the supersaturated carbon in ferrite is partitioned with austenite due to a displacive mechanism [28,29]. It is known that in steels containing high Si, the carbide precipitation in bainitic ferrite is retarded [15-17,30,56,66,69]. As a result, more carbon is partitioned between ferrite and austenite causing supersaturation of austenite. Upon cooling to room temperature, the carbon enriched austenite retains in the microstructure either in the form of thin films between the bainite sheaves or in the form of bulk islands (named as M/A).

Several thermodynamic conditions must be met for carbide-free bainite formation to take place [36,56,70]. These conditions are as follows: 1. Carbon concentration in

austenite must be less than T_0', 2. The carbon content in austenite must be above the para-equilibrium curve of austenite-cementite (A/A_p+Fe_3C) so that no cementite precipitation takes place and 3. No martensite must form at that temperature, i.e. temperature must lie above M_s.

The T_0' and para-equilibrium curves are calculated for both C-Mn-Si and C-Mn-Si-Mo alloys and shown with dashed lines in Figure 4.34 using Thermo-Calc software. For C-Mn-Si alloy, the feasible region for carbide-free bainitic transformation is bounded by T_0', Para-equilibrium, and M_S curves. In the case of C-Mn-Si alloy, the higher amount of retained austenite in specimens transformed at elevated temperatures (300°C vs. 250°C) can be related to T_0' phenomena. As seen in Figure 4.34, at higher temperatures, the bainite reaction stops at an earlier stage because beyond the T0' line bainite reaction cannot proceed. The contradictory results on the effect of retained austenite can possibly be related to the carbide precipitation kinetics and mechanisms in the different alloy systems. In this study, an increase in volume fraction of retained austenite due to longer transformation time (from 12 h to 24 h) at 250°C can be explained with the same mechanism: A longer transformation time causes formation of more bainite and hence high amount of carbon rejection into austenite. This results in a highly supersaturated austenite in terms of carbon. However, the bainitic transformation at 300°C exhibits a higher amount of retained austenite than that of samples transformed at 250°C which is believed to be due to the T_0 phenomena. A very similar result has been reported by Caballero et. al. [11] who studied the bainitic transformation of 1.0wt%C-1.6wt%Si-1.9wt%Mn-1.3wt%Cr steel at high temperatures and indicated that the retention of the high amount of austenite at around 300°C occurs due to T_0' phenomena.

It is seen from Figure 4.34 that for C-Mn-Si-Mo alloy, both T_0' and para-equilibrium curves shift to higher carbon percentages, hence the carbide-free bainite area is enlarged. This implies that bainite transformation should go into completion more easily than transformation of Mo free alloy. However, the plots of Thermo-Calc cannot explain the absence of retained austenite in Mo-containing alloy, as the

carbide-free bainite region is larger than that of C-Mn-Si alloy, there should be no carbide precipitation and consequently the supersaturated austenite should remain in the microstructure. The effect of Mo in a quenched and partitioned low carbon and high Si steels has been studied by E. De Moor et.al [71] and G.A. Thomas et.al [72] and it has been found that the Mo-containing alloy exhibits greater austenite fractions than the base alloy and the stability of retained austenite is increased.
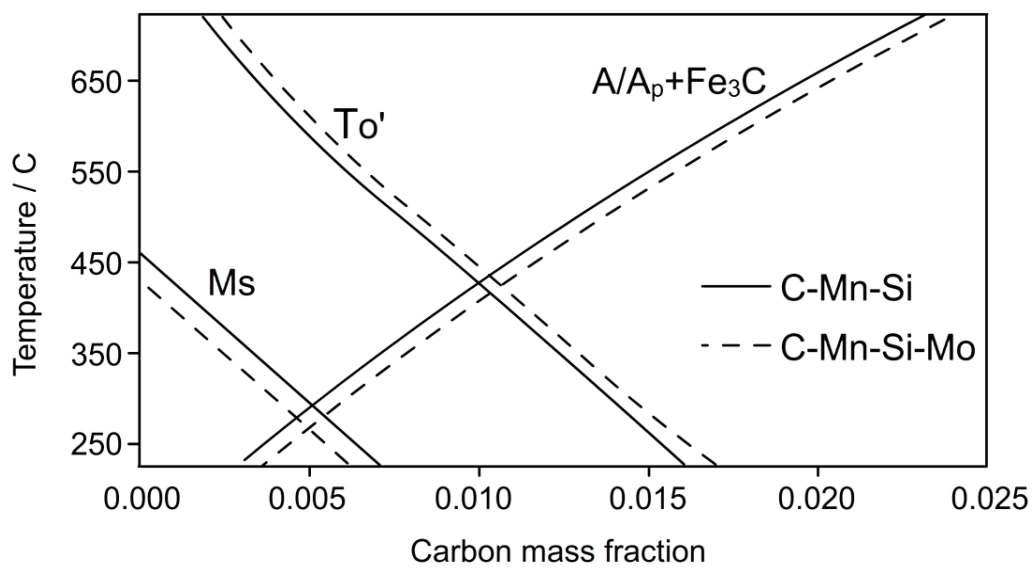
Figure 4.34. The schematic drawing of T_0' curve. At the right of this curve, the bainitic reaction cannot proceed.

In this study, the carbide extraction studies have shown that there is epsilon carbide precipitation in Mo-containing alloy during bainitic transformation (section 4.3.4). The epsilon carbide precipitation in bainite would inhibit the partition of carbon with austenite and avoid formation of supersaturated austenite. This means that all the austenite will transform to martensite. Indeed, as seen in Figure 4.35, a very fine carbide precipitation is present in the form of parallel thin carbide films in specimen C-Mn-Si-Mo alloy after transformation at 280ºC. However, a carbide precipitation

is not observed in C-Mn-Si alloy. It seems that presence of 2%Mo, an addition of 1.2%Si is not enough to prevent carbide precipitation.
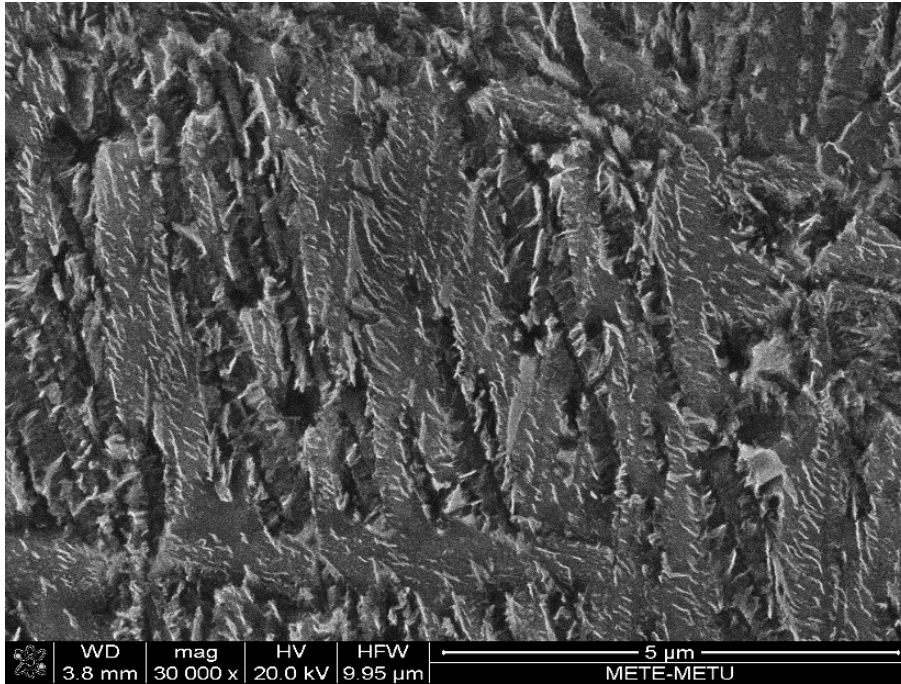
Figure 4.35. SEM micrograph of Mo-IT-280-12. Very thin, elongated carbide precipitation within and between the sheaves can be seen (white precipitates).

All these results indicate that the effect of Si on the retardation of carbide precipitation is complex and needs further study in different alloy systems including the high carbon content and Mo systems.

It is important to evaluate the microstructural analysis of the samples together with the calculated TTT diagrams. At low transformation temperatures, the bainite formation starts and finishes later. As expected, the hardnesses of bainitic microstructures are closely related to the transformation temperature. As the amount of bainite increases, hardness decreases. Since the hardness of the phases cannot be determined separately, the obtained hardness is an average and belongs to the phase mixtures. As the bainite transformation temperature and time increase, it can be said

that the amount of martensite decreases by looking at the hardness. After the transformation is completed, the hardness of the bainite transfomed at 230°C is higher than the hardness of the bainite transformed at 280°C as expected. This variation can be explained by the coarser bainite sheaves at higher temperatures.

It is known that both Mn and Cr shift the T_0' curve to lower carbon content and thus, the bainitic transformation stops at an earlier stage as the T_0' curve will be reached more quickly. In our study, the Mn and Cr contents of the alloys are minimized for shifting the T_0' curve to higher carbon concentrations, but the formation of blocky M/A regions at the high transformation temperatures cannot be avoided. The diffusivities of Cr and Mo atoms are very low at the bainitic transformation temperatures, therefore precipitations of M_6C and M_2C alloy carbides are not expected [15]. The carbide precipitation from supersaturated bainitic ferrite follows similar stages as in the case of the tempering of martensite. First, ε-carbide is seen and then it is replaced with Fe_3C at higher temperatures [15,42]. Also, there is experimental evidence that the precipitation of the transition ε-carbide is enhanced in the presence of silicon [59,73,74] and even an attempt was made by D.V. Edmonds et.al. [75] to draw two different C-curves for the precipitation of transition ε-carbide and cementite.

The bainitic transformation just above M_s may result in formation of very narrow bainitic sheaves. In fact, to enhance the mechanical properties, formation of blocky austenite (M/A) regions has to be minimized as it is known that it causes brittleness. Looking at the microstructures (Figure 4.36), it can be seen that bainite sheaves at 200°C and 230°C are quite narrow for C-Mn-Si and C-Mn-Si-Mo alloy, respectively. In C-Mn-Si alloy, bainitic sheaves are much narrow at 200°C than at 250°C due to kinetics of transformation. It can be seen in Figure 4.36(a), Figure 4.36(b) and Figure 4.36(c) that the number of sheaves on the 1μm line is 8 at 200°C, 10 at 250°C and 12 at 300°C. In C-Mn-Si-Mo alloy, bainitic sheaves are much narrow at 230°C than at 280°C due to kinetics of transformation. It can be seen in Figure 4.36(d) and Figure 4.37 that the number of sheaves on the 1μm line is 5 at 230°C and 10 at 280°C.

Increase in the transformation temperature shortens the transformation time required to form 100% bainite, increases the amount of retained austenite, and coarser bainitic ferrites are obtained.

(a)

WD 6.2 mm | mag 30 000 x | HV 20.0 kV | HFW 9.95 µm | 5 µm | METE-METU

(b)

WD 6.2 mm | mag 20 000 x | HV 20.0 kV | HFW 14.9 µm | 5 µm | METE-METU
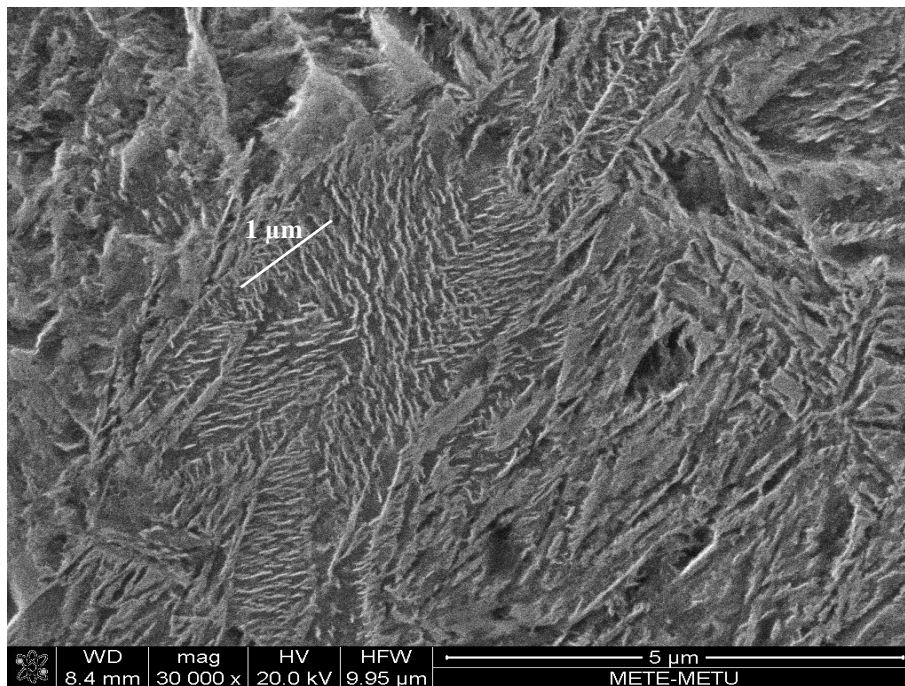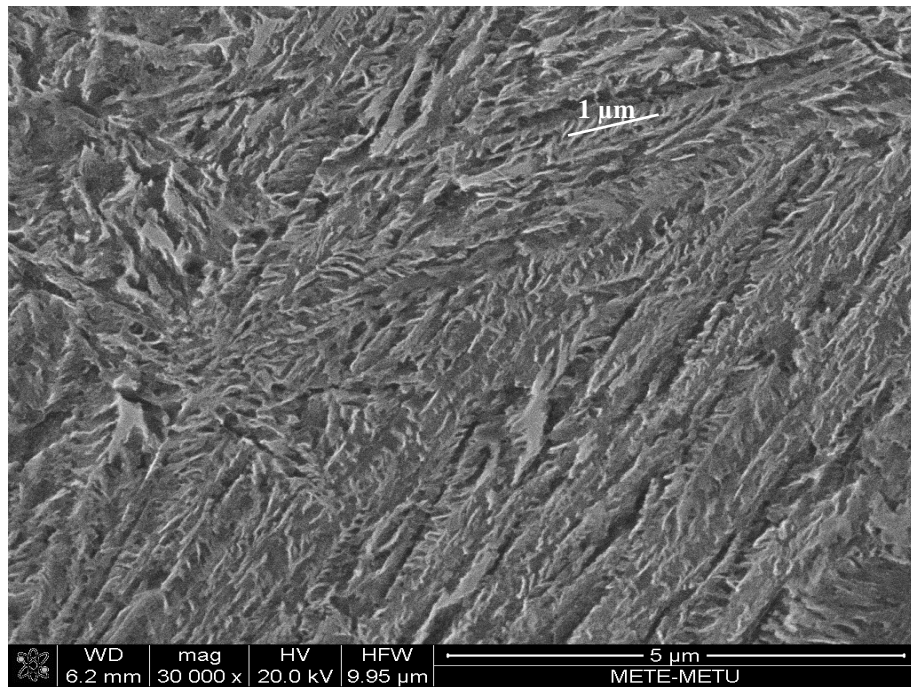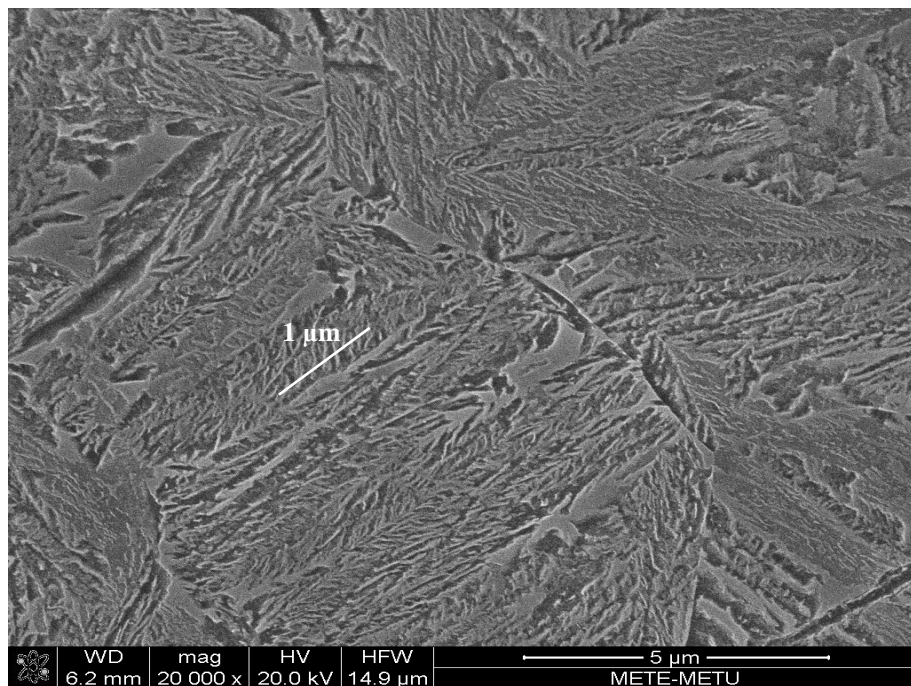
(c)
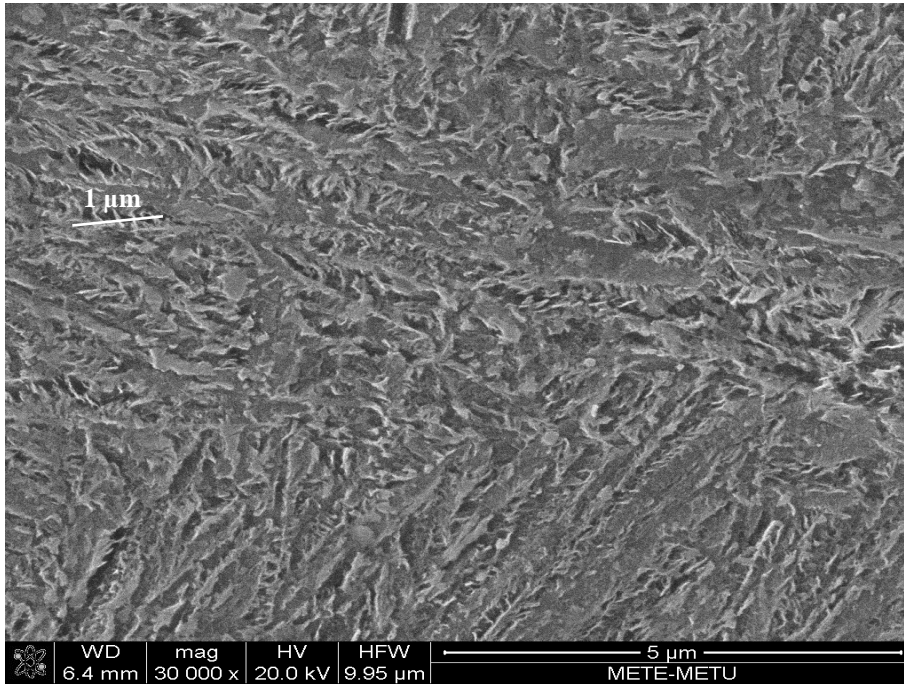
(d)

Figure 4.36. SEM micrographs of IT-200-24, IT-250-12, IT-300-3 and Mo-IT-230-48, respectively.

In Mo-IT-280-12 specimens, a change in the morphology of bainite is observed. It appears that bainite sheaves become coarser and more flat (Figure 4.37). Also, it is evident that there is a very thin, carbide-like precipitates are located within the sheaves (white precipitates in Figure 4.37).
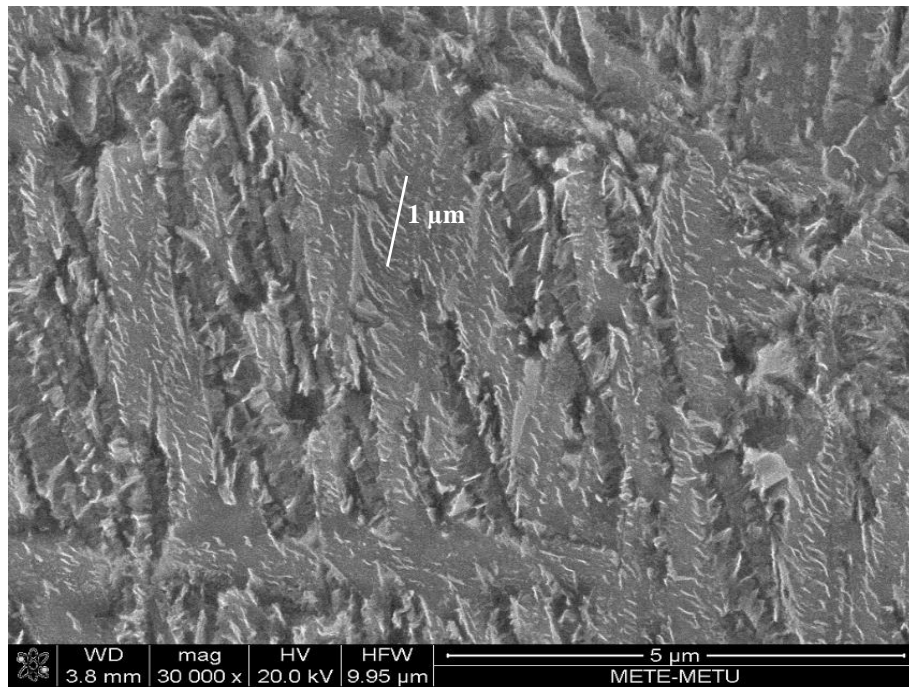
Figure 4.37. SEM micrograph of Mo-IT-280-12. Very thin, elongated carbide precipitation within the sheaves can be seen (white precipitates).

CHAPTER 5

CONCLUSION

In this thesis study, the effect of Si and Mo on the isothermal transformation treatment and tempering of a bainitic medium C steel is studied. The following conclusions are drawn:

1.   In both C-Mn-Si and C-Mn-Si-Mo steel, the bainitic transformation is completed after an isothermal treatment just above their Ms temperatures, i.e. at 250°C and 230°C respectively, although at later stages than dictated by calculated TTT diagrams.

2.   In C-Mn-Si steel, the amount of retained austenite increases with an increase in isothermal transformation time. When bainitic transformation is completed, the specimen transformed at 250°C contains nearly 11% retained austenite whereas the one transformed at 300°C yielded 15% retained austenite at room temperature. In C-Mn-Si-Mo alloy, the retained austenite phase could not be detected after 100% bainitic transformation at either 230°C for 48 h or 280°C for 12 h.

3.   In C-Mn-Si steel, the carbide extraction results have shown that the bainitic structure in this steel is nearly free of carbide. In contrast to C-Mn-Si steel, the bainitic specimens of C-Mn-Si-Mo steel contains Ɛ-carbide. This indicates that the presence of 2%Mo shadows the effect of the 1.2%Si and contribute to fine epsilon carbide precipitation during bainitic transformation. This finding also explains the absence of retained austenite in C-Mn-Si-Mo specimens, because precipitation of epsilon carbide in bainitic ferrite will avoid formation of a supersaturated austenite with respect to carbon.

4.   Tensile testing of C-Mn-Si alloy specimens have shown that fully bainitic specimens have equal or higher tensile strength values than that of the tempered martensitic specimens. The fully bainitic specimen exhibited yielded a UTS of 2200

MPa with an elongation of 8% whereas a quenched and tempered specimen yielded 1900MPa and 7% respectively. Tensile strength decreases as the bainitic transformation temperature increases.

5.   When the "Product of Strength and Elongation (PSE=UTSx%Elongation)" parameter of C-Mn-Si alloy specimens are compared, the 100% bainitic specimen treated at 250°C yielded nearly 15% higher PSE values than other bainitic and martensitic specimens.

REFERENCES

1. R. Rana and S.B. Singh, "Automotive Steels; Design, Metallurgy, Processing and Applications", Woodhead Publishing (Elsevier), 2017, https://doi.org/10.1016/C2015-0-00236-2.

2. V.K. Sikka, R. Klueh, P. J. Maziasz, S. Babu, M.L. Santella, H. Maan, J. Paules, K.E. Orie, "Mechanical Properties of New Grades of Fe–3Cr–W Alloys", Amer Soc Mech Eng Pressure Vessel Piping, vol. 476, pp. 97-106, 2004, https://doi.org/10.1115/PVP2004-2576.

3. F. Abe, "Bainitic and Martensitic Creep-Resistant Steels", Curr Opin Solid State Mater Sci, vol. 8, no. 3-4, pp. 305-311, 2004, https://doi.org/10.1016/j.cossms.2004.12.001.

4. D. K. Matlock, G. Krauss, J. G. Speer, "Microstructures and properties of direct-cooled microalloy forging steels", J Mater Process Technol, vol. 117, pp. 324–328, 2001, https://doi.org/10.1016/S0924-0136(01)00792-0.

5. L. Ceschini, A. Marconi, C. Martini, A. Morri, A. Di Schino, "Tensile and Impact Behaviour of a Microalloyed Medium Carbon Steel: Effect of The Cooling Condition and Corresponding Microstructure", Mater Des, vol. 45, pp. 171–178, 2013, https://doi.org/10.1016/j.matdes.2012.08.063.

6. F. Harrier et.al., Hardness of a Low Alloyed Complex Phase Steel, MS&T 2009: Proceedings from the Materials Science & Technology Conference, Oct 25–29, 2009 (Pittsburgh, PA), MS&T Partner Societies, pp. 78–83, 2009.

7. M.Y. Demeri, "Advanced High Strength Steels. Science, Technology and Applications", ASM International, Materials Park, Ohio, 2013.

8. F.G. Caballero, H.K.D.H. Bhadeshia, K.J.A. Mawella, D.G. Jones, P. Brown, "Design of Novel High Strength Bainitic Steels. Part 1", Mater Sci Technol, vol. 17, pp. 512–516, 2001, https://doi.org/10.1179/026708301101510348.

9. F.G. Caballero, H.K.D.H. Bhadeshia, K.J.A. Mawella, D.G. Jones, P., Brown, "Design of Novel High Strength Bainitic Steels. Part 2", Mater Sci Technol, vol. 17, pp. 517–522, 2001, https://doi.org/10.1179/026708301101510357.

10. F.G. Caballero, M.J. Santofimia, C. Capdevila, C. Garcia-Mateo, C. Garcia de Andres, "Design of Advanced Bainitic Steels by Optimization of TTT Diagrams and T_0 Curves". ISIJ Int, vol. 46, pp. 1479–1488, 2006, https://doi.org/10.2355/isijinternational.46.1479.

11.   F.G. Caballero, H.K.D.H. Bhadeshia, "Very Strong Bainite", Curr Opin Solid State Mater Sci, vol. 8, pp. 251–257, 2004, https://doi.org/10.1016/j.cossms.2004.09.005.

12.   F.G. Caballero, H.K.D.H. Bhadeshia, K.J.A. Mawella, D.G. Jones, P. Brown, "Very Strong Low Temperature Bainite", Mater Sci Technol, vol. 18, pp. 279–284, 2002, https://doi.org/10.1179/026708301225000725.

13.   C. Garcia-Mateo, F.G. Caballero and H.K.D.H. Bhadeshia, "Development of Hard Bainite", ISIJ Int, vol. 43, no. 8, pp. 1238-1243, 2003, https://doi.org/10.2355/isijinternational.43.1238.

14.   C. Garcia-Mateo, F.G. Caballero, H. K. D. H. Bhadeshia, "Acceleration of Low-Temperature Bainite". ISIJ Int, vol. 43, pp.1821-1825, 2003, https://doi.org/10.2355/isijinternational.43.1821.

15.   H.K.D.H. Bhadeshia, "Bainite in Steels", 3rd ed, IOM Communications, London, (2015).

16.   H.K.D.H. Bhadeshia, D.V. Edmonds,   "Bainite in Silicon Steels: A New Composition-Property approach. Part I", Met Sci, vol. 17, pp. 411-419, 1983, https://doi.org/10.1179/030634583790420600.

17.   H.K.D.H. Bhadeshia, D. V. Edmonds, "Bainite in Silicon Steels: A New Composition-Property approach. Part II", Met Sci, vol. 17, pp. 420- 425, 1983, https://doi.org/10.1179/030634583790420646.

18.   H.K.D.H. Bhadeshia, "High Performance Bainitic Steels", Materials Science Forum,   vol.   500-501,   pp.   63-74,   2005, https://doi.org/10.4028/www.scientific.net/MSF.500-501.63.

19.   M.N. Yoozbashi, S. Yazdani, T.S. Wang, "Design of A New Nanostructured, High-Si Bainitic Steel with Lower Cost Production", Mater Des, vol. 32, pp. 3248–3253, 2011, https://doi.org/10.1016/j.matdes.2011.02.031.

20.   H.K.D.H. Bhadeshia, R.W.K. Honeycombe, "Steels Microstructure and Properties". 3rd ed., 2006.

21.   J. Kang, F.C. Zhang, X.W. Yang, B. Lv, K.M. Wu, "Effect oOf Tempering on the Microstructure and Mechanical Properties of a Medium Carbon Bainitic Steel". Mater Sci Eng A, vol. 686, pp.150–159, 2017, https://doi.org/10.1016/j.msea.2017.01.044.

22.   M. Zhu, G. Xu, M. Zhou, Q. Yuan, J. Tian, H. Hu, "Effects of Tempering on the Microstructure and Properties of a High-Strength Bainite Rail Steel with Good Toughness", Metals, vol. 8, no. 484, pp. 1-11, 2018, https://doi.org/10.3390/met8070484.

23.   K. Junhua, Z. Lin, G. Bin, L. Pinghe, W. Aihua, X. Changsheng, "Influence of Mo Content on Microstructure and Mechanical Properties of High Strength

Pipeline Steel", Mater Des, vol. 25, pp. 723-728, 2004, https://doi.org/10.1016/j.matdes.2004.03.009.

24.   F.G. Caballero, M.J. Santofimia, C. García-Mateo, J. Chao, C. Garcia de Andres, "Theoretical Design and Advanced Microstructure in Super High Strength Steels", Mater Des, vol. 30. pp. 2077-2083, 2009.

25.   C. Garcia-Mateo, F.G. Caballero, H.K.D.H. Bhadeshia, "Low Temperature Bainite", Journal de Physique IV, vol. 112, pp. 285–288, 2003.

26.   F.G. Caballero, C. Garcia-Mateo, H.K.D.H. Bhadeshia, "Very Strong Bainitic Steels", https://www.phase-trans.msm.cam.ac.uk/2005/Rome1.pdf.

27.   E. C. Bain, Functions of The Alloying Elements in Steel, 1st ed, American Society for Metals, Cleveland, Ohio, 1939.

28.   F.G. Caballero, C. Garcia-Mateo, M.J. Santofimia, M.K. Miller, C. García de Andrés, "New Experimental Evidence on the Incomplete Transformation Phenomenon in Steel", Acta Mate, vol. 57, pp. 8-17, 2009, https://doi.org/10.1016/j.actamat.2008.08.041.

29.   H.K.D.H. Bhadeshia, "The Bainite Transformation: Unresolved Issues", Mater Sci Eng A, vol. 273-275, pp. 58-66, 1999, https://doi.org/10.1016/S0921-5093(99)00289-0.

30.   H.K.D.H. Bhadeshia, "Developments in Martensitic and Bainitic Steels: Role of The Shape Deformation", Mater Sci Eng A, vol. 378, pp. 34-39, 2004, https://doi.org/10.1016/j.msea.2003.10.328.

31.   M. Soliman, H. Palkowski, "Development of The Low Temperature Bainite", Archives of Civil and Mechanical Engineering, vol. 16. pp. 403-412, 2016.

32.   T. Sourmail, F.G. Caballero, C. Garcia-Mateo, V. Smanio, C. Ziegler, M. Kuntz, R. Elvira, A. Leiro, E. Vuorinen, T. Teeri, "Evaluation of Potential of High Si High C Steel Nano Structured Bainite for Wear and Fatigue Applications", Mater. Sci. Technol., vol. 29, no. 10, pp. 1166-1173, 2013, https://doi.org/10.1179/1743284713Y.0000000242.

33.   G. Sidhu, S.D. Bhole, E. Essadiqi, D.L. Chen, "Characterization of Isothermally Heat-Treated High Carbon Nano bainitic Steels, Journal of Materials Engineering and Performance", vol. 22, no. 10, pp. 3070-3076, 2013, https://doi.org/10.1007/s11665-013-0581-4.

34.   F.G. Caballero, J. Chao, J. Cornide, C. García-Mateo, M.J. Santofimia, C. Capdevila, "Toughness Deterioration in Advanced High Strength Bainitic Steels", Mater Sci Eng A, vol. 525, no. 1, pp.87-95, 2009, https://doi.org/10.1016/j.msea.2009.06.034.

35. U. P. Singh, B. Roy, S. Jha, S.K. Bhattacharyya, "Microstructure and Mechanical Properties of as Rolled High Strength Bainitic Rail Steels", Mater Sci Technol, vol. 17, pp. 33–38, 2001, https://doi.org/10.1179/026708301101509098.

36. H. Huang, M.Y. Sherif, P.E.J. Rivera-Díaz-del-Castillo, "Combinatorial Optimization of Carbide-Free Bainitic Nanostructures", Acta Mater, vol. 61, pp. 1639–1647, 2013, https://doi.org/10.1016/j.actamat.2012.11.040.

37. M. Soliman, H. Palkowski, "Controlled Setting of the Transformation Kinetics and The Structure Constituents in Low-Temperature Bainite Steels", in: The Minerals, Metals & Materials Society (Ed.), TMS 2013 Supplemental Proceedings, John Wiley & Sons, Inc., Hoboken, NJ, USA, pp. 901–908, 2013.

38. M. Soliman, H. Palkowski, "Verfahren Zum Herstellen Eines Bauteils Mit Bainitischem Gefüge und Entsprechendes Bauteil", DE102012017143 B3, 2012.

39. H. Amel-Farzad, H.R. Faridi, F. Rajabpour, A. Abolhasani, S. Kazemi, Y. Khaledzadeh, "Developing Very Hard Nanostructured Bainitic Steel", Mater Sci Eng A, vol. 559, pp.68–73, 2013, https://doi.org/10.1016/j.msea.2012.08.020.

40. F.G. Caballero, M.K. Miller, S.S. Babu, C. Garcia-Mateo, C. Garcia de Andrés, "Low Temperature Bainite: An Analysis at Atomic Level. Solid-to-Solid Phase Transformations in Inorganic Materials", vol. 1: Diffusional Transformation, pp. 511-516, 2005.

41. K.J. Irvine, F.B. Pickering, W.C. Heselwood, M. Atkins, "The Physical Metallurgy of Low-Carbon, Low-Alloy Steels Containing Boron", JISI, vol. 195, pp. 54-67, 1957.

42. R.G. Baker, J. Nutting, "The Tempering of 2.25Cr%-1%Mo Steel After Quenching and Normalizing", JISI, vol. 192, no. 3, pp. 257-268,1959.

43. G. Jha, S. Das, S. Sinha, A. Lodh, A. Haldar, "Design and Development of Precipitate Strengthened Advanced High Strength Steel for Automotive Application", Mater Sci Eng A, vol. 561, pp. 394-402, 2013, https://doi.org/10.1016/j.msea.2012.10.047.

44. V.F. Zackay, E.R. Parker, D. Fahr and R. Bush, "The Enhancement of Ductility in High-Strength Steels", Trans Am Soc Met, vol. 60, pp. 252-259, 1967.

45. A. Zarei Hanzaki, P.D. Hodgson, S. Yue, "The Influence of Bainite on Retained Austenite Characteristics in Si-Mn TRIP Steels", ISIJ Int, vol. 35, no. 1, pp. 79-85, 1995, https://doi.org/10.2355/isijinternational.35.79.

46. J.A. Jimenez, M. Carsi, O.A. Ruano, G. Frommeyer, "Effect of Testing Temperature and Strain Ration the Transformation Behavior of Retained Austenite in Low-alloyed Multiphase Steel", Mater Sci Eng A, vol. 508, no. 1–2, pp. 195-199, 2009, https://doi.org/10.1016/j.msea.2008.12.048.

47. C. Keul, V. Wirthsn, W. Bleck, "New Bainitic Steels for Forgings", Archives of Civil and Mechanical Engineering, vol. 12, pp. 119–125, 2012, https://doi.org/10.1016/j.acme.2012.04.012.

48. H. K.D.H. Bhadeshia, "Rationalisation of Shear Transformations in Steels", Acta Metall., vol. 29, pp. 1117-1130, 1981.

49. W. Steven, A.G. Haynes, "The Temperature of Formation of Martensite and Bainite in Low-Alloy Steels." Journal of the Iron and Steel Institute, vol. 183, no. 8, pp. 349–59, 1956.

50. K.W. Andrews, "Empirical Formulae for The Calculation of Some Transformation Temperatures", JISI, vol. 203, pp. 721-727, 1965.

51. H.K.D.H. Bhadeshia, "52nd Hatfield Memorial Lecture Large Chunks of Very Strong Steel", Mater Sci Tech, vol. 21, 1293-1302, 2005, https://doi.org/10.1179/174328405X63999.

52. F. G. Caballero, H.K.D.H. Bhadeshia, "High-Strength Bainitic Steels", IJISSI, vol. 1, pp. 15-23, 2004.

53. N.E. Tenaglia, R.E. Boeri, A.D. Basso, "Mechanical Properties of a Carbide-Free Bainitic Cast Steel with Dispersed Free Ferrite", Mater Sci Technol, vol. 36, no.1, pp.108-117, 2020, https://doi.org/10.1080/02670836.2019.1684658.

54. K. Tsuzaki, C. Nakao, T. Maki, "Formation Temperature of Bainitic Ferrite in Si-Containing Steels", Mater Trans, vol.32, no. 8, pp. 658-666, 1991, https://doi.org/10.2320/matertrans1989.32.658.

55. C. Hofer, F. Winkelhofer, H. Clemens, S. Primig, "Morphology Change of Retained Austenite During Austempering of Carbide-Free Bainitic Steel", Mater Sci Eng A, vol. 636, pp. 236-246, 2016, https://doi.org/10.1016/j.msea.2016.04.005.

56. E. Kozeschnik, H.K.D.H. Bhadeshia, "Influence of Silicon on Cementite Precipitation in Steels", Mater Sci Technol, vol. 24, pp. 343–347, 2008, https://doi.org/10.1179/174328408X275973.

57. H.K.D.H. Bhadeshia, A.R. Chintha, S. Lenka, "Critical Assessment 34: Are χ (Hägg), η and ε carbides transition-phases relative to cementite in steels?", Mater Sci Technol, vol. 35, no. 11, pp. 1301-1305, 2019, https://doi.org/10.1080/02670836.2019.1625526.

58.   Xing-Wu Liu, Z. Cao, S. Zhao, R. Gao, Y. Meng, Jian-Xin Zhu, C. Rogers, Chun-Fang Huo, Y. Yang, Yong-Wang Li, Xiao-Don Wen, "Iron Carbides in Fischer−Tropsch Synthesis: Theoretical and Experimental Understanding in Epsilon-Iron Carbide Phase Assignment", J Phys Chem C, vol. 121, pp. 21390−21396, 2017, https://doi.org/10.1021/acs.jpcc.7b06104

59.   J. Jang, I. Kim, H. K. D. H. Bhadeshia, "ε-Carbide in Alloy Steels: First-Principles Assessment", Scripta Materialia, vol. 63, no. 1, pp. 121-123, 2010, https://doi.org/10.1016/j.scriptamat.2010.03.026.

60.   M.M. Sandomirskii, V.I. Grigorkin, "Influence of Phase Composition and Structure on The Temper Resistance and Brittle Fracture Resistance of 15Kh2NMFA and 10GN2MFA Steels" Met Sci Heat Treat, vol. 25, pp. 849-854, 1983, https://doi.org/10.1007/BF00703899.

61.   C. Garcia-Mateo, M. Peet, F. G. Caballero, H. K. D. H. Bhadeshia, "Tempering of Hard Mixture of Bainitic Ferrite and Austenite", Mater Sci Technol, vol. 20, no. 7, pp. 814-818, 2004, https://doi.org/10.1179/026708304225017355.

62.   W.J. Nam, "Effect of Initial Microstructure on the Coarsening Behavior of Cementite Particles", ISIJ Int, vol. 39, no. 11, pp. 1181-1187, 1999, https://doi.org/10.2355/isijinternational.39.1181.

63.   K.J. Irvine, F.B. Pickering, "The Tempering Characteristics of Low-Carbon Low-Alloy Steels", JISI, vol. 194, pp. 137-153, 1960.

64.   K. Zhang, M. Zhu, B. Lan, P. Liu, W. Li, Y. Rong, "The Mechanism of High-Strength Quenching-Partitioning-Tempering Martensitic Steel at Elevated Temperatures", Crystals, vol. 9, no. 2, pp. 94-103, 2019, https://doi.org/10.3390/cryst9020094.

65.   K. Sugimoto, M. Murata, T. Muramatsu, Y. Mukai, "Formability of C–Si–Mn–Al–Nb–Mo Ultra High-strength TRIP-aided Sheet Steels", ISIJ Int, vol. 47, no. 9, pp. 1357-1362, 2007, https://doi.org/10.2355/isijinternational.40.902.

66.   K. Sugimoto, M. Tsunezawa, T. Hojo, S. Ikeda, "Ductility of 0.1–0.6C–1.5Si–1.5Mn Ultra High-Strength TRIP-Aided Sheet Steels with Bainitic Ferrite Matrix", ISIJ Int, vol. 44, no. 9, pp.1608–1614, 2004, https://doi.org/10.2355/isijinternational.44.1608.

67.   K. Sugimoto, T. Iida, J. Sakaguchi, T. Kashima, "Retained Austenite Characteristics and Tensile Properties in a TRIP Type Bainitic Sheet Steel", ISIJ Int, vol. 40, no. 9, pp. 902-908, 2000, https://doi.org/10.2355/isijinternational.40.902.

68. C. Garcia-Mateo, F.G. Caballero "The Role of Retained Austenite on Tensile Properties of Steels with Bainitic Microstructures", Mater Trans, vol. 46, no. 8, pp. 1839-1846, 2005, https://doi.org/10.2320/matertrans.46.1839.

69. K. Sugimoto, T. Hojo, J. Kobayashi, "Critical Assessment 29: TRIP-Aided Bainitic Ferrite Steels", Mater Sci Technol, vol. 33, no. 17, pp. 2005-2009, 2017, https://doi.org/10.1080/02670836.2017.1356014.

70. C.M. Amey, H. Huang, P.E.J. Rivera-Díaz-del-Castillo, "Distortion in 100Cr6 and nanostructured bainite", Mater Des, vol. 35, pp. 66-71, 2012, https://doi.org/10.1016/j.matdes.2011.10.008.

71. E. De Moor, C. Föjer, A.J. Clarke, J. Penning, J.G. Speer: Proc. on New Developments on Metallurgy and Applications of High Strength Steels Conf., Minerals, Metals & Materials Soc, Buenos Aires, 721, 2008.

72. G.A. Thomas, E. De Moor, J.G. Speer: E. De Moor, H.J. Jun, J.G. Speer, M. Merwin (Eds.) Proc. of the International Symposium on New Developments in Advanced High-Strength Sheet Steels, (AIST), Vail, Colorado, 153, 2013.

73. D.V. Edmonds, K. He, M.K. Miller, F.C. Rizzo, A. Clarke, D.K. Matlock, and J.G. Speer, "Microstructural Features of 'Quenching and Partitioning': A New Martensitic Steel Heat Treatment", Mater. Sci. Forum, vol. 539–543, pp. 4819-4825, 2007, https://doi.org/10.4028/www.scientific.net/MSF.539-543.4819.

74. E. De Moor and J.G. Speer, "Automotive Steels: Design, Metallurgy, Processing and Applications", pp. 289-316, 2017, https://doi.org/10.1016/B978-0-08-100638-2.00010-9.

75. D.V. Edmonds, K. He, F.C. Rizzo, B.C. De Cooman, D.K. Matlock, J.G. Speer, "Quenching and Partitioning Martensite—A Novel Steel Heat Treatment", Mater Sci Eng A, vol. 438–440, pp. 25-34, 2006, https://doi.org/10.1016/j.msea.2006.02.133.

CURRICULUM VITAE

PERSONAL INFORMATION

Surname, Name: Kafadar, Gülten
Nationality: Turkish (TC)
Date and Place of Birth: 2 January 1989, Ankara
Marital Status: Married
Phone: +90 533 741 38 14
email: gultenkilickafadar@gmail.com

EDUCATION

Degree	Institution	Year of Graduation
MS	METU Metallurgical and Materials Engineering	2013
BS	METU Metallurgical and Materials Engineering	2011
High School	Çankaya Anadolu High School, Ankara	2006

WORK EXPERIENCE

Year	Place	Enrollment
2019-Present	Turkish Aerospace	Technology Development Engineer
2015-2019	Presidency of Defence Industries	Project Engineer

FOREIGN LANGUAGES

Advanced English, Basic German

PUBLICATION

Kafadar G., Kalkanlı A., Özdemir A.T., and Ögel B. "Effect of Isothermal Transformation Treatment and Tempering on the Microstructure and Hardness of a Medium C and High Si Steels", ISIJ International, 61(5), 1679-1687(2021), https://doi.org/10.2355/isijinternational.ISIJINT-2020-419.

HOBBIES

Running, Travel, Movies.